Influence of fungal morphology on the performance of industrial fermentation processes for enzyme production

Quintanilla Hernandez, Daniela Alejandra

Publication date:
2017

Document Version
Publisher's PDF, also known as Version of record

Influence of fungal morphology on the performance of industrial fermentation processes for enzyme production

Daniela Alejandra Quintanilla Hernández

PhD Thesis

January 2017

DTU Chemical Engineering
Department of Chemical and Biochemical Engineering

Influence of fungal morphology on the performance of industrial fermentation processes for enzyme production

PhD thesis

Daniela Alejandra Quintanilla Hernández

Department of Chemical and Biochemical Engineering
Technical University of Denmark

January 31st 2017

Supervisors:
Krist V. Gernaey
Ole Hassager
Anna Eliasson Lantz
Kim Hansen

Evaluation committee:
Assoc. Professor Timothy John Hobley
DTU
Assoc. Manager Mhari Workman
Novo Nordisk A/S
Professor Gunnar Lidén
Lund University

Address: Department of Chemical and Biochemical Engineering

Technical University of Denmark

Søltofts Plads, Building 229

Dk-2800 Kgs. Lyngby

Denmark

Phone: +45 4525 2800

Web: www.kt.dtu.dk

Print: STEP

DTU Chemical Engineering
Department of Chemical and Biochemical Engineering

Abstract

Production of industrial enzymes is usually carried out as submerged aerobic fermentations. Filamentous microorganisms are widely used as hosts in these processes due to multiple advantages. Nevertheless, they also present major drawbacks, due to the unavoidable oxygen transfer limitations as a consequence of the high viscosity of the medium that they develop, which is believed to be related to the biomass concentration, growth rate and morphology. This last variable is one of the most outstanding characteristics of the filamentous fungi due to its great complexity and it was extensively studied in this work, along with its correlation to viscosity and other process variables.

Considerable research work has been conducted through the years to study fungal morphology and its relation to productivity. However, the work reported in the literature lacks relevant industrial data. In this work, a platform was developed which was able to produce high enzyme titers in comparison with what has been reported thus far in fed-batch fermentation using a soluble inducer (lactose). Different nitrogen sources were compared, and it was found that soy meal allowed for higher enzyme titers compared to what has been reported in the literature.

The developed platform was used to study the influence of agitation intensity on the morphology, rheology and protein production capability of *Trichoderma reesei* RUT-C30. Eight fed-batch fermentations were conducted in bench scale fermenters at two different media concentrations and four different agitation speeds. The morphology was measured with laser diffraction and the 90^{th} percentile of the particle size distribution (PSD) was chosen as the characteristic morphology parameter. No significant difference in biomass concentration, carbon dioxide production rate and enzyme production was observed as a function of agitation speed, even at the very high power inputs. However, the morphology and rheology were considerably affected. The data produced was used to create a novel method to predict filamentous fungi rheology based on simple measurements of biomass and morphology.

Thus, morphology is an important variable in industrial submerged fermentation since it highly impacts the broth rheology. Therefore, it is important to understand the factors that affect it. One important factor is agitation-induced fragmentation since it will dictate the size of the particles, which will then affect rheology. A well-established state of the art function, the Energy Dissipation Circulation Function (EDCF), has been used to correlate hyphal fragmentation over a range of scales and impeller types. This correlation was however developed for non-growing systems (off-line fragmentation), and no attempts have been made for testing its application across different scales in actual fermentation broths. Thus, to test the validity of this correlation, a scale-down experiment was carried out. A production batch from Novozymes A/S operated in a production scale bioreactor ($\approx$ 100 m^3) was scaled down to pilot scale ($\approx$1 m^3) and to bench scale ($\approx$0.001 m^3). The EDCF was calculated for each batch along with other mixing parameters and they were

correlated to the characteristic morphological parameter, the 90th percentile of the PSD. The data showed that other more simple scale up parameters are equally good at predicting mycelial fragmentation across scales, compared to the EDCF.

Furthermore, the morphological development of an industrial strain of *T. reesei* was monitored in pilot scale fermentations. This study showed that the morphology monitored with laser diffraction also granted the possibility to study direct physiological responses to environmental conditions in stirred bioreactors. The obtained results indicate that the nutrient depletion induced foraging due to starvation, which caused the increase in hyphal length.

Finally, a novel, fast and easy method for statistically-verified quantification of relative hyphal tensile strength was developed in the last part of this PhD project. Fungal hyphal strength is an important phenotype which can have a profound impact on bioprocess behavior. The applicability of this novel method was demonstrated by estimating relative hyphal strength during growth in control conditions and rapamycin-induced autophagy conditions for two strains of *Aspergillus nidulans*. Both strains were grown in shake flasks, and relative hyphal tensile strength was compared. The findings confirmed the utility of the developed method in strain selection and process development.

This PhD thesis brings more knowledge to the understanding of the relationship between growth kinetics, environmental conditions and the morphological structure of the filamentous fungi, which can help to tailor the morphology for a given industrial strain.

Dansk Resumé

Produktion af industrielle enzymer udføres typisk som vandige aerobe fermenteringer. Filamentøse mikroorganismer er udbredte som værtsorganismer i disse processer pga. adskillige fordele. Samtidig har de store ulemper som følge af den uundgåelige begrænsning i iltoverførselen pga. den høje viskositet af mediet de udvikler, og som menes at være relateret til biomasse koncentrationen, væksthastigheden og morfologien. Den sidste variabel er blandt de mest betydningsfulde egenskaber på grund af sin store kompleksitet, og den er blevet grundigt undersøgt i dette arbejde samt dens korrelation til viskositet og andre procesvariabler.

En betydelig mængde forskning er blevet udført igennem årene i forbindelse med svampes morfologi og deres relation til produktivitet. Dog er bidragene i litteraturen kendetegnet ved mangel på relevante industrielle data. En platform er blevet udviklet, som giver anledning til høje enzymproduktiviteter sammenlignet med hvad der tidligere er rapporteret i litteraturen for fed-batch fermentering ved anvendelse af en opløselig inducer (lactose). Forskellige nitrogenkilder er blevet sammenlignet, og det blev konstateret, at sojamel muliggør en højere enzymtiter i sammenligning med hvad der er blevet rapporteret i litteraturen.

Den udviklede platform blev anvendt til at undersøge indflydelsen af omrøringsintensiteten på morfologien, rheologien og proteinproduktionsevnen af *Trichoderma reesei* RUT-C30. Otte fed-batch fermenteringer blev udført i lab-skala fermentorer ved to forskellige mediekoncentrationer og fire forskellige omrøringshastigheder. Morfologien blev målt med laserdiffraktion og den 90. percentil af partikelstørrelsesfordelingen (PSD) blev valgt som den karakteristiske morfologiske parameter. Ingen signifikant forskel i biomassekoncentration, kuldioxidproduktionshastigheden og enzymproduktionen blev observeret som funktion af omrøringshastigheden, selv ved meget høj omrøringseffekt. Imidlertid blev morfologien og rheologien betydeligt påvirket. De indsamlede data blev brugt til at skabe en ny fremgangsmåde til at forudsige filamentøse svampes rheologi, baseret på simple målinger af biomasse og morfologi.

Eftersom at morfologi er en vigtig variabel i industrielle vandige fermenteringer, er det vigtigt at forstå de faktorer, der påvirker den. En vigtig faktor er omrøringsinduceret fragmentering, da det vil afgøre størrelsen af partiklerne, som derefter vil påvirke rheologien. En veletableret state-of-the-art funktion, Energy Dissipation Circulation Function (EDCF), er blevet anvendt til at korrelere hyfe fragmentering over et område af reaktorskalaer og omrører typer. Denne korrelation (EDCF) blev dog udviklet til ikke-voksende systemer (off-line fragmentering), og der er ikke foretaget forsøg for at teste dens anvendelse på tværs af forskellige skalaer i egentlige fermenteringsvæsker. For at teste validiteten af denne korrelation, blev et nedskaleringsforsøg udført. En produktionsbatch fra Novozymes A/S, som blev kørt i en produktionsskala bioreaktor (≈

100 m^3) blev skaleret ned til pilotskala (≈1 m^3) og lab-skala (≈0.001 m^3). EDCF blev beregnet for hvert batch sammen med andre blandingsparametre, og de blev korreleret til den karakteristiske morfologiske parameter, den 90. percentil af PSD. Dataene viste, at andre mere enkle opskaleringsparametre er lige så gode til at forudsige mycelie fragmentering på tværs skalaer.

Endvidere blev den morfologiske udvikling af en industriel stamme af *T. reesei* overvåget i pilotskalafermenteringer fodret med en hidtil ukendt strategi, udviklet i et parallelt projekt. Denne undersøgelse viste, at når morfologien overvåges med laser diffraktion, åbnes muligheden for at studere direkte fysiologiske reaktioner på vækstbetingelser i omrørte bioreaktorer. De opnåede resultater indikerer, at forbrug af næringsstofferne og de resulterende lave koncentrationer af næringsstofferne inducerede fouragering grundet sult, der forårsagede en stigning i hyfe længde.

Endelig blev en ny, hurtig og nem metode til statistisk-verificeret kvantificering af den relative hyfe trækstyrke udviklet i den sidste del af dette ph.d.-projekt. Hyfestyrke af svampe er en vigtig fænotype, som kan have en dybtgående indvirkning på bioprocessens adfærd. Anvendeligheden af denne nye metode blev demonstreret ved en estimering af den relative hyfestyrke under vækst i kontrollerede forhold og rapamycin-induceret autophagy for to *Aspergillus nidulans* stammer. Begge stammer blev dyrket i rystekolber, og den relative hyfe trækstyrke blev sammenlignet. Resultaterne bekræftede anvendeligheden af den udviklede metode i udvælgelse af stamme og procesudvikling.

Denne ph.d.-afhandling bringer mere viden til forståelsen af forholdet mellem vækstkinetik, vækstbetingelser og den morfologiske struktur af filamentøse svampe, som kan bidrage med at skræddersy morfologien af en given industriel stamme.

Preface

This thesis is submitted in partial fulfilments of the demands for obtaining a Ph.D. degree from the Technical University of Denmark (DTU). The PhD project was conducted at the Department of Chemical and Biochemical Engineering in the period November 2013 to January 2017. The study was carried out at the research group CAPEC-PROCESS in collaboration with Novozymes A/S. Professor Krist V. Gernaey was the main supervisor of this project and it was co-supervised by Associate Professor Anna Eliasson Lantz and Professor Ole Hassager. Senior Science Manager Kim Hansen was the co-supervisor from Novozymes A/S.

I would like to express my gratitude to my supervisors for their excellent guidance. Kim, thank you for sharing some of you huge knowledge with me; without question you have thought me a lot; thanks for all the patience you had, thanks for always making time and be willing to guide me. Anna, thank you for the valuable discussions and indispensable feedback during this period. Krist, thank you for all the trust and for believing in me; thank you for being such a caring supervisor.

The work presented in this thesis was conducted in the laboratories of Novozymes A/S. During the project, I had the opportunity to work in different departments - the Fermentation Technology Department and the Fermentation Pilot Plant-, but I also had the chance to collaborate with people from other departments - Recovery Pilot Plant and Solid Product Development-. I am grateful to all of you whom directly and indirectly contributed to this project. Special thanks to Lone and Paul which were always willing to help me with everything I needed. I would also like to express my gratitude to Stuart Stocks who gave me advice during the project and who contributed with ideas.

During my PhD studies, I had the opportunity to do an external research stay at the University of Maryland Baltimore County (UMBC), at the research group of Mark Marten. Thank you Mark for welcoming me at the group and make me feel part of it; thanks for all your guidance in that three months period and more. It has been a pleasure to have you as a supervisor. Also, I would like to thank Cindy for the help in the project I conducted at UMBC.

Finally, I would like to express my gratitude to my family and friends which have always been there for me. You all are also part of this achievement.

Table of Contents

Chapter 1. Introduction 1
1.1 Project motivation 1
1.2 Thesis outline 3
Chapter 2. Literature Review: Fungal Morphology in Industrial Enzyme Production .. 7
2.1 Introduction 7
2.2 Filamentous fungi for enzyme production 9
2.2.1 Important strains and products 9
2.2.2 Introduction to Morphology of Filamentous Fungi 10
2.2.3 Complexity of the subject 11
2.3 Modelling the Morphology 12
2.3.1 Micromorphology and productivity 13
2.3.2 Shear stress and morphology 14
2.3.3 Morphology and rheology 16
2.3.4 Process conditions and morphology 18
2.4 Conclusion 19
Chapter 3. Morphological and Rheological Characterization of Fungal Fermentation Broth 25
3.1 Identification of fungal morphology characterization technologies 26
3.1.1 Description of the technologies 26
3.1.2 Technologies' comparison 28
3.2 Comparison of LD and FBRM for the characterization of fungal morphology 30
3.2.1 Materials and methods 30
3.2.2 Results and discussion 32
3.2.3 Conclusions 38
3.3 Rheological characterization 39
Chapter 4. Platform Development for Enhanced Enzyme Expression 43
4.1 Introduction 43
4.2 Materials and Methods 44
4.2.1 Strain and propagation 44
4.2.2 Fermentation conditions and media 45
4.2.3 Sampling and analysis 45
4.2.4 Carbon balances and yield calculations 46
4.3 Results 46
4.3.1 Fermentation reproducibility 46
4.3.2 Influence of nitrogen source on cellulase production 47
4.3.3 Control and scalability 51
4.3.4 Statistics of the yield coefficients 53
4.4 Discussion 53
4.5 Conclusions 55
Chapter 5. Influence of process variables on morphology and rheology 57

5.1 Abstract 57
5.2 Introduction 57
5.3 Materials and Methods 60
5.3.1 Strain and propagation 60
5.3.2 Fermentation conditions and media 60
5.3.3 Morphology 61
5.3.4 Rheology characterization 61
5.3.5 Power input determinations 61
5.4 Results and discussion 62
5.4.1 Measurements of power draw for the 2L bioreactor 62
5.4.2 Fermentation Reproducibility 63
5.4.3 Respiration 65
5.4.4 Biomass and enzyme production 66
5.4.5 Morphology 68
5.4.6 Rheology 69
5.4.7 A simple rheological prediction model 72
5.5 Conclusions 73
Chapter 6. Influence of scale on the morphology of filamentous fungi 75
6.1 Introduction 75
6.2 Materials and Methods 76
6.2.1 Fed-batch cultivations 76
6.2.2 Power input measurements and calculations 77
6.2.3 Agitation conditions 77
6.2.4 Off-line measurements 78
6.3 Results 79
6.3.1 Agitation conditions 79
6.3.2 Biomass concentration and rheology 79
6.3.3 Morphology development 80
6.3.4 Fragmentation prediction across scales 84
6.3.5 Fermentations at bench scale 86
6.3.6 Validation of the fragmentation prediction model 87
6.4 Discussion 89
6.4.1 EDCF vs Energy Dissipation Rate 89
6.4.2 Shear rate in a turbulent stirred tank reactor 90
6.4.3 Higher viscosity at the production scale 91
6.4.4 Averages values vs maximum values 91
6.5 Conclusions 92
Chapter 7. Physiological responses of filamentous fungi in submerged fermentation 93
7.1 Introduction 93
7.2 Materials and methods 94
7.2.1 Fermentation samples 94
7.2.2 Sample characterization 94
7.3 Results 95
7.3.1 On-line biomass estimation dynamics 95

7.3.2 Dry cell weight and viscosity evolution 96
7.3.3 On-line measurements 97
7.3.4 Morphology development monitored as particle size distribution with laser diffraction 98
7.4 Discussion 100
7.5 Conclusions 103
Chapter 8. Dependence of hyphal tensile strength on environment and genetic variation 105
8.1 Abstract 105
8.2 Introduction 106
8.3 Materials and Methods 108
8.3.1 Strains and growth conditions 108
8.3.2 Modifications to the fragmentation test of fungal hyphae 109
8.4 Results and Discussion 109
8.4.1 Method Development 109
8.4.2 Finding a measuring window to estimate a constant specific fragmentation rate 111
8.4.3 Hyphal tensile strength in autophagy conditions 113
8.4.4 Studying the role of Anatg8 in hyphal strength 114
8.4.5 Normalization of the relative fragmentation rate for inter-laboratory comparison 116
8.5 Conclusions 116
Chapter 9. General conclusion and future perspectives 117
Appendix 121

Nomenclature

Roman letters

D	Impeller diameter	m
Fl	Flow number	-
k'	Geometric constant	-
k_{bran}	Branching frequency	tip/µm/h
k_{frag}	Relative fragmentation rate	$\mu m^{-1}\ s^{-1}$
k_s	Metzner and Otto proportionality constant	-
K	Power law consistency index	Pa s^n
K_{HB}	Herschel and Bulkley consistency index	Pa s^n
n	Power law flow behavior index	-
n_{HB}	Herschel and Bulkley flow behavior index	-
n_i	Count number in channel i	-
n_{PL}	Power law flow behavior index	-
N	Agitation speed	1/s
N_v	Number of vortices	-
P	Power	W
Po	Power number	-
s_{90}	90^{th} percentile of the PSD	µm
s_i	Size of channel i	µm
t	Time	s
t_c	Circulation time	s
T	Tank diameter	m
ν	Kinematic viscosity	m^2/s
v_i	Volume in channel i	μm^3
vp_i	Percentage distribution in channel i	%
v_T	Total volume occupied by counted particles	μm^3
V	Volume	m^3
W	Impellers blade width	m
X	Biomass concentration	g/kg
$Y_{S\,CO2}$	Yield coefficient CO_2 over substrate	C-mol/C-mol
Y_{SP}	Yield coefficient product over substrate	C-mol/C-mol
Y_{SX}	Yield coefficient biomass over substrate	C-mol/C-mol

Greek letters

$\dot{\gamma}$	Shear rate	1/s
ε	Energy dissipation rate	W/kg
η	Kolmogorov's microscale	m
μ_{app}	Apparent viscosity	Pa s
ρ	Density	Kg/m^3
τ_{HB}	Yields stress	Pa

Abbreviations

BCA	Bicinchoninic acid assay
CPR	Carbon Dioxide Production Rates
DCW	Dry Cell Weight
DOT	Dissolved Oxygen Tension
EC	Extracellular
EDCF	Energy Dissipation Circulation Function
FBRM	Focused Beam Reflectance Measurement
FPU	Filter Paper Units
IA	Image Analysis
LD	Laser Diffraction
LOFC	Large Object Flow Cytometry
MAG	Maltose Agar Glucose
NT	Normalized Fermentation Time
OTR	Oxygen Transfer Rate
OUR	Oxygen Uptake Rate
PLS	Partial Least Square
PSD	Particle Size Distribution
STR	Stirred Tank Reactor
VSC	Vesicle Supply Center

Chapter 1. Introduction

Fermentation processes for the production of industrial enzymes are under continuous optimization so that the enzymes can be produced at a lower cost. Some of these improvements have to do with process understanding and the comprehension of the interaction of all the variables involved in the fermentation processes. Filamentous fungi are widely used in these processes due to diverse advantages. Nevertheless, they also present major disadvantages, due to the unavoidable oxygen transfer limitations as a consequence of the high viscosity of the medium that they develop, which is believed to be related to the biomass concentration, growth rate and morphology (Metz et al. 1979; Olsvik & Kristiansen 1994). Furthermore, it is believed that the morphology of filamentous fungi is closely associated with productivity in fermentation processes. However, until now there is no clear evidence of this relation and there is an ongoing discussion around the topic. Therefore, fungal morphology is usually a bottleneck for productivity in industrial production, and will be extensively studied in this work. This will allow to determine whether a certain microorganism's phenotype has an influence on process performance, and how this performance can be influenced actively by manipulating different process variables or by genetic engineering, as a means of improving the design and operation of filamentous fungi fermentations.

1.1 Project motivation

For aerobic fermentation processes with filamentous fungi, one of the most critical indirect considerations during the scale up/scale down is viscosity. Viscosity will highly influence the oxygen transfer rate, substrate diffusivity, mixing efficiency, heat transfer and aeration (Metz et al. 1979; van Suijdam & Metz 1981). All these factors will affect the performance and efficiency of a bioreactor. This in turn will influence the operating conditions and is thus affecting growth, morphology and product formation (Oniscu et al. 2003). The difficulty of scaling up/scaling down aerobic bioprocesses is dictated by the continuously increasing complexity of the fermentation broth as the process proceeds,

e.g. the viscosity of the broth increases as a result of biomass growth and biosynthesized product accumulation (Cascaval et al. 2003). In addition, the rheological properties of these fluids are quite complex and differ significantly from the ideal behavior, i.e. most fermentation broths of filamentous fungi will behave as non-Newtonian fluids. This flow behavior is highly dependent on production scale, fermenter geometry and fermentation broth type. Cooke et al. (1998) exemplify that an apparent viscosity of 0.4 Pa s will give a Reynold's number in the turbulent flow regime in a 20 m^3 fermenter, while in a 30 L fermenter it will give a Reynold's number in the transitional regime. The change of the hydrodynamics will have a major impact on the mass transfer. Thus, mixing data on small scale are inappropriate to predict mixing at large scale because of the rheological properties of fermentation broths (Cooke et al. 1988). Therefore, it is very important to investigate the rheological behavior of fermentation broths as well as to quantify the rheological parameters (viscosity, shear stress, shear rate, power law index, consistency index, yield stress), since they are directly correlated to the fermentation stage. It is expected that the results of such an investigation would allow to have a better control of the process development (Oniscu et al. 2003)

In filamentous fermentation broths, the viscosity is mainly influenced by the concentration of biomass, its growth rate and morphology. Additional factors related to morphology are: the geometry of hyphae (i.e. length, diameter, branching frequency), hyphal flexibility and hyphal-hyphal interactions. These factors can all be affected by the operating strategy of the reactor. For example, agitation of the culture broth can have a variety of effects on filamentous microorganisms' morphology, which can include rupture of the cell wall, fragmentation, hypha damage, etc. (Smith et al. 1990). These phenomena might lead to decrease in process' yields. Sophisticated methods to measure the rheological properties of fermentation fluids have been developed. Nevertheless, the challenge relies in how to predict all these parameters and/or how to correlate them to other process variables as e.g. biomass concentration and morphology. In general, highly viscous broths are usually related to high biomass level; however, there is no simple correlation between the rheological properties of the broth and the biomass concentration, since this correlation will be affected by other variables and parameters as well (Olsvik & Kristiansen 1994). Thus, correlations describing viscosity as a function of biomass concentration solely are of limited value. A better understanding of the relation between morphology and rheology may be achieved by a combination of more extensive rheological and morphological models. This will precisely be investigated in the proposed project. It is furthermore important to carry out studies on the non-homogeneous fermentation fluids, and to develop correlations based on these studies. Better models might combine population data from image analysis, including data on compactness, maximum dimension, etc. with the multivariate approach. Furthermore, due to the nonlinearity of the rheological phenomena, nonlinear methods would potentially be able to cover a wider range of morphologies and scales.

At the start of the project, there are a lot of unanswered questions such as: Which is the best way to model rheology? How many different parameters/variables apart from biomass concentration need to be used in order to model viscosity? Is image analysis, size distribution, polymer solution models, or on-line viscosity the best way to study morphology and rheology? As a starting point, a limited number of model strains will be selected, and their morphology will be characterized (e.g. using image analysis or other methods) in lab scale fermentations. Rheological properties of the resulting fermentation broth will also be measured, and it will be evaluated which are the best data/methods to link morphological characterization to rheological properties. This data set will then be extended with pilot scale data, to further extend the validity of the obtained correlations. In a second phase of the project, it will be investigated whether morphology can be influenced actively, for example by modifying the strains genetically or by changing the operating mode of the fermenter, in order to improve mass transfer and thus the process' performance.

1.2 Thesis outline

The contents of this thesis have been organized in four sections and each section consists of different chapters. It is the intention that each chapter can be read individually. Therefore, the introduction to each chapter might sound redundant at times. But in general, the thesis has been organized as follows:

Introduction (Chapter 1 and Chapter 2)
This section contains the project motivation. Furthermore, the literature from the past years with respect to the morphology of filamentous fungi has been reviewed. Chapter 2 presents a summary of the most important findings. This literature review was published in the review series "Advances in Biochemical Engineering/Biotechnology" in the book "Filaments in Bioprocesses" edited by Rainer Krull and Thomas Bley.

Experimental tool box (Chapter 3 and Chapter 4)
Before embarking on a study for aiming at linking the morphology of filamentous fungi to the different variables in industrial enzyme production, it is necessary to define and establish the experimental tool box. A crucial step is to determine how the fungal morphology will be quantified. Chapter 3 discusses the most interesting technologies for morphology characterization. The technologies are described and benchmarked. The most novel and advantageous technology, focused beam reflectance measurement (FBRM), is compared to an established method, laser diffraction. The FBRM was found not to be suitable for fungal morphological characterization for highly concentrated samples, but some recommendations upon further use are provided.

Also, some different considerations when making rheological characterizations of *T. reesei* fermentation broths are discussed in Chapter 3. The ultimate contribution for the

rheological characterization section is the definition of which rheological model should be used, and the value at which one of the parameters for the model should be fixed.

Another aspect of the experimental tool box involves the specifications of the parameters and process conditions for the fermentations conducted in this work, e.g. strain, media, temperature, pH, etc. Chapter 4 describes how the reference process is established and how all the conditions were selected. The platform developed in this project can be used as a reference process for a highly productive system for further studies, since the productivities obtained here are larger than the highest values found in literature.

Influence of process variables on morphology (Chapter 5 and Chapter 6)
Deeper understanding of how fungal morphology and enzyme production are connected and how they are influenced by the process conditions will allow targeted process improvements in industrial enzyme production. Based on the investigations reported up to now it seems as it has not been possible to manipulate one process variable while keeping the remaining process variables constant, thereby complicating the interpretation of experimental data. The motivation for Chapter 5 arises from the lack of attention that has been paid until now to this issue. Thus, in this chapter, the direct influence of agitation intensity on different variables involved in submerged fermentation including morphology, rheology and protein production capability is studied. Furthermore, a novel method of characterization of fungal broths with respect to rheology is introduced and validated. The method is based on morphological measurements with laser diffraction and biomass concentration. This very simple and straightforward method offers a very interesting new possibility to be used as a routine measurement in strain selection stages in order to get quantitative descriptions of strain morphology, since the time required to get the information is very short and the sample demands are low.

After the influence of agitation intensity on different variables involved in submerged fermentations has been studied, the next step is to determine if it is possible to predict this influence across scales and to see if the behavior is consistent. This activity involves collecting data from a production batch from Novozymes A/S and measuring the variables of interest in this PhD project: morphology and rheology. The process is scaled down to pilot scale and bench scale. The most important variables to be considered when scaling up/scaling down a fungal fermentation process are discussed. Furthermore, the applicability of a well-established state of the art function to predict fragmentation across scales, the energy dissipation circulation function (EDCF), was tested. It was found that the specific power input is a more suitable parameter to predict fragmentation across scales when actual fermentations broths are considered. These findings are presented in Chapter 6.

Physiology and genetics of filamentous fungi (Chapter 7 and Chapter 8)
This section deals with two important aspects of filamentous fungi, physiology and genetics. In Chapter 7, the physiology under starvation conditions is discussed. It is

shown that the morphology characterization technology used in this PhD project, cannot just give information about rheology and particle size distribution, but is also suitable for physiological studies.

In addition, a fast and easy method to characterize the relative hyphal tensile strength, a very interesting phenotype in bioprocesses, is introduced for the first time in Chapter 8. Furthermore, the use of this method for strain optimization and process development is investigated.

The general conclusions and future perspectives are presented in Chapter 9

Chapter 2. Literature Review: Fungal Morphology in Industrial Enzyme Production

The contents of this chapter are based on an article published in the book review series Advances in Biochemical Engineering/Biotechnology. The review article was written mainly by the two first authors, but this chapter presents only the contributions by D. Quintanilla.

"Fungal morphology in industrial enzyme production – Modelling and monitoring"

Quintanilla, D., Hagemann, T., Hansen, K., Gernaey, K.V.

Advances in Biochemical Engineering Biotechnology 149:29-54 (2015)

2.1 Introduction

Filamentous fungi are widely used in the biotechnology industry for the production of different compounds like organic acids, industrial enzymes, antibiotics, etc.; for an extensive list see (Papagianni 2004). The widespread use of filamentous fungi as production host is due to three main advantages which the fungi possess: 1) Filamentous fungi have an exceptional ability of secreting large amounts of proteins (Peberdy 1994); 2) They possess a special posttranscriptional modification machinery which allows for glycosylation, correct protein folding, etc. (Punt et al. 2002); and, 3) A large number of species are approved by the regulatory authorities and generally recognized as safe

(GRAS). Nevertheless, operating a process with filamentous fungi also has a few major disadvantages due to the unavoidable oxygen transfer and mixing limitations that occur as a consequence of the high viscosity of the medium, which is due to the combination of the high biomass concentration and the fungal morphology (van Suijdam & Metz 1981).

Filamentous microorganisms manifest two main types of morphology in submerged fermentations, usually classified as dispersed and pelletized morphology. The first category is characterized by biomass that grows in the form of freely dispersed hyphae or mycelial clumps, see Figure 2.1. In the second category, pellets are highly entangled and dense spherical agglomerates of hyphae which can have diameters varying between a couple of micrometers up to several millimeters (Cox et al. 1998). Depending on the desired product, the optimal morphology for a given bioprocess varies and cannot be generalized; in some cases both types of morphology are even combined in one process (Barry & Williams 2011). The pelleted morphology type is often preferred because of the resulting Newtonian fluid behavior of the medium which allows for better mixing and simplifies downstream processing in terms of pumping and separation of the biomass. However, the pelleted morphology results in nutrient concentration gradients within the pellet (Hille et al. 2005). This situation is not observed in freely dispersed mycelia allowing for enhanced growth and production (provided sufficient bulk mixing capacity is available), which has been attributed to the fact that the morphology at the microscopic level has an influence on the production kinetics, e.g. on the secretion of enzymes. The latter was reported by Spohr et al. (Spohr et al. 1997) who observed an increase in protein secretion from a more densely branched mutant of *Aspergillus oryzae* in comparison with the wild type. However, on the macroscopic level this type of morphology greatly affects the rheology of the fermentation broth, and therefore the transport processes in the bioreactor, and will thus increase the required power input for broth mixing. So, the morphology of filamentous fungi is double edged, as the productivity as well as the fermentation conditions can be affected by the outer appearance of the fungus. The challenge is to separate these effects to be able to connect productivity gains to the correct phenomenon causing it. If this challenge could be overcome, the process knowledge of the fermentation scientist would be enriched tremendously, and would undoubtedly result in productivity gains, (Timo Hegemann, personal communication).

The aim of this chapter is to give a review of the research work that has been done in order to elucidate the relation between morphology and productivity and all the related variables in filamentous fungi fermentations, specifically for the production of industrial enzymes. In order to do this, an introduction to the main industrial strains is given, followed by a brief review of the morphology and physiology of filamentous fungi. A short description of the complex interaction of the different variables involved in submerged fermentations is presented. In the final section, the chapter links the capacity to characterize and model morphology to potential applications for influencing or controlling morphology as a tool for future process optimization.

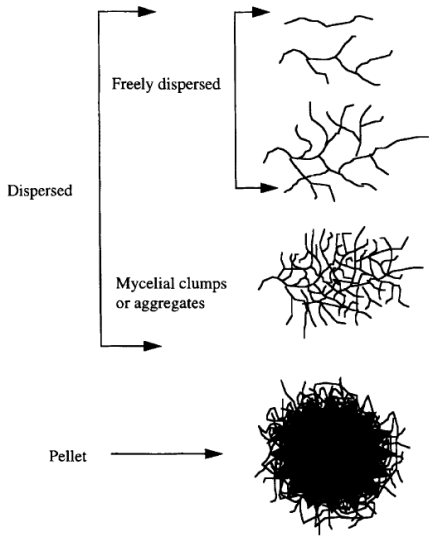

Figure 2.1. Types of morphology typically found in submerged cultures of filamentous fungi (Cox et al. 1998).

2.2 Filamentous fungi for enzyme production

2.2.1 Important strains and products

Due to their exceptionally high capacity to express and secrete proteins, filamentous fungi have become indispensable for the production of enzymes of fungal and non-fungal origin. Currently, native or recombinant industrial enzymes are mainly produced by *A. niger*, *A. oryzae* and *T. reesei* (Meyer 2008; Nevalainen et al. 2005).The *Aspergillus* genus is one of the favorite expression systems in the production of industrial enzymes, and in particular the species *A. niger* and *A. oryzae* have been frequently used, due to their high titers of native hydrolytic enzymes, especially amylases and proteases (Lubertozzi & Keasling 2009). Glucoamylase (AMG) is a homologous protein of *A. niger* used for the conversion of starch to sweeteners and in the production of first generation ethanol (Cherry et al. 2009). Amylases are also added to detergents to assist in stain removal (Cherry & Fidantsef 2003). Other enzymes produced by these microorganisms include glucose oxidases, catalases, pectinases, lipases, phytases and xylanases, which are usually used in the food, detergent, textile, pulp and paper industry (Fleissner & Dersch 2010).

T. reesei is mainly known for producing cellulases, which are enzymes capable of degrading cellulose into simple sugars. They are widely used in the pulp and paper industry for the reuse of waste paper (Lee & Kpp 2001). In addition, cellulases are also used within the textile industry for cotton softening and denim finishing. Another important application of these enzymes is within detergents, where they are used for color care, cleaning and anti-redeposition in washing powders (Cherry & Fidantsef 2003).

Also, an enormous interest in these enzymes has arisen in the biofuel industry, as they are used in the saccharification of lignocellulosic materials which will be converted to bioethanol later (Lynd et al. 2005; Horn et al. 2012)

2.2.2 Introduction to Morphology of Filamentous Fungi

Filamentous fungi are complex microorganisms constituted by complicated hyphae. A hypha is formed by one or more cells surrounded by a tubular cell wall. A hyphal element is formed by a main hypha that emerges from one spore; this main hypha is typically branched, and these branches have their own sub-branches and so on (Kossen 2000), as displayed in Table 2.1. *Ascomycota*, the group of organisms in which the fungi covered in this review are included, have hyphae that are divided into compartments by internal cross-walls called septa. Each septum possesses a pore large enough to allow cell organelles to flow between compartments. The collective term for the mass of hyphae is mycelium, Figure 2.1. Furthermore, a hyphal element can entangle with another hyphal element and form more complex structures. The morphology of filamentous fungi is usually characterized by four variables: the length of the main hyphae (L_e), the total length of all the hyphae (L_t), the number of tips (n) and the length of a hyphal growth unit (L_{hgu}) (Kossen 2000). The reader is referred to Table 2.1 for the definitions of additional morphological terms. The hyphal cell wall is formed by polymeric microfibrils of various biochemical composition arranged in a series of layers (Berry 1988). The microfibrils forming the hyphal wall usually consist of chitin, a polymer of *N*-acetyl-glucosamine (Berry 1988).

Table 2.1 Common morphological terms (Thomas 1992).

Area or projected area – Area of the projection of a three-dimensional object into a two-dimensional image.
Main hyphal length – Length of the main hypha in a mycelium, which might be taken as the longest connected path though a mycelial tree.
Branch length- Length of an individual hyphal branch.
Total hyphal length- Sum of main hyphal length and all branch lengths in a mycelial tree.
Branching frequency- Number of branches (and sub-branches) in a mycelial tree.
Number of tips- Number of branches plus two (for the main hypha. Some tips might be extending (growing); others not.
Hyphal growth unit- Total hyphal length divided by the number of tips; the mean length of hypha with each tip (ideally each growing tip).

One of the most important and interesting things to recognize in filamentous fungi is their apical extension just at the hyphae tips. This theory was established in the 19th century, when Reinhardt (Reinhardt 1892) proposed that fungal growth takes place by enlargement of the hyphae only at the apices. The elongation occurs by means of wall expanding according to a gradient, maximally at the extreme tip, and the materials necessary for cell wall expanding are provided by the cytoplasm (Reinhardt 1892). Several growth models aiming to describe the exact mechanisms of how this process takes place have been proposed, and the most important ones are the steady state model (Wessels 1993)(Wessels 1990) and the hyphoid model (Harold 1997). Some other models have also been developed but these should rather be considered as combinations of the

two former models (Bartnicki-García 1999) (Moore 1998). This is probably how the process is indeed carried out, since the main two theories are not self-exclusive given that they describe different features of the wall building process during tip growth (Bartnicki-García 1999).

In general, the theories describe hyphal growth as a consequence of a combination of wall biogenesis and turgor pressure. Wall biogenesis is ultimately an activity of the cytoplasm and that is where the building materials and necessary enzymes are synthetized; they are then later on transported in vesicles to the hyphal tip. These vesicles are accumulated in the apical dome forming a moving vesicle supply center (VSC). The VSC is an organelle from which vesicles move radially to the hyphal surface in all directions at random, and the forward migration of this pseudo-organelle is what generates the hyphoid shape (Moore 1998). Then, in the hyphal tip there are two main processes taking place, softening and hardening of the apical cell wall caused by the enzymes carried out in the vesicles. This process makes the hyphae tip more plastic and that is precisely where protein secretion takes place, carried out by a bulk flow from the cytoplasmic side to the wall. Wösten et al. showed with immunological techniques that secretion of glucoamylase in *Aspergillus niger* was carried out at the hyphal tips (Wösten et al. 1991). It is important to have this fact in mind, since it gave direction to the different research projects that were done in the area, as further described below.

2.2.3 Complexity of the subject

In terms of mass transfer and rheology, filamentous fungi are very challenging hosts for the production of proteins in submerged fermentation, since their morphology is connected to these two variables, both at the microscopic and macroscopic level. Therefore, studying the relationship between fungal morphology and productivity in submerged fermentations is not an easy task due to the abundance of interrelated factors, which affect directly and indirectly the microorganism's morphology and product formation.

The particular morphology of a filamentous fungus leads to entanglements of the hyphae at high biomass concentrations (20-50 g/L); this phenomenon causes very high viscosities with non-Newtonian fluid behavior (Metz et al. 1979). Considering a typical stirred tank reactor, it is well-known that the shear rate is at its maximum at the agitator tip, and it decreases when approaching the vessel walls. Therefore the viscosity will be low close to the impeller, and will increase towards the vessels walls. This results in a lot of problems with respect to mass transfer, moment transfer and heat transfer (Metz et al. 1979). Metz et al. describe the viscosity as the center of the multi-directional and circular interrelation of all the factors, see Figure 2.2; the broth viscosity has a major effect on the transport phenomena in the bioreactor which then will affect the process conditions (Metz et al. 1979). Metz et al. considered the process conditions at the top of the complex interactions. These process conditions include the medium composition, mode of operation, temperature, pH, etc. The process conditions will directly affect the

morphology, product formation and growth; all these variables are correlated with each other (Metz et al. 1979).

In addition to all the above-mentioned factors, there is also the fungal physiology and metabolism, which will affect morphology. For example, there is a continuous discussion with respect to shear damage of filamentous fungi; i.e. damage and fragmentation of filaments can be caused by shear forces from the impeller and by aeration. However, the aging factor of the microorganisms also plays a role making the cell walls weaker when cells grow older, and thus more susceptible to fragmentation (van Suijdam & Metz 1981). Autolysis is another phenomenon observed in filamentous fungi which in addition contributes to hyphal fragmentation (White et al. 2002). Also strain optimization plays a role, especially classical mutagenesis, since selected strains might increasingly form more single cell like structures. This results in lower viscosities, and thus better oxygen transfer, rather than higher titers (Peter et al. 2004).

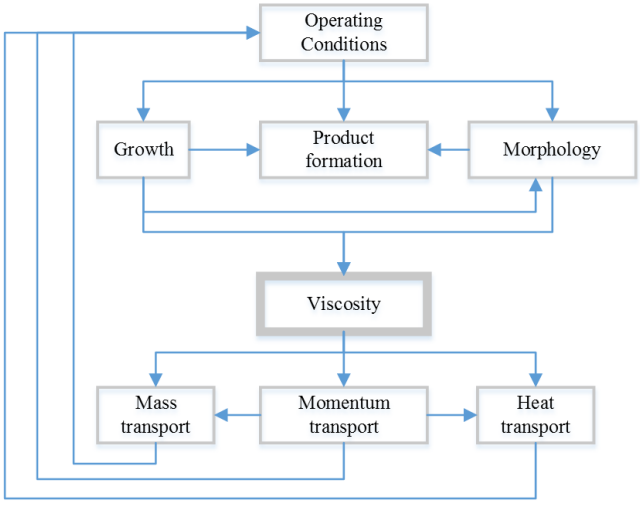

Figure 2.2. Representation of all the interrelated variables in submerged fermentation. Adapted from (Metz et al. 1979).

2.3 Modelling the Morphology

In an effort to achieve process improvements within the biotechnology industry, considerable focus has been put in the developing and maturing of engineering tools which facilitate process optimization. One of these tools is mathematical modelling, including both empirical and first-principles models. For a review of more engineering tools see (Formenti et al. 2014). Different research projects have been carried out with the objective to model and understand the different phenomena taking place in submerged fermentation, and to develop an improved understanding of the interactions between the variables illustrated in Figure 2.2. These attempts have mainly been focused on modeling

micromorphology, hyphal fragmentation and rheology, and on developing an understanding on how this affects productivity.

2.3.1 Micromorphology and productivity

Since the early 90's, it has been demonstrated that protein secretion in *A. niger* was carried out mainly in the tips of fungal hyphae (Wösten et al. 1991). Therefore, several studies have been conducted aiming at correlating the number of hyphal tips with enzyme production. As an example, *A. oryzae* producing α-amylase was further investigated by comparing three different strains in batch cultivations (Spohr et al. 1997). The strains were: a wild-type (A1560), a transformant with extra copies of the coding gene and a morphological mutant (made from the transformant). By comparing the α-amylase concentration at the end of the batch and the specific branching frequency of the two recombinant strains, it was concluded that a more densely branched strain is superior in protein production (Table 2.2). This higher productivity might be attributed to the fact that the limiting step in high yielding protein strains is the secretion process (Spohr et al. 1997).

Bocking et al. (Booking et al. 1999) investigated the topic in the same strain (A1560). In addition, they studied a transformant strain able to produce glucoamylase along with α-amylase (AMG#13). Nine morphological mutants were generated from these two strains: 4 from A1560 and 5 from AMG#13. The mutants were screened such as to keep the same maximum specific growth rate and a lower hyphal growth unit length (more branched strains). All the strains were studied in batch, continuous and fed-batch cultivations. No clear correlation between branch frequency and ability of secreting protein was observed for the highly branched mutants in the fed-batch and continuous fermentations. They however, found a correlation between higher branch frequency and viscosity reduction. This could lead to the conclusion that the observed productivity increase by Spohr et al. (Spohr et al. 1997) was achieved due to a better OTR rather than a higher productivity. However, one should be aware that the comparisons are done in different operating modes (batch vs fed-batch); thus different physiological state due to different grow rates might have an effect on the rate of fragmentation resulting in systems with different viscosity. Though, in the batch experiments for AMG#13 and its highly branched mutant, the latter did have an increase in glucoamylase compared with AMG#13. This might suggest that under maximum growth rate conditions there is a correlation between branch frequency and secretion, as suggested by Spohr et al. (Spohr et al. 1997).

Table 2.2. Final amylase concentration and specific branching frequency of the three strains of *Aspergillus oryzae*. Adapted from (Spohr et al. 1997).

Strain	**Final concentration α-amylase (FAU/ml)**	**Branching frequency k_{bran} (tip/µm/h)**
Wild-type	0.63	0.0023
Transformant	2.22	0.0010
Morphological mutant	3.09	0.0021

For the first time, Haack et al. reported the swelling of the hyphal tips as a consequence of high productivity in a recombinant strain of *A. oryzae* producing lipase (Haack et al. 2006). It was suggested that tip swelling and productivity are linked, since the hyphae tips return to normal shape after the productivity stops due to oxygen limitations. It was indicated that these findings could help to identify the fraction of productive cells in industrial fermentation, since it is known that production heterogeneities occur in full scale due to poor mixing (Formenti et al. 2014).

Most of these models are purely empirical without any structured background, and have been mainly developed using image analysis. Nonetheless, they have been used as practical tools for comparison. Agger et al. developed a morphologically structured model able to describe growth and product formation in batch, continuous and fed-batch cultivations for *A. oryzae* (A1560) (Agger et al. 1998). By dividing the fungal hyphae into three different regions - extension zone representing the tips of the hyphae, active zone which is responsible for growth and product formation and an inactive hyphal region, Figure 2.3 - a model able to predict product formation as a function of morphology was developed. Different to the previous models, it was verified by image analysis combined with fluorescence microscopy. The model performed well in batch and continuous cultivation. However, there seemed to be an under-prediction of product formation for fed-batch fermentation. This difference was attributed to rheological changes or hyphae fragmentation not accounted for in the model.

As seen in Figure 2.2, due to the complex interactions between the variables in a fermentation process it is also possible to affect morphology by changing the process conditions (media composition). Ahamed and Vermette (2009) conducted a study where they indirectly affected morphology by varying the carbon source in the batch phase of a fed-batch process. The study was performed in *T. reesei* in the strain RUT-C30 producing cellulases. They observed a more branched morphology in the medium which also presented the highest enzyme titers. A non-linear correlation for the volumetric enzyme productivity was developed as a function of the average projected area of the total mycelia (entangled mycelia plus branched mycelia) and the number of hyphae tips. This study confirms the relation between enzyme productivity and number of tips.

2.3.2 Shear stress and morphology

One of the problems with filamentous microorganisms relies in the oxygen mass transfer limitations in the culture broth due to the high viscosities and the non-Newtonian behavior. An obvious strategy to overcome this problem is to increase agitation power. However, the question of shear damage due to fragmentation or morphological changes

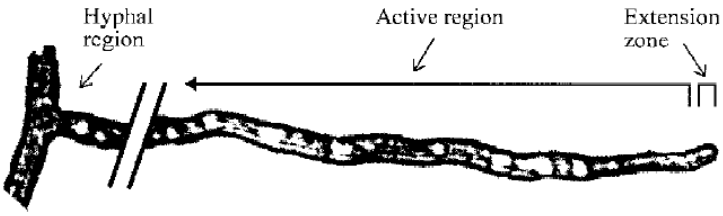

Figure 2.3. Illustration of the structuring of the hyphal elements in the model presented by (Agger et al. 1998).

arises. Early works indicated that there is shear damage to the cells caused by the impeller which usually leads to reduced productivity. Nevertheless, these studies were conducted in *Penicillium chrysogenum* for penicillin production (Makagiansar et al. 1993; Smith et al. 1990)order to understand the relation of shear stress caused by the impeller in morphology for filamentous fungi producing industrial enzymes will be summarized, and only for the cases where dispersed mycelium is observed (i.e. not pellets). The other focus will be the work of Jüsten et al. who developed a function capable of correlating mycelial fragmentation and power inputs at different scales and agitator types, the so called energy dissipation circulation function (EDCF) (Jüsten et al. 1996). The EDCF is defined as the ratio of energy dissipation in the dispersion zone to the liquid circulation time. This model considers the specific energy dissipation and the amount of time that the cells are subject to the shear caused by the impeller (circulation frequency). The theory is an extension of the work done by Smith et al. which managed to account for the circulation frequency (Smith et al. 1990). However, Jüsten et al. accounted for different impellers types. Even though the function was developed for *P. chrysogenum*, its applicability was later tested in *A. oryzae* managing to successfully correlate fragmentation (Amanullah et al. 2000); therefore, in this review the EDCF is considered as the standard tool for comparison of the different works.

Amanullah et al. studied the effect of agitation on mycelial morphology and enzyme productivity in continuous cultures of a recombinant strain of *A. oryzae* producing α-amylase and amyloglucosidase. They found that agitation intensity has an effect on morphology. When the agitation speed was reduced by half, the mean projected area increased almost 3-fold. Productivity, however, was not affected (Amanullah et al. 1999). A later study of the same group carried out with the same strain in fed-batch fermentations confirmed that mycelial morphology (measured as a mean projected area) is dependent on agitation intensity but that there is no correlation with enzyme production assuming a non O_2 limited process for the fed-batch phase. However, in the batch phase there was a direct correlation with agitation intensity and productivity, which led to higher biomass concentration and growth rates at higher agitation speeds (Amanullah et al. 2002). An important conclusion of these two studies was that given a specific growth rate, it is possible to correlate EDCF with morphology measured as the mean projected area (Amanullah et al. 2002).

Fragmentation caused by different specific power inputs measured as EDCF was investigated by Li et al. for full scale fed-batch fermentations (Li et al. 2000). The shear forces caused by the impeller on *A. oryzae* resulted in mycelial fragmentation; however, this fragmentation was not correlated to the specific power input since a similar morphology was observed at the two levels of EDCF. Hence, fungal morphology does not seem to be dependent on mixing intensity at production scale. Effects of changes on impeller power input on productivity were not studied. In a later study this correlation was investigated. Yet again, two specific power inputs measured as EDCF were tested, neither the morphology, productivity nor rheology differ at these two levels of EDCF under non-oxygen limited conditions (Li et al. 2002b).

Albæk et al. developed a correlation able to predict viscosity based on the mentioned EDCF and biomass measurements in fed-batch fermentation with *A. oryzae* (Albaek et al. 2011). The correlation does not take into consideration morphological data; however, the accuracy of the general model prediction demonstrates the ability of EDCF to correlate morphological data as a function of viscosity. They also observed a positive correlation with increasing agitation speed and product formation. This might be correlated to a better OTR, indicating that morphology actually does not necessarily play the major role in productivity (Albaek et al. 2011).

2.3.3 Morphology and rheology

The study of the rheology of culture broths has a crucial importance in the design of fermentation processes; viscosity will affect the transport phenomena taking place in a bioreactor. Fluid viscosity appears in several correlations involved in mixing and mass transfer, e.g. the Reynolds number and correlations for the volumetric mass transfer coefficient. Also, the yield stress appears in relationships used to estimate cavern sizes (Petersen et al. 2008). Therefore, it is important to study the rheology of fermentation broths, and if possible to predict it. The traditional approach for modelling the rheology of filamentous fermentations broths is based on attempts to correlate the parameters for different viscosity models (e.g. power law model) to the biomass concentration (Allen & Robinson 1990) (for a review of rheology see (Metz et al. 1979; Wucherpfennig et al. 2010)). However, these correlations are of a limited value (Olsvik & Kristiansen 1994). Viscosity is a property that is not only dependent on biomass concentration, but is affected by the structure and extent of physical interlacing of hyphal networks (Deindoerfer & Gaden 1955). Thus, several other studies have focus on correlating viscosity not only to the biomass concentration, but also to the different morphological parameters, i.e. projected area, hyphal growth unit, etc., typically characterized by image analysis. Other authors have characterized the morphology by other methods in order to correlate it to rheology. These attempts are further described in below.

The direct relation between the consistency index parameter of the power law model and different morphological parameters was studied for continuous cultivations of *A. niger* (Olsvik et al. 1993). The dissolved oxygen and growth rate were varied at two different

biomass concentrations. It was found that at constant biomass concentration the consistency index could be linearly correlated to the roughness. By including a biomass term in a linear model, a good correlation was obtained. In this work, the correlation was not further tested for different levels of biomass concentration or for batch or fed-batch fermentations. It has to be kept in mind that this is one of the first attempts to quantitatively model the rheology of filamentous fungi based on morphology parameters. As a continuation of this work, Riley et al. developed a model to predict the consistency index based on biomass concentration and the mean mycelial maximum dimension for *P. chrysogenum*. The model was able to predict the parameter with an average root-mean-squared deviation below 30%, which despite all the sources of errors is considered good (Riley et al. 2000). This microorganism is not included within the strains considered in this chapter. However, as an extension of this work, Riley and Thomas checked the relevance of the correlation to other fungi (Riley & Thomas 2010). They reformulated the model at a different magnification for *P. chrysogenum* and tested its applicability to predict the values of the consistency index for fermentation broth of *A. niger* and *A. oryzae*. The biomass concentration and the mean mycelial maximum dimension are also used in this model as the morphological parameters. The correlation performed well for fermentation broths of *A. oryzae*, but failed to describe the consistency index for *A. niger*. No simple model was found for the flow behavior index. In fact, it was considered as a constant value, which is not always the case. Similarly, Malouf aimed at correlating the rheology properties of *T. reesei* fermentation broths to morphological parameters (Malouf 2008). The Herschel-Bulkley consistency index was successfully correlated to the mean roundness by two separate correlations for the batch and fed-batch phases.

Wucherpfennig et al. studied the rheology of culture broths from *A. niger* in shake flask fermentations (Wucherpfennig et al. 2013). Image analysis was used for morphological characterization, which was described by conventional and fractal morphological parameters. Two different fractal parameters where good at predicting rheology properties; nevertheless they were not superior to the parameters developed using conventional particle shape analysis (e.g. Morphology number (Wucherpfennig et al. 2011)).

Other authors have used laser diffraction and multivariate data analysis as a tool to model the rheology of fermentation broths. Petersen et al. correlated the rheological properties of commercially relevant *A. oryzae* fermentations with respect to particle size distribution data (Petersen et al. 2008). The study was conducted in fed-batch fermentations where different feed strategies were applied, similar to the work of Bhargava et al. (2003a) . A partial least squares regression model was able to predict viscosity by using particle size distribution, biomass concentration and process information. In terms of practical applicability, this model is superior to the models that have been developed using image analysis due to the simplicity of the measurements; however a limitation is that the model was not able to predict the rheological properties of fermentation broths of different strains and/or scales.

Another aspect which is important to consider when dealing with rheology of filamentous fungi, is how to evaluate the shear rate in the tank. Until now, it has not been possible to estimate a reliable shear rate in the fermentation tank itself. As mentioned before, in an STR it is well-known that the shear rate is at its maximum at the agitator tip and decreases towards the vessel walls. Calculating shear rate can therefore be expressed as the maximum or the average shear rate. Hitherto, it is not clear which shear rate is governing the mass transfer processes, and the way of calculating this shear rate is limited to the Metzner and Otto correlation (Metzner & Otto 1957). According to Stocks (2013), it should not be forgotten that this empirical correlation was developed for Reynolds numbers in the laminar and transitional regime and not for turbulent conditions where it is also frequently used in practice. Thus its applicability is limited to laboratory and pilot-scale fermenters, even though it has been typically employed for calculating shear rates in full-scale fermenters also (Stocks 2013). A special challenge emerges when a reliable shear rate to evaluate the viscosity across different scales has to be estimated. This might be the reason why the developed models were not able to make predictions that apply across scales; therefore, the applicability of other correlations should be explored (Sánchez Pérez et al. 2006). Adding on to that challenge is the use of different instrument to measure rheology (Olsvik & Kristiansen 1994). Developing models that could predict performance of fermentations with filamentous fungi across scales with a (relatively) high accuracy is therefore still considered to be one of the major scientific challenges in this field.

2.3.4 Process conditions and morphology

Bhargava et al. (2003a) performed a study where they investigated the effect of different feeding strategies on morphology, protein expression and viscosity during a fed-batch fermentation. The work was done with *A. oryzae* (A1560). Tests with varying the feeding profile were carried out, keeping the same total amount of glucose, but fed in cycles (pulsed feeding). These experiments were compared with a continuously fed fermentation. The biomass, oxygen uptake rate (OUR) and total base added for pH control showed no significant difference indicating that pulsed feeding during fed-batch operation has no apparent effect on cellular metabolic activity. Neither was there a significant difference for the different cultivations in the measured extracellular protein content. Nevertheless, a considerable effect on fungal morphology (measured as average projected area) from the start of the fed-batch phase was observed. The pulsed feeding resulted in smaller hyphal elements in comparison to the elements resulting from continuous feeding. The smaller elements lead to a significant decrease in viscosity. As a consequence, the effect of the cycle time on morphology, rheology and productivity on the same strain was tested in a later work (Bhargava et al. 2005). As before, no effect on biomass was observed, while the mean projected area and the viscosity decreased with the increase in cycle time. Shorter cycles resulted in constant productivity and oxygen uptake rate while longer cycles caused a decrease in productivity at a higher OUR – it appeared that the fungus was forced to form conidia due to starvation. This yet again shows the double sided effect of morphology, viscosity and product formation.

Other authors have also studied the effect of agitation intensity on other process variables, rather than just in morphology. Marten et al. (1996) studied the relation between rheology, mass transfer and mixing for *T. reesei* in batch fermentations. They concluded that the Casson model and the Herschel-Buckley model are better in describing the rheological behavior of *T. reesei* broths in comparison with the power law model. However, a practical correlation was not obtained with respect to the effect of agitation intensity on rheology and biomass concentration.

In an attempt to understand the effect of shear stress on morphology and rheology also in *T. reesei*, Patel et al. studied the effect of agitation intensity in fed-batch fermentations (Patel et al. 2009). With respect to shear stress and productivity, no clear correlation was observed. With respect to morphology, in the batch phase of the fermentation, no effect on agitation intensity was observed either. However, for carbon source limiting growth, there seemed to be an effect of agitation intensity on morphology, since a higher degree of fragmentation was observed as the fed-batch phase proceeded. It is not clear whether this degree of fragmentation is caused by the agitation or by self-fragmentation of the microorganisms. This however, resulted in a lower viscosity towards the end of the fermentations. A higher apparent viscosity was observed in the experiment with the highest agitation speed, which might be attributed to the higher biomass concentration. The apparent viscosity of all the experiments was evaluated at a constant shear rate and not at the shear rate in the tank, making the comparison difficult.

2.4 Conclusion

The key issue relies on how to incorporate all the work that has been done for the past years in order to optimize the filamentous fermentation process. As illustrated in Figure 2.2, there are many variables which will influence the performance of fermentation processes, and in order to study all of them, an extensive (up to now impossible) design of experiments needs to be performed. The complex inter-correlation renders it impossible to affect a variable while keeping the rest constant, as seen in Table 2.3 and Table 2.4. Thus, until now the best way of dealing with this appears to be data reconciliation for the work that has been done, which is not an easy task, due to the different set-ups used. For example, Li et al. (2000, 2002a) found no effect on the different variables from changes in specific power input; these results at full scale production differ significantly from the findings at bench scale (Amanullah et al. 1999; Amanullah et al. 2002), which again makes it very difficult to draw a practical conclusion about the relation and interaction of all the variables involved in fermentations processes with filamentous fungi.

In addition to this, one of the biggest challenges with respect to the study of filamentous fungi in the production of enzymes is the lack of relevant industrial data. The difference between data generated by academia and the industry is enormous. E.g. processes studied in this review, and typically reported as a result of a study that has taken place at a

university department, deal with titers of barely a couple of grams per liter of extracellular protein. In industry there are reports of titers up to hundreds of grams per liter (Cherry & Fidantsef 2003). The question remains on whether it is possible for industry to apply the results of the model studies developed by academia. It is to expect that the behavior of the industrial microorganisms would be completely different due to the stress on the host organism that is caused by such high expression levels. Therefore, if the aim is to produce results with both academic value and industrial relevance, then it is important to have a proper collaboration between industry and academia in order to overcome this issue. So, there is a need for the definition of one or more well-defined case studies that should be available publicly, with limited but sufficient industrial value to be of practical use. The case studies should allow academia to work in concentration ranges which are relevant for industry. The same is valid for the scale: Bench reactors are just much smaller and not all effects, especially regarding mixing can be studied properly in regards to industrial challenges. However, this is not an easy task, since very different – often competing – interests might be involved: indeed, a problem is that a case study with practical value does not automatically have sufficient academic value, and the other way around.

Table 2.3. Effects of morphology alteration on productivity, biomass and rheology

Authors	Microorganism	Operation Mode	Growth rate (1/h)	Affected morphology parameter	Effect on productivity	Effect on growth rate/biomass	Effect on rheology	Notes
Spohr et al. 1997	*Aspergillus oryzae* (A1560)	Batch	0.18-0.27	Morphology-Branching frequency	Yes. Higher productivity in the more branched strain	Yes. Lower growth rate for the more branched strain	N/A	Comparison at an specific biomass concentration
Bocking et al. 1999	*Aspergillus oryzae* (A1560)	Batch	0.28	Morphology-Branching frequency	No	No	N/A	
	Aspergillus oryzae (AMG#13)	Batch	0.30	Morphology-Branching frequency	Yes. Higher productivity for the more branched mutants	No	Yes. Lower viscosity for the highly branched mutants	
	Aspergillus oryzae (AMG#13)	Fed-batch	-	Morphology-Branching frequency	Yes. Lower productivity for the more branched mutants	Yes. Lower biomass for the more branched mutant	N/A	Constant feed rate
	Aspergillus oryzae (AMG#13)	Fed-batch	-	Morphology-Branching frequency	Yes. Slightly more productivity for one of the more branched mutant s	Yes. Slightly less biomass for one of the more branched mutants	Yes. Lower viscosity for the highly branched mutants	DOT controlled feed rate

Table 2.4. Effects of shear stress on morphology, productivity, biomass and rheology

Authors	Microo.	Operation Mode	Growth rate (1/h)	Conditions	Effect on morphology	Effect of productivity	Effect on growth rate/biomass	Effect on rheology	Notes
Amanullah et al. 1999	*Aspergillus oryzae* (A1560)	Continuous	0.05	Agitation intensity reduction 1000 min^{-1} to 550 min^{-1}	Yes. Increase in mean project area. Increase in hyphae length. Increase in number of tips	No	No	N/A	
Amanullah et al. 2002	*Aspergillus oryzae* (A1560)	Batch	Max	Agitation intensity 825 min^{-1}, 675 min^{-1}, 525 min^{-1}	Yes. Higher mean projected area at lower agitation speed	Yes. Higher productivity at higher agitation speed	Yes. Higher growth rates and biomass at higher agitation speed	N/A	
	Aspergillus oryzae (A1560)	Fed-batch	<0.02	Agitation intensity 825 min^{-1}, 675 min^{-1}, 525 min^{-1}	Yes. Higher mean projected area at lower agitation speed	No	No	N/A	These under no oxygen limited conditions
Li et al. 2000	*Aspergillus oryzae* (A1560)	Fed-batch	<0.03	Power input	No	N/A	No	N/A	Change in morphology as a function of time
Li et al. 2002a	*Aspergillus oryzae* (A1560)	Fed-batch	<0.03	Power input	No	No	No	No	These under no oxygen limited conditions

Albaek et al. 2011	*Aspergillus oryzae* (property strain)	Fed-batch	Function of the feed flow rate	Agitation power	N/A	Yes. Higher productivity at higher agitation power	Yes. Higher biomass at higher agitation power	No significant	For the same impeller choice
	Aspergillus oryzae (property strain)	Fed-batch	Function of the feed flow rate	Impeller type	N/A	No	Yes. At some conditions higher biomass for the axial impeller	Yes. Lower viscosity for the axial impeller	At the same conditions
Marten et al. 1996	*Trichoderma reesei* RUT-C30	Batch	-	Agitation intensity 250, 400, 500 min^{-1}	N/A	Yes. Higher productivity at the higher agitation speed	No	Yes. Higher viscosity at higher agitation speed	
Patel et al. 2009	*Trichoderma reesei* RUT-C30	Batch	-	Agitation intensity	No	Not clear	Yes Lowest growth rate at the lower agitation speed	Yes Lower viscosity at the lowest agitation	
	Trichoderma reesei RUT-C30	Fed-Batch	-	Agitation intensity	Yes Lower clump fragmentation at the lower agitation speed	Not clear	Yes Higher biomass at the higher agitation speed	Yes but not clear correlation	

Chapter 3. Morphological and Rheological Characterization of Fungal Fermentation Broth

Filamentous fungi are great hosts for the production of industrial enzymes since they are able to grow at very high biomass concentration, as already discussed in the previous two chapters. Nevertheless, the high biomass concentration also has disadvantages, since it leads to oxygen transfer limitations as a consequence of the high viscosity of the medium. The high viscosity is believed to be related not only to the biomass concentration but also to morphology (Metz et al. 1979).

In light of the above, and considering the objectives of this thesis, the purpose of this chapter is to establish a morphology characterization technology which allows its quantitative study. First, different technologies are identified and benchmarked, and then, the most auspicious method is tested in a pilot study and compared to a validated method.

Furthermore, it is important to consider the fact that characterizing the viscosity properties of a fungal fermentation broth may not be straightforward. The presence of large clumps and pellets results in sedimentation in samples taken from the broth, and combined with the shear thinning nature of the broth, this represents vast challenges when characterizing the viscosity properties (Kold 2010). Further challenges, besides the selection of the most adequate characterization method, have to do also with the selection of a rheological model for shear thinning fluids, limitations of the measuring technology, etc. The last part of this chapter addresses and discusses these aspects.

3.1 Identification of fungal morphology characterization technologies

This section does not intent to give a detailed review of all the available technologies for fungal morphology characterization. The reader is referred to (Krull et al. 2013) for an extensive review. The aim of this section is to identify the most relevant technologies and to make an objective comparison to find the most suitable one for the purpose of this thesis.

3.1.1 Description of the technologies

Image analysis (IA)

When it comes to the morphological characterization of filamentous fungi, image analysis is the obvious choice since more information can be obtained in comparison with all the other available technologies (Papagianni 2014); e.g. detailed characterization of physiological parameters as branching frequency, nuclei number, etc. By taking pictures, the different morphologies (macro or micro, depending on the degree of magnification) are digitally frozen and the obtained picture has to be processed to provide quantitative information (Quintanilla et al. 2015). This is the most frequently used technique for morphological characterization of filamentous fungi, but it is also the most tedious and time consuming one.

Laser diffraction (LD)

Laser diffraction or light scattering offers an alternative fast solution for the characterization of fungal fermentations broths. Laser diffraction estimates the particle size distributions by measuring the angular variation in the intensity of light scattered as a laser beam passes through a dispersed sample containing particles. The angular scattering intensity data is then analysed to calculate the size of the particles responsible for creating the scattering pattern. The particle size is reported as a volume equivalent sphere diameter[1].

Petersen et al. (2008) were the first to report the use of laser diffraction for fungal fermentation broth characterization. A detailed morphology description is not discussed, but the particle size distribution was correlated to rheological properties which are believed to be directly related to morphology (Petersen et al. 2008). LD has also been used to characterize pellet growth with *A. niger*, demonstrating its applicability for this type of morphology (Lin et al. 2010). Rønnest et al. compared image analysis with laser diffraction for the characterization of *S. coelicolor* cell clumps and pellets proving that both methods can provide similar particle size distributions (Rønnest et al. 2012).

[1] http://www.malvern.com/en/products/technology/laser-diffraction/

Focused beam reflectance measurement (FBRM)

The measuring technology for the focused beam reflectance measurement (FBRM) is also based on laser light. The probe optics are rotated at a constant high speed. The focused laser beam scans continuously across the sample in a circular path. When the laser beam finds a particle, the reflected light is detected by the probe as a pulse measured from one edge of the particle to an opposing edge. The chord length across the particle is calculated by multiplying the duration of the pulse from the backscatter light times the scan speed[2].

The application of the FBRM in biological systems has been evaluated in plant suspension cultures (McDonald et al. 2001). These authors correlate non-linearly the mean of the FBRM cube-weighted distribution to the aggregate size provided by in-situ microscopic images in rice and cucumber cultures (McDonald et al. 2001). This technology was also applied for the characterization of the pelleted morphology from *A. niger* cultivations; a qualitative correlation was obtained between measurements done with the FBRM and microscopic images (Nielsen 2015). The application in dispersed fungal growth has not been tested. Thus the FBRM represents a very interesting new alternative for in-situ quantitative morphological measurements of filamentous fungi.

Large object flow cytometry (LOFC)

Flow cytometry is a technology that is used to analyze cells individually based on physical and chemical characteristics using light-scattering, fluorescence, and absorbance measurements (Rieseberg et al. 2001). As the cells travel through a fluid stream, they are exposed to a source of excitation usually coming from a light beam or mercury lamp that is orthogonal to the flow direction. The resulting light scatter gives information on specific cellular characteristics including granularity, cell size and cell morphology. Intracellular molecules that have an intrinsic fluorescence or are strained with specific fluorescence dyes allow further characterization of certain cell components. Both, the scattering and fluorescence signals, can be integrated in different ways that allow all subpopulations to be observed (Rieseberg et al. 2001). Dual-parameter plots are usually used to visualize cytometric data, but multivariate data analysis methods are most suitable to analyze the data when multiple parameters are obtained (Davey et al. 1999).

Traditional flow cytometry can analyze up to 10,000 particles/s in a size range from 0.2 to 150 µm, but this size range is not suitable for filamentous fungi. Alternatively, the COPAS (Complex Object Parametric Analyzer and Sorter) was introduced to deal with larger particles ranging from 20-1500 µm in diameter. The system measures size, optical density and fluorescence emissions[3]. The COPAS technology has been used to analyze

[2]http://www.mt.com/us/en/home/library/videos/automated-reactors/Lasentec-FBRM-Method-of-Measurement.html

[3] http://www.unionbio.com/product/

and sort microcolonies of *Aspergillus niger* with respect to size and gene expression (de Bekker et al. 2011). It was found that two populations of microcolonies could be distinguished with respect to size distribution. Furthermore, heterogeneities with respect to gene expression were also observed (de Bekker et al. 2011).

3.1.2 Technologies' comparison

Once the different candidate technologies have been identified, the next step is to make an objective comparison with respect to the different attributes that are desired from the user perspective. Below follows a list of desired attributes/needs as identified at the start of this PhD project, as well as a clear definition of each attribute.

- Time consumption: This attribute refers to the time required from withdrawing the broth sample to the time where the quantitative morphological information is obtained.
- Availability: An important attribute, indicating if the equipment is available or whether it has to be purchased/borrowed.
- Information: Refers to the amount of information that is obtained by the technology.
- Validation literature: This attribute indicates whether the technology has been applied before in other works for the morphological characterization of filamentous fungi (dispersed morphology).
- Throughput: A measure for the number of samples that can be processed within a given time period.
- Novelty: This attribute ranks opposite compared to the Validation literature attribute. In this case, it will be an advantage that the method has not been used before.
- Sample demands: An indication of how much sample has to be withdrawn for making the morphological characterization.

Table 3.1 shows the comparison of the technologies based on the above-mentioned features. Image analysis is the state of the art technology, thus it is ranked with zero in all attributes. The other three technologies, laser diffraction, FBRM and flow cytometry, are evaluated relative to image analysis (competitive benchmarking) (Kamrani & Salhieh 2002). Three points are given as maximum when the technology is very advantageous compared to image analysis. Minus three points are given when a technology is not suitable at all. The explanation for the selected weight for each attribute is presented in Table 3.2.

Table 3.1. Comparison of fungal morphology characterization technologies for different attributes

Characteristic	Weight	IA	LD	FBRM	LOFC
Novelty	0.30	0	1	3	1
Time consuming	0.25	0	2	3	2
Throughput	0.15	0	2	-2	2
Availability	0.10	0	3	3	-3
Information	0.10	0	-2	-2	-1
Sample demands	0.05	0	2	3	2
Validation literature	0.05	0	-2	-3	-2
Total	1	0	1.2	1.45	0.7

Focused beam reflectance measurement ranks as the best technology for characterizing the morphology of fungal fermentation broths. Thus, it is selected as the potential technology for the morphological characterization in this thesis. However, the fact that there is no validation of the technology available in the literature is an important issue; therefore, a pilot experiment was performed to compare the FBRM to a validated technology. LD was chosen as validated technology since it ranked second in the benchmarking inTable 3.1. This pilot study is described in more detail in the next section.

Table 3.2. Explanation for the given weight to each attribute in the benchmarking for the morphology characterization technologies.

Characteristic	Weight	Explanation
Novelty	0.30	This is considered as the most important attribute. In scientific research, the novelty of a method/technique is very important since most journals aim to public work that is novel.
Time consuming	0.25	In a country where the minimum wage ranks as one of the highest in the world, it is desired to have a measuring method that consume as little time as possible. This is important if the technology will be further implemented as standard morphology characterization technique.
Throughput	0.15	This is related to the previous attribute.
Availability	0.10	Scientific laboratory equipment is very costly, thus is desired that the technology is available. But if the technology is very advantageous, it is possible to allocate founding to purchase it.
Information	0.10	This attribute is very important since it is desired to get as much information as possible. But is also depends of which type of information is needed and how it will be used.
Sample demands	0.05	All the technologies do not require large amounts of sample. Therefore this attribute is not critical
Validation literature	0.05	Even though the technology is not validated in the literature, it still can be used if the application is proven.

3.2 Comparison of LD and FBRM for the characterization of fungal morphology

In the previous section, the FBRM was identified as the most advantageous technology for the morphological characterization of fungal fermentation broth in the frame of this thesis. A very important feature of the FBRM is that it represents a potential tool for on-line morphology characterization. Nevertheless, the suitability of the method has to be proven before investing any further time in formal studies. Thus, this section aims at setting up a pilot study on the applicability of the FBRM by comparing it to a laser diffraction; a validated method which can provide particle size distribution that are very similar to those obtained with image analysis (Rønnest et al. 2012).

3.2.1 Materials and methods

Fermentation samples

Samples were collected from four fed-batch fermentations of a filamentous fungal strain (*Trichoderma reese*i, proprietary strain) conducted in a parallel PhD project. This set of fermentations is part of the work reported in (Mears et al. 2017). All fermentations were conducted in bioreactors of 550 L total volume. 16 time samples were collected for each batch. The fermentations were conducted at different conditions by varying the back pressure, agitation speed and air flow rate. The experiment was carried as a 2^{3-1} fractional factorial design, as explained in Table 3.3 .A more detailed description of the experimental setup cannot be given due to confidentiality of the industrial data, but the process is very similar to previously described experiments (Albaek et al. 2011; Albaek et al. 2012). The samples were analysed for biomass concentration and particle size distribution. The particle size distribution was measured both with the LD and the FBRM. Approximately 200 ml of sample were collected for each data point.

Sample characterization

The biomass concentration was measured as dry cell weight by double centrifugation and re-suspension of 2-3 grams of the fermentation broth, followed by drying to constant weight at 110°C, as described by (Albaek et al. 2011). The results are reported as normalized values on the same basis for this section of the thesis.

Table 3.3. Experimental design of the four fed-batch fermentations sampled in this study. Two levels for each factor were used, a high and a low variation, they are indicated by the plus and minus sign, respectively.

Fermentation ID	Agitation speed	Aeration	Back pressure
Batch 1	+	+	+
Batch 2	+	-	-
Batch 3	-	+	-
Batch 4	-	-	+

The particle size distribution measurements with laser diffraction were done with the Mastersizer 3000, with a Hydro SM manual small sample dispersion unit (Malvern Instruments Ltd. Worcestershire, UK). The method in this project was similar to the one described by Rønnest et al. (2012), with some differences in the selection of the microorganism refractive index and the absorption related to the imaginary part of the refractive index. Value of 1.59 for the refractive index and 0 for the absorption were used in this work. 30% laser saturation was used as a maximum. Three to four successive measurements were made for each sample and the average of the whole particle size distribution was estimated by the Mastersizer 3000 software.

The ParticleTrack G400 (Mettler Toledo) was used for measuring the particle size distributions with the FBRM technology. Appendix A presents a detailed description of the measuring technology. This instrument is the next generation of the widely used Lasentec FBRM instruments (McDonald et al. 2001; Heath et al. 2002; Ge et al. 2005; Greaves et al. 2008). The scanning speed was set at 2 m/s and the data was analyzed by the iC FBRM 4.3 software using the Macro discrimination settings. In the literature this setting is widely referred as Coarse. Even though one of the main advantages of the FBRM technology is the possibility for in-situ characterization, the proof of concept data collection should be performed off-line. Measurements were done in a 0.5 L plastic cup filled with approximately 200 ml sample. The system was adapted with an external stirrer to prevent sedimentation. Preliminary work was done to determine the influence of the external stirrer on the measurements of particle distribution, and thus to establish the optimal agitation speed for the measurements. An agitation speed of 200 vs 400 rpm was compared. Data was collected every 15 s for 5 min at 200 rpm. After 5 min, the stirrer speed was changed to 400 rpm and data was collected for another 5 min. 400 rpm was chosen as the optimal operating agitation speed.

For the pilot experiment, samples were collected analyzed at the previously established optimal stirrer speed, 400 rpm. Data were collected every 15 s for 5 min and exported to MATLAB®. The average number of counts in each channel over the 5 min period was estimated. The counts for each channel were transformed into a volume distribution considering:

$$v_i = \frac{4}{3}\pi\left(\frac{s_i}{2}\right)^3 \cdot n_i \qquad \textbf{Equation 3-1}$$

v_i corresponds to the total volume occupied by the particles of size s_i in channel *i*, which is calculated by multiplying the representative volume of the channel times the number of counts n_i in that channel. The total volume occupied by all the particles in all 100 channels is estimated as:

$$v_T = \sum_{i=1}^{100} v_i \qquad \textbf{Equation 3-2}$$

The percentage distribution at each channel is estimated as follows:

$$vp_i = \frac{v_i}{v_T} \cdot 100 \qquad \textbf{Equation 3-3}$$

3.2.2 Results and discussion

Biomass concentration dynamics

The biomass concentration evolution as a function of time is shown in Figure 3.1 for the four fed-batch fermentations. The results are reported as normalized values over the same basis. Real values are not displayed for reasons of confidentiality, but similar values have been previously reported for other filamentous fungi processes (Amanullah et al. 2002; Bhargava et al. 2003b; Bhargava et al. 2005). The high biomass concentration values at the beginning of the process are caused by the particles from the non-soluble nitrogen source. The biomass concentrations for Batch 3 and Batch 4 are very similar at all times. The biomass concentration for Batch 1 and Batch 2 are also rather similar, but more differences are observed.

Determination of measurement conditions and sample stability

For this pilot study where the FBRM technology will be used as off-line measurement, the first step is to determine the conditions at which the measurements should be performed. Since the ultimate goal is to make on-line measurements, it was decided that samples for the off-line FBRM characterization should be un-diluted. However, the agitation conditions for the external stirrer should be determined first, and there should be focus on whether this agitation speed will have an influence on the measurements. The latter is referred as sample stability; samples could indeed agglomerate or de-agglomerate over the period of analysis

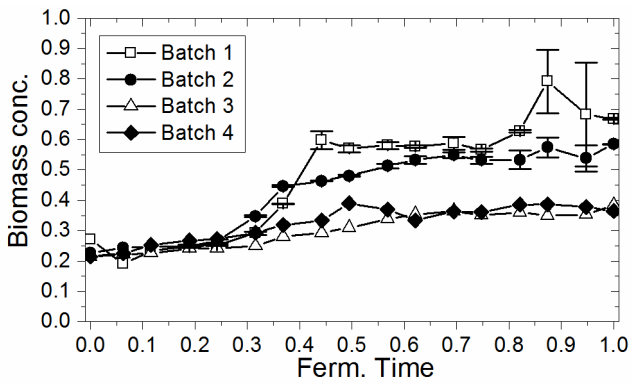

Figure 3.1. Biomass concentration dynamics for the fed-batch fermentations. Lines were drawn to indicate trends. Error bars represent standard deviation. In Batch 3 and Batch 4 the bars are smaller than the symbols at all sample times. Biomass concentrations were normalized on the same basis.

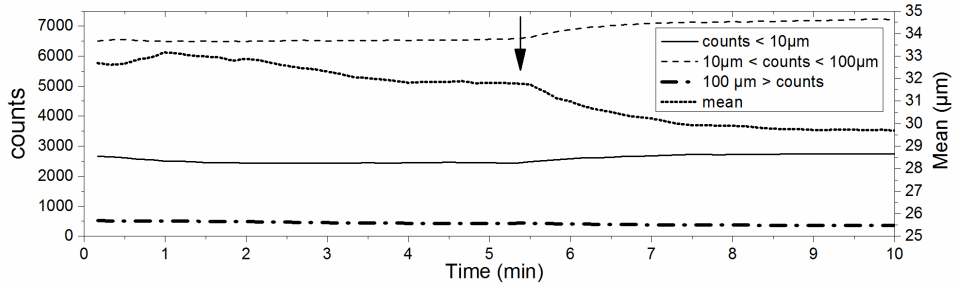

Figure 3.2. Measurements in time of particle counts classified in three size categories (counts < 10 µm, 10 µm < counts < 100 µm, counts > 100 µm. The mean of the particle size distribution (un-weighted) is presented as a function of time. The arrow represents the time point when the speed from the external agitator was changed from 200 RPM to 400 RPM.

Two agitation speeds were selected, 200 vs 400 rpm, and the differences in counts and in mean sizes were compared. Figure 3.2 shows the results for this experiment, where the black arrow illustrates the point when the agitation speed was changed from 200 rpm to 400 rpm. The counts have been classified in three categories: counts < 10 µm, 10 µm < counts < 100 µm, counts > 100 µm. The mean average size (un-weighted) has been calculated as:

$$mean\ size = \frac{\sum_{i=1}^{100} n_i \cdot s_i}{\sum_{i=1}^{100} n_i} \qquad \textbf{Equation 3-4}$$

Differences in the counts and the particle size mean can be clearly observed after the agitation speed was changed. Figure 3.2 shows the averages and the standard deviation of the variables shown in Table 3.4 for the two different agitations speeds. The averages have been calculated over the first two minutes of measurements at 200 rpm, and over the last 2 minutes of measurements at 400 rpm. The total number of counts increases when switching from 200 to 400 rpm, and forms an indication of hyphal de-agglomeration due to the higher agitation rates. It is important to emphasize that the phenomenon observed is not hyphal fragmentation due to agitation. The shear developed by the external stirrer is not high enough to have an impact on the hyphal strength, according to the Kolmogorov theory of isotropic turbulence, as further discussed in this thesis.

Table 3.4. Mean and standard deviation for the counts by the FBRM in a filamentous fungi fermentation broth observed at two agitation speeds in the external stirrer. Mean and standard deviation of the particle size are provided.

External stirrer speed (rpm)	**Counts <10µm** (1/s)	**10 µm < counts < 100 µm** (1/s)	**Counts > 100 µm** (1/s)	**Total counts**	**Chord length mean** (µm)
200	2525±81.5	6503±22	501±11.7	9530	32.9±0.2
400	2735±8.3	7182±32.2	365±4.1	10 282	29.8±0.1

A t-test over the differences in the mean of the chord length for 200 rpm and 400 rpm indicates a very significant difference (p=6E-32). Thus, it was decided to perform the off-line measurements with the FRBRM at the higher stirrer speed (400 rpm), considering the fact that the ultimate goal is to perform on-line measurements. Therefore, in the pilot experiment the hydrodynamic conditions in the bioreactor should be mimicked (transitional to turbulent flow for pilot scale fermenters). A higher external stirrer speed was not tested due to vortex formation.

Reproducibility

The quality of scientific work highly depends on replicate measurements. Replicates can help to evaluate and identify sources of variation in measurements and to isolate the effect of random variation when testing a hypothesis and estimating parameters (Blainey et al. 2014). Two types of replicate measurements are usually considered in experimental design: technical replicates and biological replicates. "Technical replicates are repeated measurements of the sample that represent independent measures of the random noise associated with protocols or equipment. Biological replicates are parallel measurements of biologically distinct samples that capture random biological variation" (Blainey et al. 2014). Figure 3.3 shows the results for the technical and biological reproducibility test. Both the laser diffraction and the FBRM technologies were tested. The technical reproducibility was tested by measuring the media before inoculation for Batch 2, Batch 3 and Batch 4. Although the measurements are not done for exactly the same sample, it can be assumed that this is the case, since the error for preparing the media is very small when large quantities are handled and when all compounds come from the same batch of medium. Figure 3.3a shows the cumulative volume distribution for the media measurements with laser diffraction. The results are the same for all samples. Figure 3.3c presents the results for the same samples but for the FBRM measurements; Batch 2 differs from the other two measurements. Biological reproducibility was tested by measuring the particle size distribution at some point in the batch phase, i.e. when the four batches are still experiencing the same conditions. Figure 3.3b shows the results for the biological reproducibility for LD. The variation has increased. Batch 2 differs from the other three measurements. In the case of the FBRM, Batch 3 is the one that differs, as can be seen in Figure 3.3d. All these sources of variation have to be considered for further data analysis.

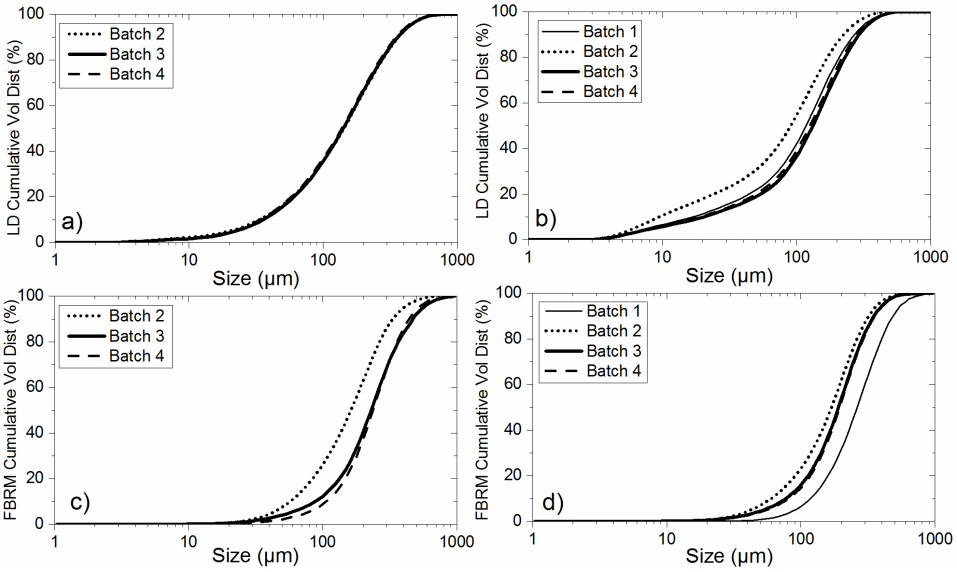

Figure 3.3. Technical and biological reproducibility for the LD and the FBRM measurements. a) LD measurements to the media before inoculation; b). LD measurements of the fermentation broth at the end of the batch phase; c) FBRM measurements for the media before inoculation; d) FBRM measurements to the fermentation broth at the end of the batch phase.

Fungal morphology measured with LD and FBRM

Now that the conditions for the measurements with FBRM have been established and the reproducibility of the measurements has been determined, the morphological evolution characterized by LD and FBRM will be compared. Figure 3.4 shows the cumulative volume percentage distribution at selected normalized time points during the fermentation: 0.07, 0.33, 0.50, 0.75 and 1. For the LD measurements, the distribution shifts to the left from NT=0.07 to NT=0.33, as an indication of hyphal fragmentation. As the fermentation proceeds, the distribution keeps shifting to the left until it stays more or less constant. The measurements done with the FBRM are different than the LD measurements. There is no trend what so ever in the measurements by itself, e.g. the measurements at the end of the fermentation, NT=1, indicate a larger average size than the measurements taken at the initial time. The cumulative particle size distribution does not move at all for some of the measurements, i.e. Batch 2. This indicates that the FBRM cannot be used as a tool for morphological characterization.

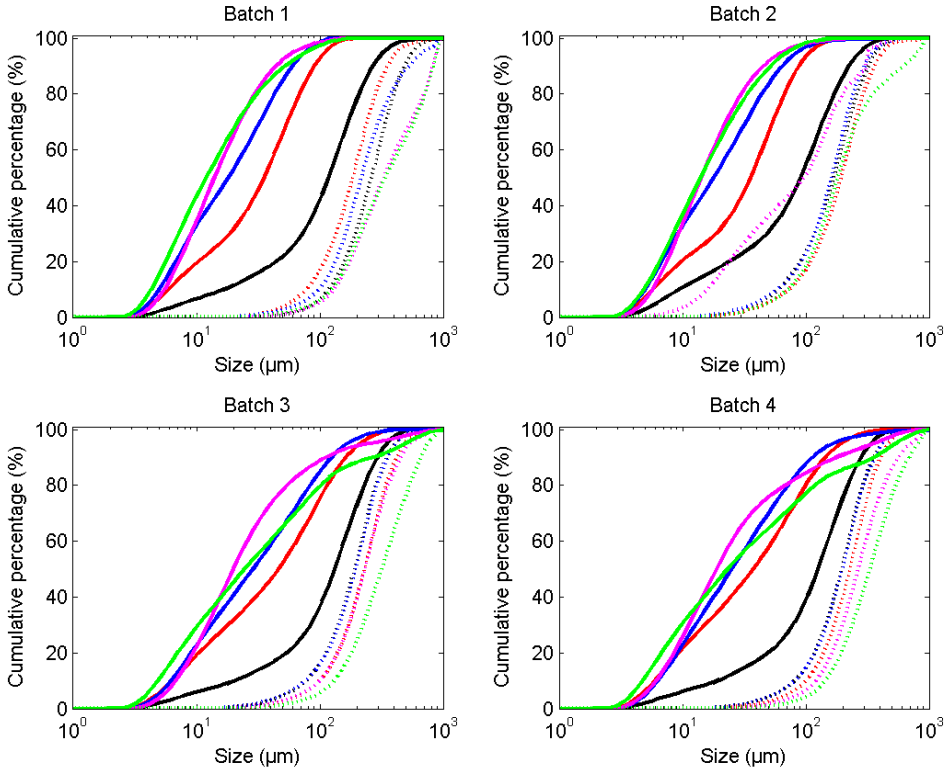

Figure 3.4. Comparison of LD (solid line) vs FBRM (dotted line) for the four batches at different normalized fermentation times. Macro electronics module. Black NT=0.07, red NT=0.33, blue NT=0.50, magenta NT=0.75, green NT=1.

It was further investigated for the FBRM if by changing the electronic modules from Macro to Primary, a more similar result to the LD measurements could be obtained. Figure 3.5 shows the comparison of the LD vs FBRM (Primary electronic modules). Again, the measurements with the FBRM technology are different than the LD measurements. However, it should be said that there is one measurement from the FBRM which is very similar to the LD cumulative volume distribution, the measurement at NT=0.07; i.e. this time point corresponds to the measurements of morphology characterization done for the batch phase of the fermentation.

It was hypothesized that the reason why similar cumulative volume distributions are obtained at the early stages of the fermentation process, i.e. the batch phase, was due to the low biomass concentration in the samples. According to Schöll et al. (2012), the FBRM can be used in a wide range of solid concentrations, i.e. there is no upper limit of suspension density that cannot be measured with FBRM for crystallization processes. However, they also point out that for very high solids concentration the counts for the chord lengths do not correlate linearly with the particle concentration (Schöll et al. 2012).

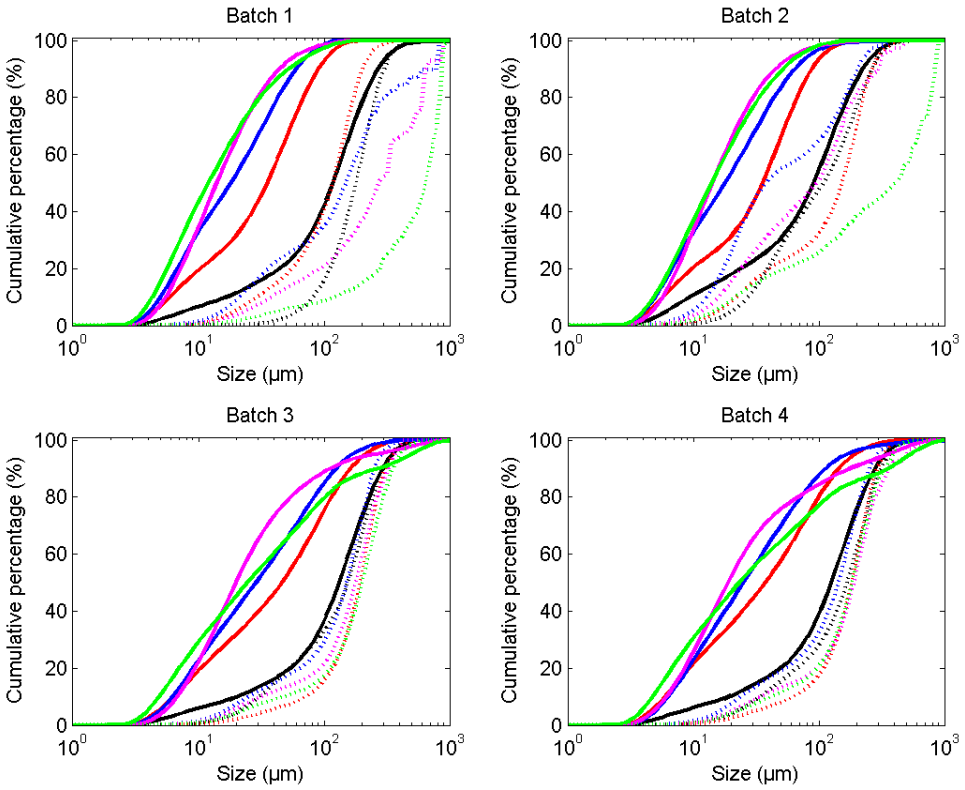

Figure 3.5. Comparison of LD (solid line) vs FBRM (dotted line) for the four batches at different normalized fermentation times. Fine electronics module. Black NT=0.07, red NT=0.33, blue NT=0.50, magenta NT=0.75, green NT=1.

Thus, it is very likely that the high biomass concentration and the very irregular fungal shape interfered with the measurements. To test this hypothesis, the cumulative volume distributions for the LD and the FBRM (Primary settings) at the early stages of the processes (NT=0.07 and NT=0.12) were compared. The measurements of the media before inoculation determined with the Primary electronic modules were also compared to the LD measurements, Figure 3.6. The cumulative volume distribution estimated with the FRMB is very similar to the distribution estimated with LD. Nevertheless, the variation of the measurements performed with LD is not very large for the different data points, and a clear trend is not observed. For Batch 1, Batch 3 and Batch 4, the cumulative volume distribution is smaller for NT=0.12, than for NT=0.07, but not for Batch 2. The cumulative volume distribution for the media measurements indicates bigger particles than when the fermentation process is started for Batch 2, Batch 3 and Batch 4. However, the FBRM does not show this trend, and there is not a specific trend in the measurements for each batch either when plotted as a function of time.

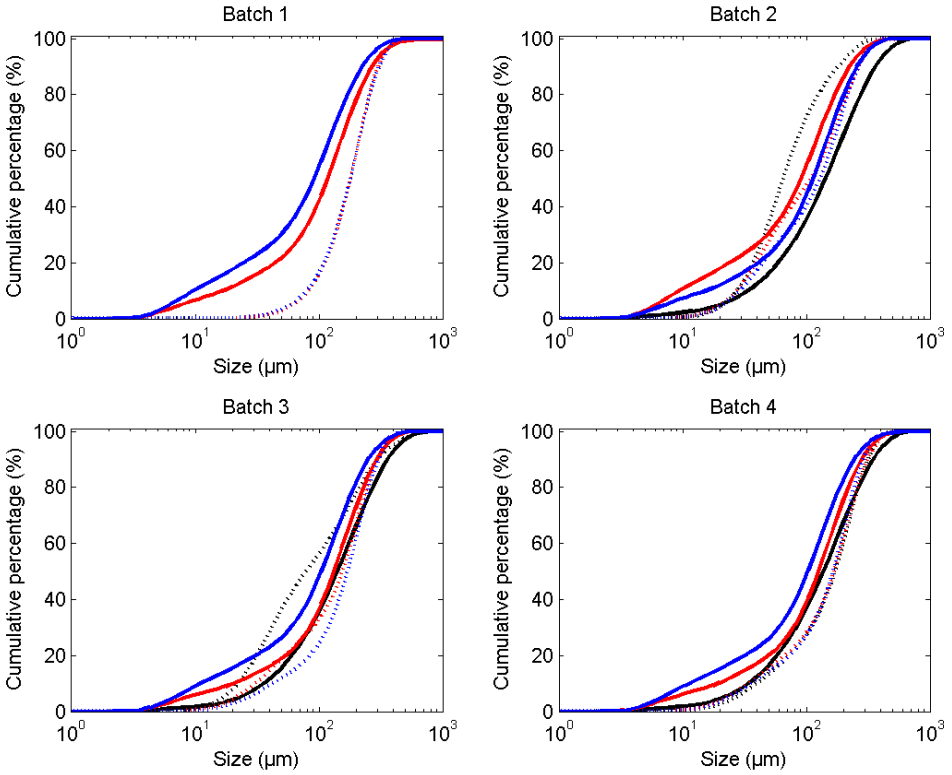

Figure 3.6. Comparison of LD (solid line) vs FBRM (dotted line) for the four batches for the first three samples. Fine electronics module. Black NT=0 (media before inoculation), red NT=0.07, blue NT=0.12.

It should be further investigated if measurements with the FBRM technology performed on diluted samples could give volume distributions that are more similar to the ones obtained with LD. This could be used as an at-line characterization system. In this case, a single probe could be used to characterize samples coming from different fermenters, but significant more infrastructure should be invested. Thus, it was decided to adopt LD as the formal fungal morphology characterization technique in this project. Very interesting physiological findings were observed by the detailed characterization of morphology with LD in the batches described here and they are further discussed in Chapter 7.

3.2.3 Conclusions

A pilot study for testing the applicability of the FBRM technology as a tool for characterization of fungal morphology in dispersed growth was performed. This was done by comparing the particle size distribution measurements as volume percentage obtained with the FBRM to the ones obtained with the previously validated LD technology. It was found that the FBRM does not give a PSD that is similar to the ones obtained with LD. Because LD was ranked second in the morphological characterization technologies benchmarking presented in the previous section, LD will from now on be used for the formal morphological characterizations in this PhD project.

It was also found that by using the Primary electronics setting when performing data analysis with the FBRM, contrary to the Macro electronics setting recommended in the literature, a similar PSD can be obtained for the FBRM as for LD for low concentration samples. This offers the possibility for monitoring morphology with an at-line system.

3.3 Rheological characterization

In fungal fermentations, mass transfer is often the main limitation; changes in the rheological properties of the fermentation broth may significantly reduce the overall performance of the bioreactor (Kold 2010). Thus, an accurate description of the broth rheology is necessary when evaluating the performance of fermentation processes. Significant work has been done to evaluate different methods to characterize fungal rheology (Marten et al. 1996; Malouf 2008; Kold 2010; Quintanilla 2013). The common characteristic is that these studies suggest the use of rotational rheometers for fungal fermentation broth characterization, in accordance with (Metz et al. 1979).

Rheological measurements were done in an AR-G2 rheometer (TA Instruments, New Castle, DE) in controlled shear rate mode. The vane and cup geometry was used for the measurements and a gap of 1 mm between the bigger radius of the vane and the outer cylinder was used. Temperature was controlled at the operation temperature in the fermenter. A continuous shear rate ramp from 20 to 600 s^{-1} was implemented over a period of 6 minutes, and 16 measurements of shear stress were taken. The information from the flow curves was retrieved, i.e. shear rate, shear stress and viscosity.

Due to the nature of the fermentation broths, i.e. non-Newtonian fluid, the ratio between the applied shear rate and the measured shear stress for a fermentation broth is not constant; therefore, the viscosity has to be expressed as a function of any of the two variables. There are several models in the literature to describe the shear stress or apparent viscosity as a function of shear rate. These models are purely empirical and they are inspired by the shape of the curve in the obtained rheogram, which can be described mathematically, e.g. shear thinning fluids are usually described by a power law function, shown in Equation 3-5, where K is the consistency index and n_{PL} is the flow behaviour index.

$$\mu_{app} = K\dot{\gamma}^{(n_{PL}-1)} \qquad \textbf{Equation 3-5}$$

When a positive offset of the shear thinning curve is observed, it can be modelled by the Herschel and Bulkley correlation, Equation 3-6.

$$\mu_{app} = \frac{\tau_{HB} + K_{HB}\dot{\gamma}^{(n_{HB})}}{\dot{\gamma}} \qquad \textbf{Equation 3-6}$$

The parameters in such an expression are typically found by fitting it to the experimentally obtained flow curves (Ratkovich et al. 2013). After the parameters are found, the model is used to calculate the apparent viscosity at the shear rate in the fermentation tank. However, the problem with these models is that the parameters are usually correlated, which appears when performing a parameter estimation: a decrease of the value of one parameter can be compensated with an increase of the value of another parameter. What it means, in fact, is that the data are not sufficiently informative to allow for an independent estimation of all parameters, a problem that is often encountered when fitting a mathematical model to data (see e.g. also Sin et al. 2009). The usual approach to overcome this problem is to fix one of the parameters. For the power law model, the flow behaviour index is usually fixed, since it is relatively constant throughout a fermentation. For comparison, Riley et al. considered a value for the flow behaviour index of 0.35 for fermentations of *Penicillium chrysogenum* for biomass levels >10 g L^{-1} (Riley et al. 2000). The consistency index for fermentation broth from *A. oryzae* and *A. niger* was fixed at 0.5 and 0.2, respectively (Riley & Thomas 2010). In the case of the Herschel and Bulkley model, Petersen et al. (2008) fixed the consistency index parameter at a value of 0.41; fixing this parameter resulted in a dramatic decrease in the variance of the other estimated parameters, the yield stress and the consistency index (Petersen et al. 2008).

In this work, the rheology of fermentation broths from *T. reesei* has been characterized at different scales and with different strains. The power law rheological model has been chosen to represent the steady shear rheological behaviour. Reuss et al. (1982) speculated

Table 3.5. Power law rheological parameters for three different fed-batch fermentations at different relative times run at pilot scale and production scale.

Strain	**Scale**	**Ferm. Time**	K	n_{PL}	**Strain**	**Scale**	**Ferm. Time**	K	n_{PL}
NZ 1	Full	0.08	0.27	0.59	**NZ 2**	Pilot	0.40	0.67	0.58
	scale	0.23	0.99	0.53			0.43	0.68	0.58
		0.38	0.66	0.66			0.54	0.89	0.56
		0.40	0.74	0.65			0.57	1.04	0.54
		0.42	0.62	0.67			0.68	1.36	0.51
		0.54	0.93	0.62			0.72	1.28	0.52
		0.56	1.15	0.60			0.86	1.22	0.51
		0.57	0.92	0.63			0.97	1.14	0.51
		0.69	1.22	0.59			1.00	1.10	0.52
		0.71	1.27	0.58	**NZ 2**	Pilot	0.13	0.04	0.60
		0.73	1.04	0.60			0.26	0.09	0.63
		0.85	1.13	0.57			0.39	0.30	0.36
		0.87	1.31	0.57			0.53	0.15	0.54
		0.88	1.21	0.58			0.66	0.15	0.58
		1.00	1.14	0.57			0.81	0.21	0.65

that any of the different shear thinning models could adequately be used to represent the rheological behaviour, and therefore they suggested using the power law model due to simplicity. Table 3.5 shows the power law rheological parameters from three fed-batch fermentations at two scales run with 2 proprietary strains from Novozymes A/S. The flow behaviour index, n_{PL}, is relatively constant despite the scale or the strain used. For the data in Table 3.5 the average flow behaviour index is 0.57 with a standard deviation of 0.06. This suggests that the flow behaviour index for *T. reesei* fermentations should be fixed around this value.

The power law rheological parameters at different times from two lab scale fermentations (TRC26 and TRC27) conducted with the strain RedTr can be found in Table 3.6. The strain RedTr and its growth conditions are described in more detail in the Chapter 4. For these processes the flow behaviour index is not constant; it is different for both fermentations and changes as a function of time. Also, the values are very different compared to the values in Table 3.5. For TRC26 the biomass concentration decreases from t = 26 h to t = 69 h, and the flow behaviour index increases, from t = 69 h to t = 98 h the biomass concentration stays relatively constant and the n_{PL} value increases. For TRC27 the biomass concentration stays constant and the flow behaviour index increases. As it will be pointed out in further chapters, fragmentation during the time course of a fed-batch fermentation occurs due to different reasons, which could explain the increase in n_{PL}; however in the pilot and production scale fermentation there is also fragmentation, but the flow behaviour index stays constant. Thus, it is hypothesized that the reason for the dramatic changes in the flow behaviour index, in comparison with the results reported in Table 3.5, is merely a problem occurring due to the correlation between the parameters. The viscosity is not high enough to have a representable measure of it. Riley et al. (2000) questioned the accuracy of the rheological measurements for fermentation broths with a dry cell weight below 8 to 10 g L^{-1}; these values are in agreement with the dry cell weight data in Table 3.6, suggesting that the method used in this work is not accurate for low dry cell weight samples.

Table 3.6. Biomass concentration and power law rheological parameters at different time points for two different fed-batch fermentations run in 2 L fermenters.

	TRC26			**TRC27**		
Ferm. Time (h)	**DCW (g/kg)**	***K***	**n_{PL}**	**DCW (g/kg)**	***K***	**n_{PL}**
26	8.9	0.09	0.64	7.9	0.14	0.59
69	7.0	0.05	0.72	8.1	0.11	0.65
98	7.1	0.02	0.82	8.4	0.04	0.79

It was further tested if by concentrating the sample, a more representative measurement could be obtained. 50 ml of extra broth were taken and centrifuged for 10 min at 2800 rpm. Then, 15 ml of supernatant were removed and the cells were suspended. Table 3.7 shows the rheological parameters for the concentrated samples. The values for the flow behaviour index are more similar between samples, and the values are also constant during the fermentation. The values are also closer to the flow behaviour index values for

fermentation broths from pilot and production scale reported in Table 3.5. The values of the flow behaviour index from Table 3.5 and from Table 3.7 were averaged and a flow behaviour index of 0.55 was obtained. It was decided that the value for the flow behaviour index for further experiments will be fixed at that value.

Table 3.7. Biomass concentration and power law rheological parameters for two different fed-batch fermentations at different times run in 2L fermenters. Rheological parameters were determined for concentrated samples. Con. factor = 1.4.

		TRC26 (concentrated)			TRC27 (concentrated)		
Ferm. (h)	**Time**	**DCW (g/kg)**	***K* (Pa s^n)**	n_{PL}	**DCW (g/kg)**	***K*(Pa s^n)**	n_{PL}
26		10.6	0.45	0.50	10.8	0.51	0.50
69		12.1	0.35	0.51	9.2	0.58	0.51
98		8.9	0.32	0.50	12.7	0.34	0.58

A control experiment was conducted in order to test whether the centrifugation could cause a change in morphology/structure, which could influence the rheological measurements when the samples were centrifuged. The rheology of a fermentation sample was measured with no centrifugation. Also, a different sample was centrifuged and re-suspended, and the viscosity was measured. The results from this experiment can be found in Figure 3.7. There are no big differences in the flow curves between samples with or without centrifugation.

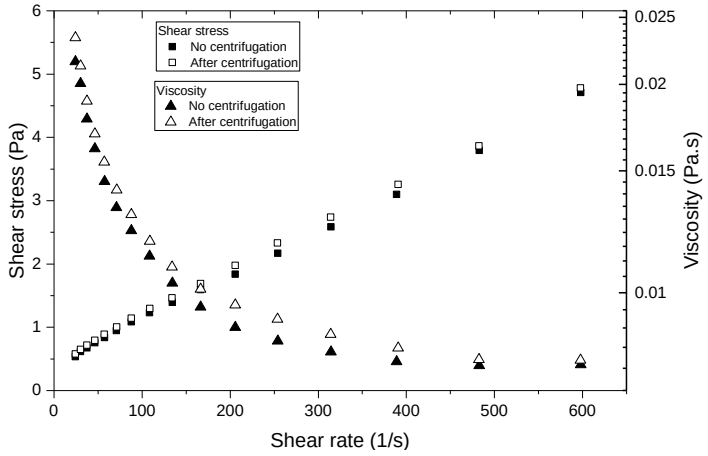

Figure 3.7. Rheological measurements for a fermentation sample before and after centrifugation and re-suspension. The filled symbols represent the rheological measurement for the normal sample. The empty symbols are for the rheological measurement performed on a re-suspended sample after 10 min centrifugation at 2800 rpm.

Chapter 4. Platform Development for Enhanced Enzyme Expression

4.1 Introduction

As described in Chapter 1, the aim of this thesis is to study the morphology and rheology in submerged fermentations with filamentous fungi. Given the importance of producing cheaper renewable fuels, *Trichoderma reesei* has become a paradigm for industrial production of cellulases and hemicellulases that are then applied to the hydrolysis of waste biomass (Martinez et al. 2008); therefore, *Trichoderma reesei* has been chosen as the fungal model for most of the work in this thesis. Before starting a detailed study to determine the relation between the different variables and parameters involved in fungal fermentations (morphology, rheology, productivity, oxygen transfer, etc.), it is desired to develop a platform which enhances enzyme expression. Thus, it is the aim of this chapter to describe such platform.

Industrial fermentation for the production of enzymes is usually carried out as a fed-batch process, since it allows to convert more carbohydrate into product (Stocks 2013). Therefore, fed-batch is also here selected as the fermentation operation mode. Manipulation of media, strain improvements and various parameter optimizations (pH, temperature, etc.) are among the most relevant strategies for promoting the overproduction of enzymes (Sivaramakrishnan et al. 2006). Different cellulases' hyperproducing strains of *T. reesei* have been developed throughout the years. The RUT-C30 strain continues to be one of the most widely used filamentous fungi strains for the production of cellulolytic enzymes and recombinant protein for academic research (Peterson & Nevalainen 2012); thus, it will be used to perform most of the work in this thesis. Throughout the years, growth parameters have consistently been used as

temperature = 28 °C and pH between 4 and 5 for RUT-C30 (Marten et al. 1996; Velkovska et al. 1997; Yu et al. 2012). Some authors have suggested that a lower temperature is beneficial for the enzyme production period, as a means of enhancing productivity (Lee & Koo 2001; Lehmann 2011). Nevertheless, from an industrial point of view, a low temperature requires more cooling, which may not be cost effective in large scale fermenters. Thus, 28°C has been chosen as the operating temperature for the experimental work in this thesis.

The cultivation medium for the production of cellulases by *T. reesei* is under continuous improvement and it has been fully reviewed (Persson et al. 1991; Peterson & Nevalainen 2012). A number of studies have reported the effects of different carbon sources on cellulases production (Olsson et al. 2003; Juhász et al. 2005; Rodriguez-Gomez et al. 2012). Although, the compounds studied in these articles (cellulose, spruce, willow, corn stover and wheat straw) are reported as strong inducers, lactose has been chosen as the carbon source to be used in this work since it is one of the most important soluble carbon sources in industry (Xu et al. 2014). Other works have aimed to improve enzyme production through manipulation of the pre-culture media composition (Ahamed & Vermette 2008). The nitrogen source has also been widely studied in the literature. Lehmann (2011) studied thoroughly the effect of different nitrogen sources on the production of cellulases in *T. reesei* RUT-C30 in batch fermentations. It was concluded that an organic nitrogen source is crucial for the proper growth of *T. reesei*. It was also found that the type of nitrogen source plays a big role; peptone was found to be the best nitrogen source for the production of cellulases (Lehmann 2011). On the other hand, Rodríguez-Gomez et al. found cellulase titers and protein patterns to be independent of the nitrogen source in batch fermentations with RUT-C30 (Rodriguez-Gomez & Hobley 2013). Thus, they recommended the use of ammonium sulphate as sole nitrogen source (Rodriguez-Gomez & Hobley 2013).

In the light of the above, it is the objective of this chapter to develop an expression platform which enhances cellulase production by testing the effect of nitrogen source in fed-batch fermentations with *T. reesei* RUT-C30. Thus, due to the discrepancies found in the literature, peptone and ammonium sulphate are compared as N sources. Furthermore, an additional nitrogen source is tested: soy meal, which is an agro-food industry by-product and it has been tested in solid state fermentations (El-Deen et al. 2014; Irfan et al. 2012). Therefore, it is a good alternative as a nitrogen source in industrial enzyme production for being a cheap nitrogen source.

4.2 Materials and Methods

4.2.1 Strain and propagation

T. reesei RedTr was used for all the experiments in this section. This strain was constructed from RUT-C30. RedTr expresses an intracellular fluorescent red protein under a constitutive promoter. Spores were propagated from frozen ampoules onto potato

dextrose agar slopes, following incubation for 7 days at 26°C. The spores were harvested with 8 mL of 0.1% Tween-80 solution. Approx. 4 mL were used to inoculate 250 mL of shake flask medium. The shake flask medium consisted of: glycerol, 15 (g/L); $(NH_4)_2SO_4$, 13.6 (g/L); bacto peptone, 6 (g/L); KH_2PO_4, 4 (g/L); $MgSO_4 \cdot 7H_2O$, 0.6 (g/L); $CaCl_2 \cdot 2H_2O$, 0.8 (g/L); $FeSO_4 \cdot 7H_2O$, 5 (mg/L), $MnSO_4 \cdot H_2O$, 1.6 (mg/L), $ZnSO_4 \cdot 7H_2O$, 1.4 (mg/L); $CuSO_4 \cdot 5H_2O$, 2 (mg/L); and pluronic, 1 (mL/L). After inoculation, the shake flasks were placed in an orbital shaker at 250 rpm and 26°C for 48h. 50 grams of vegetative growth from these shake flaks were used to inoculate the bench scale bioreactors.

4.2.2 Fermentation conditions and media

The fed-batch fermentations were conducted in 2-L bioreactors with an initial batch volume of 1.3 L. The vessel diameter was 150 mm and two Rushton turbines were used for agitation with D/T=1/3. Aeration was provided by sparging air through a micro-hole. The initial aeration set-point was 0.75 L/min, which then was ramped up to 1.5 L/min over 1 h. The temperature was set at 28°C and the pH was maintained between 4.5 and 4.8 using 10% (w/v) H_3PO_4 and 15% (w/v) ammonia solution. The agitation speed was set to 600 rpm for the batch phase. From the point the feed addition started, the stirrer speed was manipulated between 600 and 1100 rpm to maintain a dissolved oxygen tension (DOT) above 50%.

Three fermentations were conducted to determine the influence of nitrogen source on cellulase production. The composition of the media used for the fermentations was very similar. The peptone medium (PP) included 20 g/L bacto peptone. The soy medium (Soy) contained 20 g/L soy meal. The inorganic nitrogen (Inorg-N) medium included 8 g/L $(NH_4)_2SO_4$. The rest of the media components were selected based on (Ma et al. 2013): glucose, 6.0 (g/L); $(NH_4)_2SO_4$, 4.0 (g/L); KH_2PO_4, 4 (g/L); $MgSO_4 \cdot 7H_2O$, 0.6 (g/L); $CaCl_2 \cdot 2H_2O$, 0.8 (g/L); $FeSO_4 \cdot 7H_2O$, 5 (mg/L); $MnSO_4 \cdot H_2O$, 1.6 (mg/L); $ZnSO_4 \cdot 7H_2O$, 1.4 (mg/L) $CuSO_4 \cdot 5H_2O$, 2 (mg/L); and pluronic, 1 (mL/L). The glucose was sterilized separately as a 500 g/L glucose solution. All compounds were supplied by Sigma-Aldrich.

At 17 h, a ramp for adding the feed solution was implemented giving a final flow rate of 0.08 g/min at 40 h. After 40 h, the feed flow rate was kept constant. The feed solution consisted of 150 g/L lactose and 5 ml/L pluronic. During feeding, the feed solution was agitated by a magnetic stirrer at 900 rpm in order to ensure a homogenous mixture.

4.2.3 Sampling and analysis

Samples were taken at different time intervals and analyzed for biomass, extracellular (EC) protein concentration and enzyme activity. The biomass concentration was measured as dry cell weight by double centrifugation and re-suspension of 2-3 grams of the fermentation broth, followed by drying to constant weight at 110°C, as described by

(Albaek et al. 2011). When soy was present – roughly for the first 20 h of the fermentation – the dry weight included both biomass and soy. The protein concentration was determined in duplicates with the Bicinchoninic acid (BCA) assay. Enzyme activity was determined also in duplicates using a proprietary assay, and the results in this chapter are reported as normalized values on the same basis. The DOT was measured by an optical probe (Mettler Toledo). Changes in air composition (O_2 and CO_2) were also monitored on-line.

4.2.4 Carbon balances and yield calculations

Carbon balances were performed in order to estimate the biomass, CO_2 and product yields over the total amount of fed carbon. The system mass balance was done by predicting the system weight at the end of the fermentation and comparing it with the measured system weight, and this difference was then called the system error. The predicted value is estimated considering the initial broth volume, inlets (feed, acid and base addition) and system outlets (evaporation, sample, CO_2 and losses due to foaming).

The carbon mass balance was done in C-mol. The carbon inputs to the systems were the carbon from the glucose, the carbon from the nitrogen source and the carbon in the lactose feed solution. The carbon outlets were considered as the carbon going to biomass formation, product formation and respiration (CO_2). The composition for the reactants and products considered for the carbon mass balances can be found in Table 4.1

Table 4.1. Element composition for the different compounds involved in the carbon mass balances.

Compound	C-mol composition	Molecular weight (g/C-mol)	Reference
Glucose	CH_2O	30	Calculated
Soy	$CH_{1.8}N_{0.15}O_{0.46}K_{0.04}$	24.9	(Osborn 1977)
Peptone	$CH_{1.58}O_{0.3}N_{0.27}S_{0.004}$	22.5	(Villadsen et al. 2011)
Lactose	$CH_{1.83}O_{0.92}$	28.5	Calculated
Biomass	$CH_{1.72}O_{0.55}N_{0.17}$	24.9	(Villadsen et al. 2011)
Product	$CH_{1.58}O_{0.3}N_{0.27}S_{0.004}$	22.5	(Villadsen et al. 2011)

4.3 Results

4.3.1 Fermentation reproducibility

Two fermentations with bacto peptone as nitrogen source were run first in order to test for reproducibility. The results of these two fermentations are shown in Figure 4.1. Figure 4.1a compares the biomass concentrations measured as dry weight per kilogram broth. Figure 4.1b shows the extracellular protein concentrations. The integrated carbon dioxide production rates are shown in Figure 4.1c. The relative enzyme activities are displayed in Figure 4.1d. The trends in the biomass concentration profiles are similar for both fermentations, but some differences are observed. These differences could be attributed to the biomass determination method; however, since single measurements were

performed, further discussion of this explanation is not justified. Extreme foaming was observed in most of the fermentations. This is a common problem for RUT-C30 (Weber & Agblevor 2005; Patel et al. 2009), the paternal strain for RedTr. The broth became very heterogeneous due to the trapped bubbles, which could explain the differences in the biomass determination for both fermentations. The protein concentrations have the same trend for the two fermentations and the values are similar, but the EC protein concentrations for the fermentation indicated with empty squares are slightly lower. However, given the variation of the determination method, these differences may not be significant. The integrated carbon dioxide production rates are identical for both fermentations. The enzyme activities for both fermentations show similar trends, but the values for the fermentation represented by the empty squares are smaller, in agreement with the measured extracellular protein concentrations. The variation in this method is extreme, and this has to be considered for further experiments. In general, there is a large variation in the off-line measurements; nonetheless the results obtained by the on-line measurements, i.e. integrated CO_2, are identical. This indicates that the biological variation in the experiments is low.

4.3.2 Influence of nitrogen source on cellulase production

Three different fed-batch fermentations were conducted in order to test the effect of nitrogen source on enzyme production. The nitrogen sources tested were bacto peptone, soy meal and ammonium sulfate; they are referred below as PP, Soy and Inorg-N, respectively. Figure 4.2 shows the on-line measurements for dissolved oxygen tension (a), air flow rate measured before entering the bioreactor (b), agitation speed (c) and integrated carbon dioxide production rate (d). Due to some technical problems, it was not possible to calibrate the DOT probe for the Soy fermentation, and thus the agitation speed for this batch was set at 900 rpm from t = 17 h onwards.

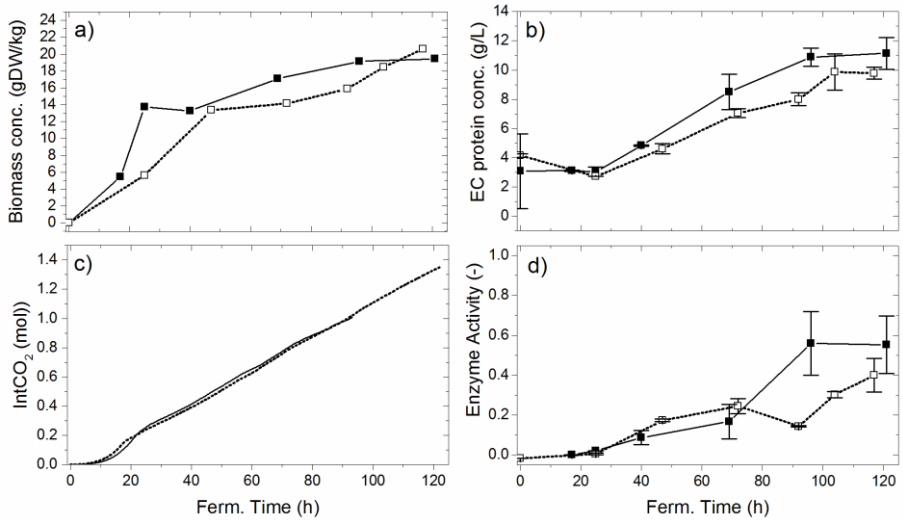

Figure 4.1. Reproducibility of two fermentations with peptone as nitrogen source. a) Biomass concentration, lines drawn to represent trends; b) Extracellular protein concentration, lines drawn to represent trends; c) Integrated carbon dioxide production; d) Normalized enzyme activity. Error bars represent standard deviations.

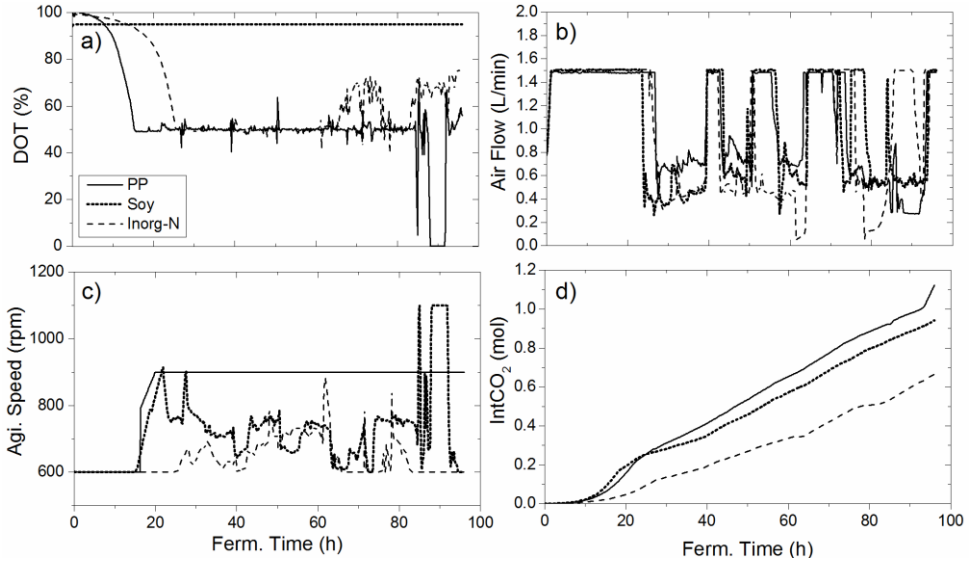

Figure 4.2. On-line measurements for three fed-batch fermentations of *T. reesei* using different nitrogen sources. a) Dissolved oxygen tension, b) Air flow rate at ambient conditions measured before entering the bioreactor, c) Stirrer speed; and, d) Integrated carbon dioxide production rates.

According to Figure 4.2a, the DOT for the PP and Inorg-N fermentations does not fall below the set point of 50% for most of the time. For PP the DOT drops to zero around t = 90 h; this was attributed to the fact that this fermentation presented severe foaming which caused outlet blockage, preventing air in-flow. Figure 4.2b shows an unstable air flow rate for the three fermentations. This was investigated thoroughly, and it was found that the air flow fluctuations were caused by the feed solution. The lactose feed solution (150 g/L) was very close to saturation (189 g/L) (Machado et al. 2000). For PP, Soy and Inorg-N, the feed solution was added together with the air; and therefore, the air flow caused water evaporation from the feed solution which resulted in lactose crystallization. These crystals were causing the air inlet blockage. This however, had no effect on protein production, since in the previous experiment for testing reproducibility one of batches was conducted with air humidification before the air was entering the rector, and the same protein concentrations are obtained for both fermentations. Air humidification was used for further experiments conducted with lactose as feed. Figure 4.2d shows the integrated carbon dioxide production rates as a function of time. The PP fermentation has the highest values, followed by the Soy and the Inorg-N fermentations.

The off-line measurements from t = 17 h onwards can be found in Figure 4.3. The evolution of the biomass concentrations as a function of time are compared in Figure 4.3a. The extracellular protein concentration data can be found in Figure 4.3b. Figure 4.3c shows the relative enzyme activity for the three fed-batch fermentations. The biomass concentration is assumed to be zero for the fermentations with soluble nitrogen sources (PP and Inorg-N) at t = 0 h. For PP the biomass concentration rapidly increases to 14 g/L at t = 25 h. The growth for Inorg-N is very slow for the batch phase and it has only

reached 4.6 g/L at t = 25 h. In the case of Soy, it is not possible to have reliable biomass concentration measurement in the first hours due to the presence of insoluble soy particles; however, at t = 25 h the biomass concentration is very similar to PP. When comparing the relative maximum growth rate – estimated on the basis of on-line measurements of carbon dioxide production rates (CPR) in the exponential growth of the batch phase, Table 4.2 – the fermentation using soy as nitrogen source has the fastest growth. This gives an indication that the measurements of dry weight for the fermentations when soy is used as nitrogen source are reliable from t = 17 h onwards. As the fermentations proceed, the growth profiles change. At the end of the fermentations, PP has the highest biomass concentration, followed by Inorg-N, whereas Soy has the lowest biomass growth. The fermentation using soy meal as nitrogen source presents the highest extracellular protein content, and then it is followed by PP and Inorg-N. These trends are the same for the relative enzyme activity, despite the variation in the enzyme activity determination assay.

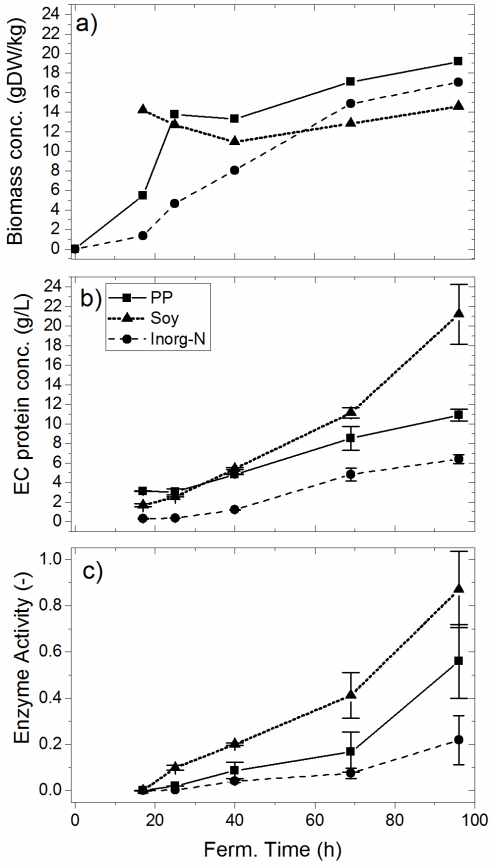

Figure 4.3. Profiles for: a) Biomass concentration; b) Extracellular protein concentration; and, c) Relative enzyme activity for three fed-batch fermentations of *T. reesei* grown with different nitrogen sources. Error bars represent the standard deviation. Lines drawn to represent trends

Table 4.2. Maximum specific growth rates for *T. reesei* grown with three different nitrogen sources in 2 L bioreactors. Refer to Appendix B for illustration of the calculations to estimate the maximum growth rate.

Nitrogen source	Max growth rate (h^{-1})
PP	0.23
Soy	0.27
Inorg-N	0.14

Carbon mass balances were made in order to estimate the yields over the total fed carbon for production of biomass, CO_2 and product, and are summarized in Table 4.3. The system error mentioned in Table 4.3 refers to the difference between the total measured amount of broth at the end of the fermentation in comparison with the predicted value on the basis of the feed flow rate. This error is low for the three fermentations, but it is not zero. One source of uncertainty is the evaporation rate, where a value of 1.5 g/h was considered. Historically, 2.5 g/h has been considered to be an appropriate value, but given the fluctuations in the inlet air flow, a lower value seems more appropriate.

The carbon mass balance closure for the fermentations differs depending on the nitrogen source. For the fermentation with peptone as nitrogen source, there is a carbon loss of 5%. The fermentation with soy has a small error: there is an overestimation of 2% more carbon in the outlets compared to the carbon fed to the system. In the case of the inorganic nitrogen source, there is an 8% error, where more carbon is apparently leaving the system compared to what has been added. See Appendix C for a detailed carbon mass balance.

Figure 4.4 shows the yields for the biomass formation, CO_2 and product formation over the total fed carbon for the three fed-batch fermentations with different nitrogen sources. The yield for CO_2 production is similar for the three fermentations; it is between 0.32 and 0.36 C-mol/C-mol. In the case of biomass and product formation, there seems to be an inverse correlation for the Inorg-N and Soy fermentations. The fermentation with soy has a Y_{SX} of 0.31 C-mol/C-mol, while the Y_{SX} for Inorg-N is 0.54 C-mol/C-mol. The yield coefficient for product formation is as follows: Soy = 0.39 C-mol/C-mol and Inorg-N = 0.19 C-mol/C-mol. The fermentation with peptone has a Y_{SX} = 0.37 C-mol/C-mol and a Y_{SP} = 0.21 C-mol/C-mol. Since the main objective in this work was to develop a platform which produces high enzyme titers, soy is selected as the best nitrogen source for further experiments.

Table 4.3. Carbon balances for three fed-batch fermentations with *T. reesei* grown with three different nitrogen sources.

N-Source	System error	In Carbon (C-mol)				Out Carbon (C-mol)				Carbon error
	%	Glc	N-source	Feed	Total	X	CO_2	P	Total	%
PP	3.1	0.26	1.16	1.66	3.08	1.15	1.12	0.65	2.92	-5%
Soy	2.9	0.26	1.04	1.66	2.96	0.92	0.95	1.14	3.01	2%
Inorg-N	-2.2	0.26	0	1.66	1.92	1.04	0.67	0.36	2.07	8%

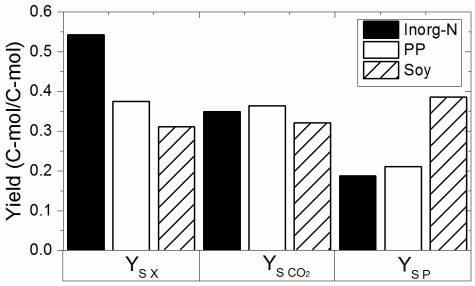

Figure 4.4. Yields for biomass ($Y_{S\,X}$), carbon dioxide ($Y_{S\,CO2}$) and cellulase ($Y_{S\,P}$) production over the total fed carbon for three fed-batch fermentations of *T. reesei* grown with different nitrogen sources.

4.3.3 Control and scalability

Two more fed-batch fermentations were conducted in order to test for reproducibility of the selected platform. One of the fermentations (Lac) was run identically as the soy fermentation in the previous section. The other cultivation (Lac/2) was run with half the concentrations for all the compounds in the medium, inoculum and feed (80 g/L Lactose); this was done in order to test the scalability of the selected platform. Furthermore, an extra fed-batch fermentation (Glc) was conducted as a control experiment. This batch was very similar to the Soy fermentation, but it was fed with glucose instead of lactose. The purpose of this experiment was to compare the basal levels of extracellular protein expression under non-enzyme induction conditions.

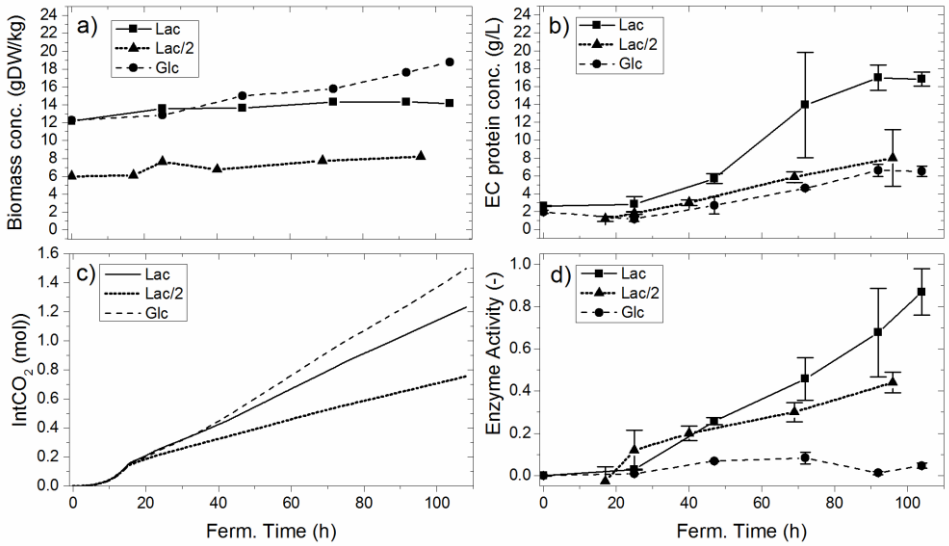

Figure 4.5. Profiles for: a) Biomass concentration; b) Extracellular protein concentration; c) Integrated carbon dioxide production; and, d) Relative enzyme activity for three fed-batch fermentations of *T. reesei* grown with soy as nitrogen source and lactose in the fed, half concentration of nutrients and glucose. Error bars represent standard deviation. Lines drawn to represent trends

Figure 4.5 shows the profiles for biomass concentration (a), EC protein concentration (b), integrated carbon dioxide production rate (c) and relative enzyme activity (d) for three batch fermentations. The Lac and the Lac/2 batches show very similar trends. The values for the four variables displayed in Figure 4.5 for Lac/2 are half the values for Lac, as expected. An important aspect to point out is the fact that the biomass concentration seems to be constant for these two fermentations. This is observed due to the highly diluted carbon solution that has been fed to the system. When looking at the total accumulated biomass (data not shown), the number increases for most of the fermentation, i.e. the fed-batch phase. Nevertheless, there is a slightly reduction in biomass content when passing from the batch to the fed-batch phase at around 25 h. It is hypothesized that the reason for this is the slow feed addition rate. A profile for a typical feed addition rate is shown in Figure. 5.5. The amount of carbon fed to the system at this time is not high enough to sustain the biomass concentration formed after the rapid growth in the batch phase. Thus, the cells are exposed to starvation and this initiates autolysis (McNeil et al. 1998) (White et al. 2002).

For the Glc process a biomass concentration of 18 g/L is observed at the end of the fermentation, in comparison with 14 g/L for the Lac batch. A higher CO_2 production is also observed for Glc. There is production of extracellular protein for Glc, reaching a concentration of 6 g/L in comparison with 17 g/L for Lac. These proteins however do not correspond to cellulases, since the relative enzyme activities for Glc are close to zero. This is in agreement with what is expected, i.e. growth on glucose as carbon source causes catabolite repression of cellulase and hemicellulase genes (Nakari-Setälä et al. 2009).

Carbon mass balances were set up for these three batches (Table 4.4), and the yields for biomass, CO_2 and product formation were estimated (Figure 4.6). The yields for Lac and Lac/2 for biomass, CO_2 and product are almost the same, except for some differences in the biomass yield. However, given the differences in the carbon mass balance closure and the biomass determination method, the differences in the yields may not be significant. The fact that the yields for Lac and Lac/2 are the same confirms the scalability of the selected platform. In the control experiment, Glc, a higher yield for biomass and CO_2 formation is obtained. The yield for product formation is however very low in comparison with the fermentations fed with Lactose, as expected.

Table 4.4. Carbon balances for three fed-batch fermentations with *T. reesei* grown with lactose as inducer (Lac), half the concentration of lactose (Lac/2) and glucose (Glu) in the feed. Soy was used as N source for all fermentations

	Gen	**In Carbon**				**Out Carbon**				
	Error	Glc	N-source	Lac Feed	Total	Biomass	CO_2	Product	Total	error
Lac	-4.7%	1.08	0.27	1.87	3.21	1.10	1.20	1.09	3.40	6%
Lac/2	0.5%	0.52	0.13	0.89	1.55	0.48	0.58	0.52	1.58	2%
Glc	0.6%	1.04	0.26	1.77	3.08	1.16	1.45	0.36	3.00	-4%

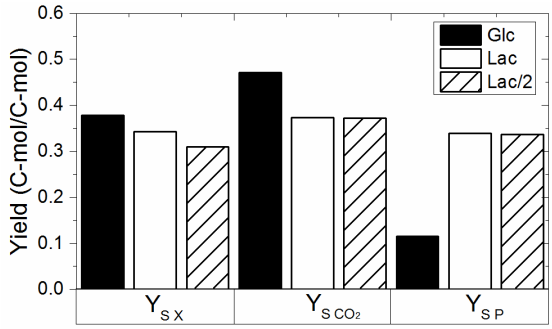

Figure 4.6. Yields for biomass ($Y_{S\,X}$), carbon dioxide ($Y_{S\,CO2}$) and cellulase ($Y_{S\,P}$) production over the total fed carbon for three fed-batch fermentation of *T. reesei* grown with soy as nitrogen source and different carbon sources in the feed.

4.3.4 Statistics of the yield coefficients

In total, three fermentations considered as biological replicates were conducted with soy as nitrogen source and lactose as inducer, they were named: Soy, Lac and Lac/2. Table 4.5 shows the yield coefficients for these three fermentations for biomass, CO_2 and product formation, including as well the mean and the confidence intervals. The confidence intervals for Y_{SX} and Y_{SP} are very large in comparison with the yield coefficient for carbon dioxide formation. This is explained by the large variation in the biomass and extracellular protein determination assays. Thus, for further experiments the biomass measurements should be done in duplicates, in order to consider this large variation. The protein and enzyme activity assay will be performed by a robot. Historical data has shown that the robot has an average coefficient of variation for repetitive measurements <5% for the BCA and enzyme activity assays (personal communication).

4.4 Discussion

The purpose of this chapter was to investigate the effect of three different nitrogen sources (peptone, soy and ammonium sulphate) on cellulase production in order to select the most productive system. The results obtained here were compared internally, but they have to be compared also to the cellulase productivities reported in the literature. The enzyme activity method employed in this work hampers the direct comparison, thus the results obtained had to be translated to filter paper units (FPU), which is the most widely used assay to evaluate cellulase activity reported in the literature (Ghose 1987). However, there is site to site variation in the assay's execution. There is even day to day variation in the assay's implementation. These facts are acknowledged, so the comparison done here may not absolute.

A different fermentation was conducted for the literature comparison. This batch was run at the same conditions as Lac/2, but it was run with a constant agitation of 600 rpm. The FPU were measured at 96 h based on the method proposed by (Xiao et al. 2004).

Table 4.5. Yield coefficients for biomass, CO_2 and product formation over the total fed carbon for the three fed-batch fermentations conducted in this section using soy as nitrogen source.

	Soy	Lac	Lac/2	Mean	Stdev	Confidence intervals
Y_{SX}	0.30	0.34	0.31	0.32	0.020	$0.27 < \bar{x} < 0.37$
Y_{SCO2}	0.37	0.37	0.37	0.37	0.001	$0.37 < \bar{x} < 0.37$
Y_{SP}	0.36	0.34	0.33	0.34	0.013	$0.31 < \bar{x} < 0.37$

Table 4.6 shows the comparison of the cellulase productivities obtained by different research groups using different nitrogen sources to the productivities obtained in this work using soy meal at different reference times. The productivity reported in this work is the second highest and it is only surpassed by the results obtained by Lee & Koo (2001); these authors used an intermittent feeding pattern with a highly inducing non-soluble carbon source. As it was mentioned in the introductory part of this section, at industrial levels these carbon sources are not desired for fed-batch processes, thus is not an alternative for our process, but it is a good a reference to include in the comparison. Table 4.6 also shows that the results obtained here are only 25 % higher than the results reported in the work of Ahamed & Vermette (2008). However, it is important to highlight that the concentration for the feeding solution used in the work of Ahamed & Vermette is 2x higher than the concentration used in this work. Thus, assuming that by doubling the concentration of the lactose feeding solution in the system reported here, a 2x higher FPU concentration should be obtained, it can be estimated that a 150% increase in productivity should in fact be observed.

Table 4.6. Comparison of cellulase productivities by *T. reesei* RUT-C30 reported in the literature.

Reference	Ferm. mode and scale	Inducer	N-source	Ferm. Time (h)	EC protein (g/L)	FPA (U/mL)	Productivity (FPU/L/h)
(Ahamed & Vermette 2008)	Fed-batch. 7 L	Lac (150 g/L) + lactobionic acid (0.1%)	Yeast extract	120	1	5	42
(Patel et al. 2009)	Fed-batch. 22 L	Lac (150 g/L)	Corn steep solids	160	2.75	5	31
(Lee & Koo 2001)	Fed-batch 50 L	Solka Floc (intermittently feeding)	Yeast extract and peptone	210	-	35	167
(Rodriguez-Gomez & Hobley 2013)	Batch 0.5 L	Avicel	$(NH_4)_2SO_4$	216	1.5	1.3	6
(Lehmann 2011)	Batch 5 L	Avicel	Peptone	180	8	7	39
This work	Fed-batch 2 L	Lac (80 g/L)	Soy meal	96	10	5	52

Another aspect for discussion of the selected nitrogen source is its solubility. Soy meal is a non-soluble substance; this is an important issue since the non-soluble particles interfere with the dry cell weight determination, as mentioned before, and it will further interfere with the viscosity measurements. However, the biomass concentration measurements can be reliable from t = 17 h onwards, as confirmed by the CO_2 profiles. Also, it should be highlighted that one of the factors influencing rheology is the shape of the suspended particles. Hyphal-hyphal interactions will have more impact on the viscosity than the sphere-sphere interactions presented by the soy.

4.5 Conclusions

Three fed-batch fermentations were conducted in order to test the effect of nitrogen source on enzyme production of *T. reesei* RedTr. The nitrogen sources tested were soy meal, peptone and ammonium sulphate. The biomass growth was greatly favoured by ammonium sulphate, followed by peptone and soy. Similar yields of carbon dioxide production were estimated for the three nitrogen sources. The highest yield coefficient for product formation was obtained when soy is used as nitrogen source. Thus, this compound will be used as nitrogen source for further experiments.

It was also found that the biological reproducibility of the fed-batch fermentations is good, when on-line measurements of carbon dioxide production rates are compared. Nevertheless, there is a lot of variation in the off-line measurements for extracellular protein and relative enzyme activity. These variations are merely human error. Considering this aspect, further measurements of extracellular protein and enzyme activity will be conducted by a robot. It is expected that automation will significantly decrease the error, as suggested by the historical data.

Furthermore, it was realized that crystallization of lactose in the air inlet port was causing blockage. In order to deal with this phenomenon, further fermentations will be performed by humidifying the air before it is blended with the fed substrate solution. This also has the benefit that evaporation is highly reduced.

Chapter 5. Influence of process variables on morphology and rheology

5.1 Abstract

The influence of agitation intensity on the morphology, rheology and protein production capability of *Trichoderma reesei* RUT-C30 was determined in bench-scale fermenters. Eight fed-batch fermentations were conducted in 2L bioreactors at two different media concentrations and four different agitation speeds. The power input was determined experimentally by calorimetry and the agitation speeds studied covered energy dissipation rates from 2 to 16 kW/m^3. The morphology was measured with laser diffraction and the 90th percentile of the particle size distribution was chosen as the characteristic morphology parameter. No significant differences in biomass concentration, carbon dioxide production rate and enzyme production were observed even at the very high power inputs. However, the morphology and rheology were considerably affected. Furthermore, we introduced a fast and easy method to predict filamentous fungi rheology based on simple measurements of biomass and morphology. This method can be used in strain selection optimization when high viscosity is an issue.

5.2 Introduction

Fermentation processes for the production of industrial enzymes are under continuous optimization so that the enzymes can be produced at lower cost. Manipulation of the medium, improvement of the strain and optimization of various process parameters (pH, temperature, etc.) are among the most relevant strategies for promoting the overproduction of bulk enzymes to meet the global demand (Sivaramakrishnan et al.

2006). However, further improvements are needed if enzyme cost has to be reduced to make some processes economically feasible. Deeper process understanding and the comprehension of the interaction of all the process variables and their influence on the process performance are of outmost importance for further optimization of industrial enzyme production.

Filamentous microorganisms are widely used as hosts for the production of industrial enzymes - mainly the *Aspergillus* and *Trichoderma* species (Demain & Vaishnav 2009) - due to the diverse advantages they possess; specifically (i) their abilities to grow at high rates and in high biomass densities inside large-scale fermenters, and (ii) their natural abilities to secrete high levels of homologous enzymes (Ward 2012). Nevertheless, they also present major drawbacks. When they grow to high biomass densities, the medium viscosity also becomes very high resulting in oxygen transfer limitations. The high media viscosity and the complex rheology is not just a consequence of the high biomass concentrations, but is also related to morphology and growth rate in dispersed fungal growth (Gibbs et al. 2000). An obvious strategy to overcome the oxygen transfer limitations is to increase agitation power. However, for a too high power input process the question of potential physiological damage due to fragmentation or/and morphological changes arises.

The effect of agitation on morphology, productivity and other process variables have been studied in different filamentous fungi species producing homologous and recombinant enzymes (for a comprehensive review see Quintanilla et al. 2015) . The effect of agitation rate at specific power input between 1 and 5 kW/m^3 has been studied in *Aspergillus oryzae* (Amanullah et al. 1999)(Amanullah et al. 2002). Amanullah et al. (2002) reported that mycelial morphology (measured as a mean projected area with image analysis) is dependent on the agitation intensity. Furthermore, the agitation intensity influenced the specific enzyme product (enzyme activity per biomass), while the total enzyme titer remained unchanged. In a different work conducted by Johansen et al. (1998) in *Aspergillus awamori*, a significant effect of agitation on morphology was also observed at specific power inputs between 0.6 and 13 kW/m^3. Nonetheless, the reported morphological differences had no effect on the product formation. Johansen et al. (1998) also characterized the morphology by image analysis and the average total hyphal length was used as the morphological parameter. The highest viscosity was observed for the lowest agitation intensity. They reported lower biomass concentrations at the highest agitation intensities (Johansen et al. 1998). Patel et al. (Patel et al. 2009) however, achieved the highest biomass concentrations at higher agitation speeds in fed-batch fermentation with *Trichoderma reesei*. They also found lower viscosities for the fermentation at the low agitation speeds. There was no clear effect on the enzyme production, since the protein titers only reached 3 g/L (Patel et al. 2009). Patel at el. (2009) also observed higher degree of fragmentation of clump morphology at high agitation intensity measured by image analysis. All these findings are contradictory and no direct correlation between agitation, morphology and enzyme production has been

elucidated. Deeper understanding of how morphology and enzyme production are related and how they are affected by the process conditions will allow targeted process improvements. Based on the investigations reported up to now, it seems as it has not been possible to manipulate one process variable while keeping the rest constant, thereby complicating the interpretation. In this study, we determined the direct influence of agitation intensity on different variables involved in submerged fermentation for the production of cellulases, under high expression, non-oxygen limitation conditions and at power inputs similar to industry, i.e. 3x higher compared to earlier reported studies.

Elucidating the direct relationship between a process variable and product formation in submerged fermentations is not an easy task due to the abundance of interrelated factors, which affect directly and indirectly the productivity (Metz et al. 1979). Therefore, the aim of this work was to make a direct comparison of the effect of agitation speed on the biomass production, morphology, rheology and enzyme production capabilities of *Trichoderma reesei* RUT-C30. The data set created here, by using a very simple set-up, presents clear trends and effects and the results are very easy to interpret. Previous work is hampered by lack of clarity in these respects. The same culture conditions were applied in the batch phase, so when the agitation ramp was implemented (at the end of the batch phase) the formed biomass had exactly the same physiological state. The agitation speeds used correspond to specific energy dissipation rates to those used industrially and even higher (2 to 16 kW/m^3). The actual specific power inputs were determined experimentally by calorimetry according to Ding et al. (Ding et al. 2005). A very low and constant feed rate was applied, which ensured that no oxygen limitations were encountered; this allowed us to remove the effect of fragmentation due to oxygen depletion. In order to achieve different biomass levels and productivities, two different media were prepared, were the second one had 2x the concentrations compared to the first one. This was done in order to test the effect of agitation on fragmentation at different hydrodynamic conditions: the initial amount of carbon in the batch phase would result in a certain biomass concentration; this would then affect the viscosity of the fermentation broth.

Furthermore, the applicability of laser diffraction to characterize fungal dispersed morphology by using the 90^{th} percentile of the particle size distribution (PSD) as the morphological parameter has been introduced. This method has been previously employed to characterize pellet growth with *A. niger* demonstrating its applicability in this type of morphology (Lin et al. 2010). Spore characterization has also been performed with this technology (Wucherpfennig et al. 2011). Rønnest et al. (2012) compared image analysis with laser diffraction for the characterization of *S. coelicolor* cell clumps and pellets proving that both methods can provide similar particle size distributions. Here, we demonstrated the applicability of laser diffraction to get quantitative description of strain morphology. This very simple/straightforward method is a very interesting new possibility to be used as a routine measurement in strain selection stages to get quantitative descriptions of strain morphology, since the time required to get the

information is very short. In addition, we present a simple empirical model to predict rheological properties using the 90th percentile of the PSD and biomass concentration. This model is proposed in accordance with Riley et al. (Riley et al. 2000), where the biomass concentration and the average projected area (measured by the time consuming image analysis) were used to create the model. In addition, the simple correlation propose in this work is an alternative model to the previously more complicated multivariate data models, where the whole PSD is used to predict the rheological properties (Petersen et al. 2008).

5.3 Materials and Methods

5.3.1 Strain and propagation

T. reesei RUT-C30 was used for the experiments. Spores were propagated from freeze-dried ampoules onto potato dextrose agar slopes, following incubation for 7 days at 26°C. The spores were harvested with 8 mL of 0.1% Tween-80 solution. Approx. 4 mL were used to inoculate 250 mL of shake flask media. The shake flask media consisted of: glycerol, 15 (g/L); $(NH_4)_2SO_4$, 13.6 (g/L); bacto peptone, 6 (g/L); KH_2PO_4, 4 (g/L); $MgSO_4 \cdot 7H_2O$, 0.6 (g/L); $CaCl_2 \cdot 2H_2O$, 0.8 (g/L); $FeSO_4 \cdot 7H_2O$, 5 (mg/L), $MnSO_4 \cdot H_2O$, 1.6 (mg/L), $ZnSO_4 \cdot 7H_2O$, 1.4 (mg/L); $CuSO_4 \cdot 5H_2O$, 2 (mg/L); and pluronic, 1 (mL/L). After inoculation, the shake flasks were placed in an orbital shaker at 250 rpm and 26°C for 48h. Different amounts of shake flask broth were used to inoculate the bioreactors according to Table 5.1.

5.3.2 Fermentation conditions and media

The fed-batch fermentations were conducted in 2-L bioreactors with an initial volume of 1.3 L. The vessel diameter was 150 mm and two Rushton turbines were used for agitation with D/T=1/3. Aeration was provided by sparging air through a micro-hole. The initial aeration set-point was 0.75 L/min, which then was ramped up to 1.5 L/min over 1 h. The temperature was set at 28°C and the pH was maintained between 4.5 and 4.8 using 10% (w/v) H_3PO_4 and 15% (w/v) ammonia solution. The dissolved oxygen tension (DOT) was measured by an optical probe (Mettler Toledo). The agitation speed was set to 600 rpm for the batch phase. Just after the start of the fed-batch phase, at 17 h, the agitation was ramped in 1 h to the set point specified in Table 5.1, and it was then kept constant for the rest of the cultivation. The agitation speeds were chosen as follows: the lowest agitation speed which will prevent oxygen transfer limitations corresponds to the lowest agitation tested, and then it was decided to cover a relative broad range of specific power inputs corresponding to realistic industrial levels (Table 5.1).

Two levels of concentrations were used for the batch growth medium. The high concentration batch medium contained the following components per liter: glucose, 6.0 (g/L); $(NH_4)_2SO_4$, 4.0 (g/L); soy meal, 20 (g/L); KH_2PO_4, 4 (g/L); $MgSO_4 \cdot 7H_2O$, 0.6 (g/L); $CaCl_2 \cdot 2H_2O$, 0.8 (g/L); $FeSO_4 \cdot 7H_2O$, 10 (mg/L), $MnSO_4 \cdot H_2O$, 3.2 (mg/L), $ZnSO_4 \cdot 7H_2O$, 2.6 (mg/L) $CuSO_4 \cdot 5H_2O$, 4 (mg/L); and pluronic, 2 (mL/L). The glucose

was sterilized separately and the necessary volume to achieve 1.3 L was added from a 500 g/L glucose solution. The medium with the lower concentration level contained half the mentioned amounts.

At 17 h, a ramp for adding the feed solution was implemented giving a final flow rate of 0.08 g/min at 40 h. After 40 h, the feed flow rate was kept constant. The feed solution consisted of 160 g/L lactose and 5 ml/L pluronic for the cultivations started with 6g/L glucose, and 80 g/L lactose and 5 ml/L pluronic for those started with 3 g/L glucose (see Table 1). During feeding, the feed solution was agitated by a magnetic stirrer at 900 rpm in order to ensure a homogenous mixture. Polypropylene glycol (P200) was added manually when needed in order to control foaming.

Samples were taken at different time intervals and analyzed in duplicates for biomass, extracellular (EC) protein concentration and enzyme activity from the point the feed addition started, when enzyme production was induced. The biomass concentration was measured as dry cell weight as described by (Albaek et al. 2011). The protein concentration was determined with the Bicinchoninic acid (BCA) assay. Enzyme activity was determined using a proprietary enzyme activity assay, and the results are here reported as normalized values on same basis. Morphology and rheological properties were also determined as described below.

5.3.3 Morphology

Laser diffraction was used to monitor fungal morphology. The Mastersizer 3000 with a Hydro SM manual small sample dispersion unit (Malvern Instruments Ltd. Worcestershire, UK) was used to measure laser diffraction. The method was similar to the one described by Rønnest et al. (2012); however 30% laser saturation was used as maximum. Three to four successive measurements were made for each sample.

5.3.4 Rheology characterization

Rheological measurements were carried out in an AR-G2 rheometer (TA Instruments, New Castle, DE) in controlled shear rate mode. The vane and cup geometry was used for the measurements and a gap of 1 mm between the bigger radius of the vane and outer cylinder was used. Temperature was controlled at 28°C. A continuous shear rate ramp from 20 to 600 1/s was implemented in 5 minutes, and approximately 16 measurements of shear stress were taken. In all cases, a power law-type fit was made to the data to give a consistency index (K). The flow behavior index (n) was fixed at a value of 0.55.

5.3.5 Power input determinations

Specific power input determinations were conducted by calorimetry as described by Ding and co-workers (Ding et al. 2005). 1.25 L of a salt solution containing sodium benzoate (0.43% w/w) and potassium dihydrogen phosphate (0.21% w/w) was used as working fluid as in Albaek et al. (Albaek et al. 2008). The heat capacity of water at 25 °C was used for the calculations. The un-gassed and gassed power inputs were measured in the

range of 600 to 1800 rpm. This agitation speed range covers Reynolds number from 25 000 to 75 000, i.e. turbulent conditions. The gassed power input was measured at 1.5 L/min. The air was humidified before entering the fermenter in order to prevent heat loss due to evaporation.

5.4 Results and discussion

5.4.1 Measurements of power draw for the 2L bioreactor

It is important to have a good estimate of the power input to compare the agitation intensity in the vessel and to support process scale-up (Ding et al. 2005). Power measurements by electrical means at this scale are not possible because of the significant losses in seals, bearings, etc. Therefore, power input determinations were done by calorimetry. Figure 5.1 shows a log-log plot of specific un-gassed power input versus agitator speed in the salt solution. Regression through all points yields a slope value of 1.69, R^2 0.99. In the fully turbulent region a constant power number should be expected. Thus, a power versus speed plot on a log-log axis should have a slope of 3 ($P = Po \cdot \rho \cdot N^3 \cdot D^5$) as discussed by (Albaek et al. 2008). This is not the case here, but it can be explained by the fact that considerable surface aeration was observed during the experiments. This surface aeration was higher as the stirrer speed was increased, which reduced the power draw. When the salt solution was aerated, there was not a significant decrease in the power draw in comparison with un-gassed conditions, given that the liquid was already very gassed, as seen in Table 5.2.

Table 5.1 Experimental conditions for fed-batch fermentations

Fermentation ID	Agitation Speed (rpm)	Specific power input (kW/m^3)[a]	Initial Glucose Concentration (g/L)	Inoculum (g)	Lactose feed concentration (g/L)
A600_C3	600	2.2	3	25	80
A1000_C3	1000	5.5	3	25	80
A1400_C3	1400	10.0	3	25	80
A1800_C3	1800	15.7	3	25	80
A600_C6	600	2.2	6	50	160
A1000_C6	1000	5.5	6	50	160
A1400_C6	1400	10.0	6	50	160
A1800_C6	1800	15.7	6	50	160

[a]The values are estimated by fitting a power law curve to the gassed power input results in Table 5.2.

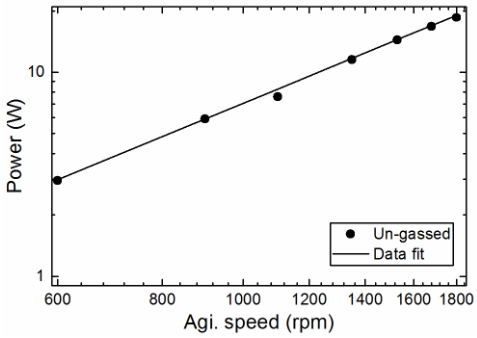

Figure 5.1. Specific un-gassed power input versus agitator speed in a log-log plot for the 2L bioreactor measured in a salt solution containing sodium benzoate (0.43% w/w) and potassium dihydrogen phosphate (0.21% w/w). A regression curve is shown as well

5.4.2 Fermentation Reproducibility

Two fermentations at identical conditions were run in order to test for reproducibility. The conditions for these fermentations were selected as center points, i.e. 1200 rpm and initial glucose concentration 4.5 g/L (the concentration for the other components and the concentrations of lactose in the feed were also modified). Due to some technical problems, it was not possible to achieve 1200 rpm, hence the agitation speed of both fermentations was set to 1050 rpm. The results of these two fermentations are shown in Figure. 5.2. Figure. 5.2a compares the 90th percentile, s_{90}, of the particle size distribution and the extracellular protein concentration. The consistency index (K) from the power law is shown in Figure. 5.2b as a means for comparison of the rheology. The biomass concentration measured as dry cell weight is displayed in Figure. 5.2c, along with the

Table 5.2 Re numbers and specific power input plus standard deviation for the 2L bioreactor measured in 1.25 L salt solution containing sodium benzoate (0.43% w/w) and potassium dihydrogen phosphate (0.21% w/w)

Agi. speed (rpm)	**Reynolds number**	**Un-gassed P/V (kW/m^3)**	**Gassed P/V (kW/m^3)**
600	25000	2.36 ± 0.22	2.33 ± 0.25
900	37500	4.71 ± 0.16	4.24 ± 0.03
1100	45833	6.06 ± 0.30	6.50 ± 0.80
1350	56250	9.23 ± 0.03	8.95 ± 1.18
1530	63750	11.50 ± 0.30	11.85 ± 1.80
1680	70000	13.38 ± 0.59	14.40 ± 0.80
1800	75000	14.84 ± 0.30	16.24 ± 0.74

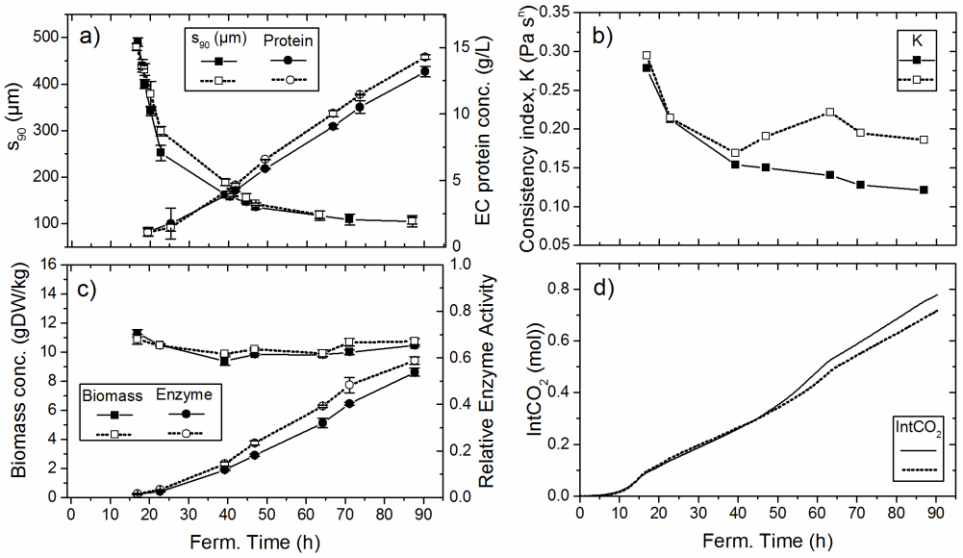

Figure. 5.2 Reproducibility of two fermentations run at 1050 rpm and at initial glucose concentration of 4.5 g/L. a) 90 percentile for particle size distributions and extracellular protein concentration, lines drawn to represent trends.; b) Power law rheological parameters, lines drawn to represent trends; c) biomass concentration and enzyme activity, lines drawn to represent trends; and, d) the produced carbon dioxide in time. Error bars represent standard deviations

relative enzyme activity. The integrated carbon dioxide production rate in time is shown in Figure. 5.2d. The results of morphology are very similar for both fermentations with some differences at the beginning; however, they are identical from t = 40 h onwards. The protein concentrations have the same trend for both fermentations and the values are very similar; nevertheless, the EC protein concentrations for the fermentation indicated with filled circles are somehow lower. The biomass measurements are very reproducible, and there is no variation in the determination method. The enzyme activities for both fermentations have similar trends, but the values for the fermentation represented by the filled circles are smaller, in agreement with the measured extracellular protein concentration. The consistency indexes are similar for the first 40 h of operation. After 40 h there are mayor differences in the measurements. The reason for this is the extreme foaming that was observed in most of the fermentations mainly after 50 h; this is a common problem for this particular strain (Weber & Agblevor 2005; Patel et al. 2009). The broth became very heterogeneous due to the trapped bubbles, which explains the differences in rheology. The morphology measurements were also affected by the foam; however, before the particle size distribution was determined, the samples were centrifuged to remove the air bubbles. This was not done for the rheological measurements, due to the demands for a larger amount of sample for such measurements. Hence, the rheology was measure until 50 h and at the end of each process for the other eight fermentations. The integrated carbon dioxide production rate is reproducible for both fermentations.

5.4.3 Respiration

Eight fed-batch fermentations were conducted at different agitation speeds and media concentrations. The fermentations lasted around 90 h. A600_C6 was shorter due to severe problems with foaming observed since 65 h. For the high media concentration the fermentations were run at 600, 1000, 1400 and 1800 rpm. The same agitation speeds were used for the batches run at low media concentration. As mentioned before, the two different levels of media concentrations were used in order to achieve two different levels of biomass concentrations, which would then give different viscosities due to variation on clump interactions (Olsvik et al. 1993). Figure. 5.3 shows the profiles for the DOT and carbon dioxide production rates (CPR). For the fermentations run at low media concentration, the DOT never falls below 60% (Figure 3a). The DOT is higher for the fermentations at higher agitation speeds, as expected. For most of the fermentations ran at high media concentration, Figure 3b, the DOT stays above the critical value of 20% (Schafner & Toledo 1992). For A1800_C6 the DOT decreases below 20% at 16 h and then it reaches 10% at 17 h. However, the short duration where the DOT is below the critical value is not enough to observe any adverse effects on growth rate and morphology. After this point, the agitation ramp was implemented and the DOT increased very fast. After the agitation ramp started, the DOT for A1400_C6 is higher than for A1800_C6, which is unexpected. But it is important to highlight than when the DOT values are very close to saturation, as for these two fermentations, any small variations during the calibration may have an influence on the measurements. Thus, it may seem that there is a higher oxygen transfer at 1400 rpm than at 1800 rpm. For A600_C6 it is possible to see an increase in DOT from 65 h to 75 h. This is due to the built overpressure caused by foam obstruction; therefore this fermentation had to be stopped at this point due to safety reasons.

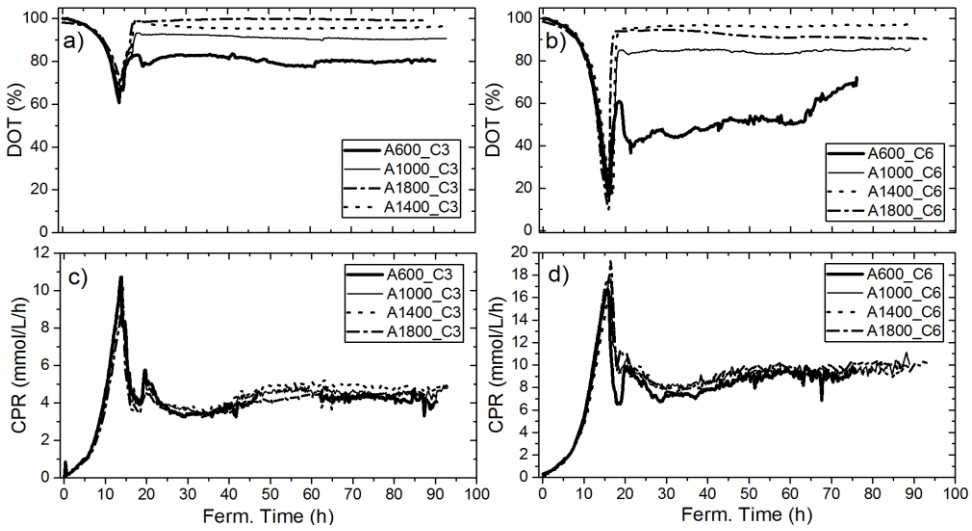

Figure. 5.3 Profiles for dissolved oxygen tension (top) and carbon dioxide production rates (bottom). The results for the fermentations at low media concentrations are illustrated in a) and c); while b) and d) corresponds to the results for the fermentations at high media concentrations

The CPR peaks at 10 mmol/L/h at the end of the batch phase for the fermentations ran at low media concentration. In the case of the fermentations ran at high media concentration, the CPR peaks around 18 mmol/L/h. After 45 h the CPR stays more or less constant. At this point in the fermentations, the CPR values for the fermentations at high media concentration are about the double of the fermentations at low media concentration. This correlates well with the amount of fed lactose and is an indication of non-oxygen limiting conditions. The carbon dioxide production rates at each media concentration are very similar despite the variations in agitation speed.

5.4.4 Biomass and enzyme production

Figure. 5.4 shows the profiles for the biomass concentration, the extracellular protein content and the enzyme activity as a function of time for the eight fermentations. Samples were taken after the batch phase ended, which is the point just before the agitation ramp was implemented, t = 17 h. All the fermentations had the same agitation speed in the batch phase. Thus, no differences in biomass concentration at each media level are expected at this point, as seen in Figure. 5.4a. The biomass content for the four fermentations with high media concentration is the double than for the other four, as expected. In general, the biomass concentration slowly decreases to its lowest level at t = 40 h (that is when the feed addition rate reaches its maximum, Figure. 5.5). From t = 40 h onwards it starts to slowly increase and remains constant for all the fermentations after t = 65 h. For each media concentration, there is no difference in the biomass concentration at the different agitation speeds. Patel et al. (2009) observed the same biomass concentration at the two highest levels of agitation intensity (when oxygen transfer was not a problem) through the batch phase of *T. reesei* RUT-C30 fermentations, i.e. when the same amount of glucose was available (Patel et al. 2009). Also, Lehmann (2011) did not observe an effect of agitation speed on the biomass development for fermentations ran at non-oxygen limiting conditions in batch cultivation using cellulose as carbon source (Lehmann 2011). In another different study with *A. oryzae*, Kold (2010) did not see an effect on biomass formation in two different mixing systems where the flow conditions and mixing mechanisms were very different (Kold 2010). These results in conjunction with ours suggest that agitation speed has no influence on biomass formation under non-oxygen limiting conditions even at very high power inputs. This is however contradictory to the findings of Johansen et al. (Johansen et al. 1998); they observed an increased agitation rate resulted in less biomass production, which was attributed to maintenance requirements.

According to Figure. 5.4b, the EC protein production starts around t = 25 h for all the fermentations. After this point, the production rate is constant. For fermentations operated with low media concentration the protein content is around 9 g/L at t = 90 h. For the fermentations operated with high media concentration there is a protein production up to 17 g/L at t = 90 h, which is almost the double compared to the fermentations at low media concentration. There is an indication of slightly lower protein production for the fermentations ran at the highest agitation speed, i.e. A1800_C3 and A1800_C6. However,

given the measurement error this difference is not large. Figure. 5.4c displays the relative enzyme activity in time; the same trend is observed as for the protein concentrations. Thus, no differences in protein concentrations and enzyme activities are observed at the different agitation speeds for each media concentration, as an indication that there is no influence of the agitation intensity on the production capabilities of T. reesei, even at very high power inputs. This is in agreement with the work of Lehmann (2011), who observed no significant differences on the enzyme production at different agitation speeds in batch cultivations with T. reesei RUT-30, using cellulose as carbon source (Lehmann 2011). These findings, however, are contradictory to an old study by Mukataka et al. conducted in T. reesei QM9414. They observed that high agitation speeds will have a negative effect on the productivity of cellulases (Mukataka et al. 1987).

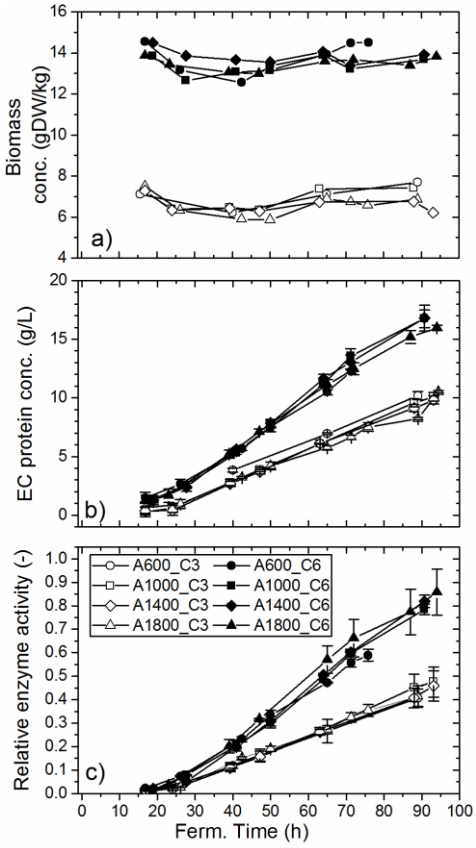

Figure. 5.4 Profiles for a) biomass concentration b) extracellular protein concentration and c) relative enzyme activity for the fed-batch fermentations ran at different agitation speeds and media concentrations. Error bars represent standard deviation, in a) they are smaller than the symbols. Lines drawn to represent trends

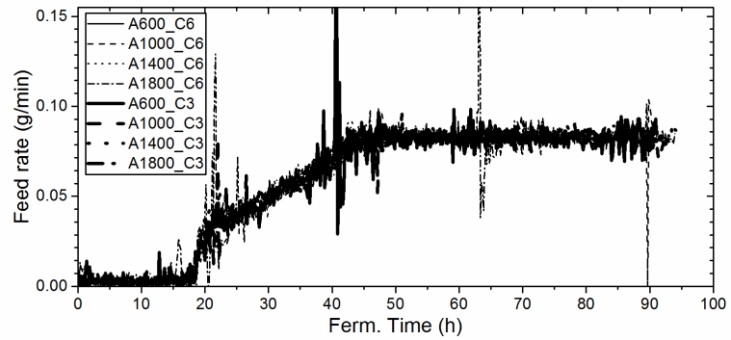

Figure. 5.5 Feed addition rate for the eight feed batch fermentations

5.4.5 Morphology

The morphology of T. reesei RUT-C30 was characterized by measuring particle size distribution with laser diffraction. Figure. 5.6 shows the particle size distribution as volume density for all the fermentations at t = 17 h, i.e. at the end of the batch phase when all the fermentation have the same agitation intensity. Fig. 6a displays the PSD for the fermentations ran at low media concentrations; the distributions are very similar for the four fermentations. Fig. 6b shows the distributions for the fermentations at high media concentration, where the variation is higher. In both figures, most of the size

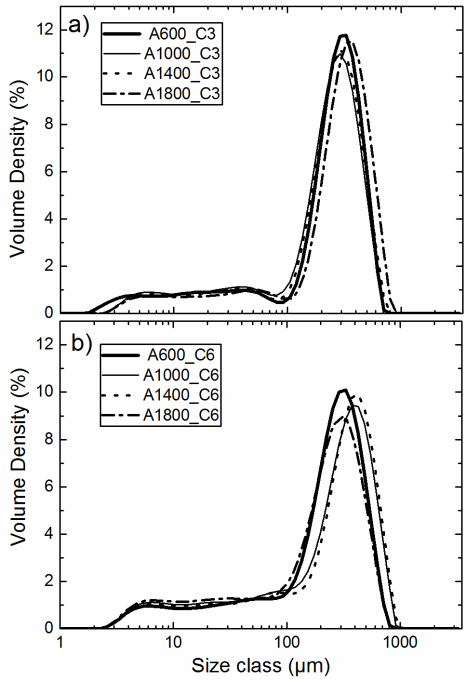

Figure. 5.6 Particle size distribution by volume density for the fermentations at 17 h. a) PSD for the fermentations at low media concentration and b) PSD for the fermentations at high media concentration

distribution is within the range from 200 and 500 µm, which is in agreement with the observations of Ahamed and Vermette, who characterized the morphology of T. reesei RUT-C30 through image analysis (Ahamed and Vermette 2009).

Figure. 5.7 shows the particle size distribution at different times for the cultivation A1400_C6. Data for the sample taken at t = 17 h show larger particles and a narrow distribution around 500 µm. When the agitation ramp has reached its maximum (18 h) the particle size distribution has shifted slightly to the left, i. e. the particles got smaller; however, the shift is more pronounced at t = 22 h. This can be attributed to the fact that the there is still remaining glucose from the batch phase at 18 h. Therefore the growth is bigger at this stage in comparison with 22 h, where the feed solution addition rate is barely 0.025 g/min, Figure. 5.5. The particle size distribution for the next fermentation samples keeps shifting to the left, as an indication of hyphal fragmentation; the clumps keep getting smaller and smaller. This decrease in particle size distribution was consistent in all batches studied.

We used the 90th percentile of the particle size distribution, s_{90}, as the characteristic morphology parameter in order to analyze the fragmentation behavior of T. reesei RUT-C30, Figure. 5.8. Figure. 5.8a shows the s_{90} for the eight fermentations at different times up to the end of each batch, Fig. 8b is a close-up of the fragmentation behaviour for the first 10 h after the agitation ramp is implemented. According to Figure. 5.8a, the 90th percentile decreases in time for all fermentations as an indication of hyphal fragmentation. The fragmentation rate is different at the different agitation speeds, where the fermentations at higher agitation speeds fragment faster, as expected. Also, the fragmentation rate seems to vary within each fermentation. The cells fragment faster at the beginning of the fermentations in comparison to the fragmentation behavior after t = 40 h, suggesting that the cells get stronger with time. This is in agreement with the work of Li et al. (2002c) who observed a change in the fragmentation constant in a fed-batch fermentation with *A. oryzae* (Li et al. 2002c). In their case the fragmentation constant (which is inversely proportional to hyphal strength) was lower for the second half of the fermentation. The 90th percentiles for all fermentations decrease until reaching a certain point, and then the value remains more or less constant. This is in agreement with Li et al. (2002) who observed that the average equivalent hyphal length decreases in time until it reaches a constant value (Li et al. 2000). This is when growth and fragmentation have reached equilibrium in accordance to Nielsen and Krabben (1995).

5.4.6 Rheology

Figure. **5.9** shows the variation of the consistency index, *K*, from the power law rheological mode as a function of time for the eight fermentations. The flow behavior index, *n*, has been fixed at 0.55. This parameter was fixed, since it is relatively constant throughout a fermentation (Olsvik & Kristiansen 1994). For comparison, Riley et al. considered a value for the flow behavior index of 0.35 for fermentations of *Penicillium*

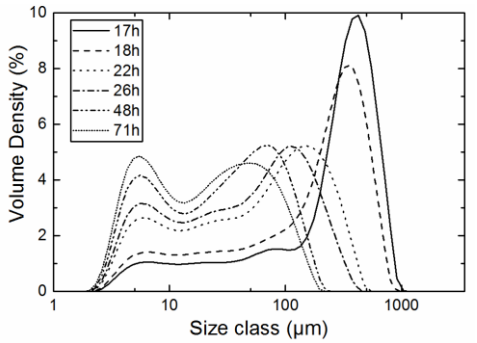

Figure. 5.7 Particle size distribution by volume density at different fermentations times for A1400_C6

chrysogenum (Riley et al. 2000). The consistency index for fermentation broths from *A. oryzae* and *A. niger* were fixed at 0.5 and 0.2, respectively (Riley & Thomas 2010). Fixing a parameter in this type of correlations usually leads to a significant decrease in the variance of the other estimated parameters, since the parameters are very correlated (Petersen et al. 2008). What it means, in fact, is that the data are not sufficiently informative to allow for an independent estimation of all parameters, a problem that is often encountered when fitting a mathematical model to data (see e.g. also (Sin et al. 2009)).

The consistency index at the end of the batch phase is very similar for the four batches at each media concentration. This is expected given that the batches have the same biomass concentration, Figure. 5.4a, and the same PSD, Figure. 5.6. For the fermentations at high media concentration the consistency index is around 0.35 Pa s^n, and for the fermentations at low media concentration it is 0.18 Pa s^n The apparent viscosity in the stirred tank reactor can be evaluated using an average shear rate according to the Metzner and Otto correlation (Metzner & Otto 1957):

$$\dot{\gamma}_{AV} = k_s N \qquad \textbf{Equation 5-1}$$

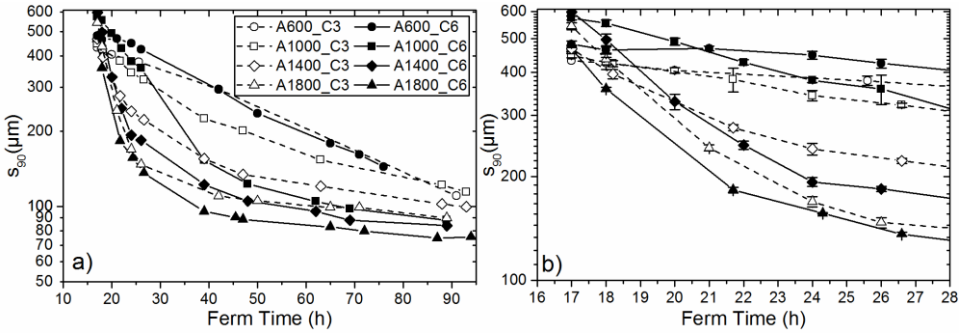

Figure. 5.8 90th percentile of the particle size distribution as a function of time for all fed-batch fermentations ran at different agitation speeds and media concentrations. Lines drawn to represent trends

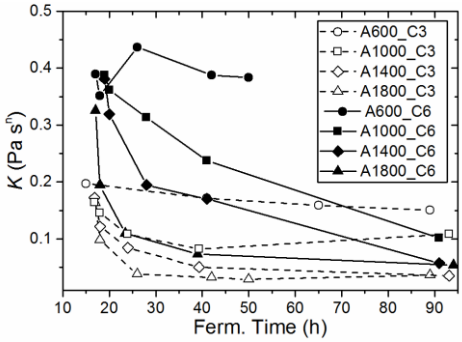

Figure. 5.9 Consistency index power law parameter for the eight fed-batch fermentations run at different agitation speeds and media concentrations

Where k_s is the proportionality constant and has a value between 10 and 13 (Nienow 1990). A value of 11 has been used in this work in agreement with (Nienow 1998) . In the above expression, N is the stirrer speed in s^{-1}. For the fermentations at high media concentration a viscosity of 0.04 Pa s is observed at the end of the batch phase and 0.0016 Pa s for the fermentations at low media concentration. For most of the fermentations, the consistency index decreases in time. This is however not the case for the fermentation operated at the lowest agitation speed, 600 rpm. For A600_C6 the consistency index increases and then remains more or less constant. For A600_C3 it remains more or less constant throughout the process.

The fermentations at low media concentrations have the lower viscosity, as expected; the biomass concentration is lower resulting in reduced hyphal-hyphal interactions (Olsvik & Kristiansen 1994). For the same media concentration, the experiments at lower agitation speeds have the higher consistency index, and it decreases as the agitation rate increases. The trends for the consistency index for the same media concentrations are very similar to the s_{90} trends. This indicates that under no oxygen limiting conditions the viscosity is just influenced by the biomass concentration and the size of the particles. A simple empirical model to predict rheology based on biomass concentration and the 90th percentile of the distribution is therefore presented in the next section.

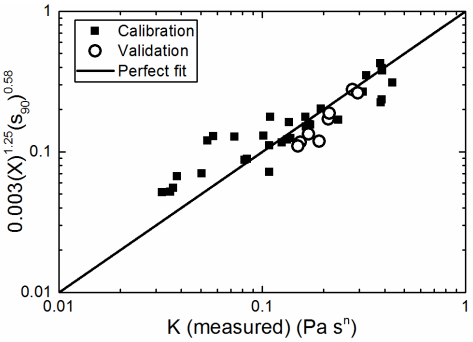

Figure. 5.10 Parity plot of the predicted values of the consistency index versus the experimentally determined values

It is important to highlight that the rheological analysis is only done for the first half of the fermentations, due to the influence of foam for the second half. The very last data point was measured after removing the foam by centrifugation and re-suspension. As pointed out in Section 3.3; no significant difference is observed when comparing samples with or without centrifugation as shown in Figure 3.7.

5.4.7 A simple rheological prediction model

Several studies have intended to correlate the rheological parameters of fermentations broths of different fungal species to morphological parameters determined through image analysis (Olsvik et al. 1993)(Riley et al. 2000)(Gupta et al. 2007)(Riley & Thomas 2010) (Wucherpfennig et al. 2013). Malouf used image analysis to correlate the parameters from the Herschel-Bulkley rheological model to different morphological parameters and biomass concentration for *T. reesei* RUT-C30 (Malouf 2008). In this work, we intended to correlate the consistency index from the power law model to the 90th percentile of the PSD and the biomass concentration. Therefore, using the data displayed in Figure. 5.4a and Figure. 5.8 for biomass concentration and s_{90}, a standard non-linear empirical model was fitted to the data:

$$K = C(X)^a(s_{90})^b \qquad \text{Equation 5-2}$$

Where C, a and b are the parameters to be estimated by the least squares method. Figure. 5.10 shows the parity plot of the predicted values of the consistency index versus the experientially determined values. The validation of the correlation is done with the data from the fermentations run as center points displayed in Figure. 5.2, considering the first 40 h and the end points. The R^2 for the validation points is 0.77, which is reasonably good. We also considered different shapes of the prediction model, however Equation 5-2 showed the lowest R^2 (data not shown). The values for C, a and b are 0.003, 1.25 and 0.58, respectively. These parameter values indicate that the biomass concentration has more influence on rheology than the morphology. These numbers however, should not be considered as absolute values but more as an indication of the influence of biomass concentration and particle size on rheology, since they probably vary with the type of microorganism. The applicability of the correlation found in this work confirms the fact that it is possible to predict rheology based on very simple measurements of morphology and biomass concentration. This method can be used as a standard tool in research and development for selecting strains with desired low viscosity. Rheological measurements are very time consuming and require large amounts of sample, which is usually not available in strain screening stages. Petersen et al. (2008) also used laser diffraction measurements to predict rheological properties of fermentation broths using the whole size distribution (Petersen et al. 2008); however, the type of models used in that work, PLS (Partial Least Square) models, are more complicated and require more advance knowledge from the user compared to the relatively simple correlation that is proposed here. Nevertheless, these more complicated models can be used further on when it is desired to predict rheological properties across scales. As future work to follow up on the

results reported here, we are currently working on a data set for predicting rheological properties across lab, pilot and production scale with more advance models using multivariate data analysis.

5.5 Conclusions

We ran a set of 8 fermentations at different conditions; the agitation speed and the media concentration were varied. The fermentations were fed at very slow feed rates, thus ensuring that no oxygen limiting conditions were encountered. No difference in biomass, product formation and carbon dioxide production over the total carbon feed were observed in our experiments conducted with *T. reesei* RUT-C30 even at very high power inputs. However, the morphology characterized as the 90^{th} percentile of the particle size distribution was significantly affected by the stirrer speed. This study has therefore allowed us to conclude that agitation intensity can be manipulated in order to reduce oxygen transfer limitations and improve bulk mixing. It can also be used to reduce viscosity by affecting the morphology without affecting productivity and it is in agreement with (Johansen et al. 1998; Amanullah et al. 2002).

Furthermore, an easy method to characterize morphology and predict rheology based on knowledge of the 90^{th} percentile of PSD and biomass concentration was introduced. This method and model could be used in strain selection stages for the production of industrial enzymes when an oxygen transfer limitation is an issue due to the high viscosities developed by the strain.

Chapter 6. Influence of scale on the morphology of filamentous fungi

Manuscript in preparation.

"Evaluation of Suitable Models for the Prediction of Fungal Fragmentation across Lab, Pilot and Production Scale"

Quintanilla, D., Hansen, K., Stocks, S. M., Lantz, A. E., Gernaey, K.V.

6.1 Introduction

Mycelial morphology is an important variable in industrial submerged fermentation since it highly impacts the broth rheology; therefore, it is important to understand the factors that affect it. An important factor is agitation-induced fragmentation. A well-established state of the art function, the Energy Dissipation Circulation Function (EDCF), has been used to correlate hyphal fragmentation over a range of scales and impellers types (Jüsten et al. 1996; Jüsten et al. 1998; Amanullah et al. 2000; Amanullah et al. 2002; Nienow 2009). This correlation was however developed for non-growing systems (off-line fragmentation), and no attempts have been made for testing its application across different scales in active fermentation broths.

To test the validity of this correlation, a scale-down experiment was carried out. A production batch from Novozymes A/S operated in a production scale bioreactor (≈ 100 m^3) was scaled down to pilot scale (≈1 m^3). The host strain employed was the filamentous fungus *Trichoderma reesei* growing in dispersed form. Four fed-batch

fermentations were conducted at pilot scale. Different agitation conditions were applied in the processes at this scale to allow a wide range of morphological sizes, while ensuring that the EDCF values for the pilot scale experiments were well below and above the values at the production scale. The morphological characterization was done by determining the particle size distribution (PSD) with laser diffraction. The 90th percentile of the distribution, s_{90}, was chosen as the characteristic morphological parameter. This parameter was chosen since it has shown to correlate well with the rheological properties of fermentations broths, as shown in Chapter 5. Measurements of biomass concentration and rheology were also conducted. The EDCF was calculated for each batch along with other mixing parameters, and they were correlated to the $s_{90.}$ Furthermore, fed-batch fermentations were also conducted at the bench scale (≈0.001 m^3) and the data were used to validate the proposed fragmentation models.

6.2 Materials and Methods

6.2.1 Fed-batch cultivations

A proprietary, recombinant strain of *T. reesei* that originated from strain QM6a was adopted in all fermentations. A complex growth medium was used which is very similar to the one previously described by (Ma et al. 2013), but a different non-soluble nitrogen source was employed in this work. The fermentations were operated as fed-batch in pilot scale and production scale reactors as described by (Albaek et al. 2012). Frozen spores were propagated onto agar plates following incubation. The spores were harvested and used to inoculate a seed tank. The vegetative growth from the seed tank was later used to inoculate the main bioreactors. The agitation conditions in the seed tanks at the pilot and production scale were chosen to match the EDCF. The fermentations were run for similar times and the time is referred as normalized time (NT) using the same basis.

Table 6.1. Equation used in the determination of the energy dissipation circulation function.

Description	Expression	Equation number
Energy dissipation circulation function (EDCF)	$\frac{P}{k' D^3 t_c}$	**Equation 6-1**
Geometric constant	$k' = \frac{\pi}{4}\frac{W}{D_i}\frac{N_V}{6}$	**Equation 6-2**
Circulation time	$t_c = \frac{V_i}{Fl\, N D_i^3}$	**Equation 6-3**
Un-gassed flow number (Radial impeller)	$Fl = \left(0.91\, P_o \frac{W}{D}\right)^{1/2}$	**Equation 6-4**
Un-gasses flow number (Axial impeller)[a]	$Fl = 0.76 P_o^{\frac{1}{3}}$	**Equation 6-5**
Un-gasses flow number (Axial impeller)[a]	$Fl = 0.784 P_o^{1/2}$	**Equation 6-6**

[a] the average of broth expressions is considered for the calculations. N_v is the number of vortices surrounding the impeller: 2 vortices per blade for radial impellers, 1 vortex per blade for axial impellers.

6.2.2 Power input measurements and calculations

Power input at the pilot scale was estimated in a tank with the same dimensions as the ones used for the fed batch fermentations, but then equipped with a torque meter. A salt solution was used as working fluid containing sodium benzoate (0.43% w/w) and potassium dihydrogen phosphate (0.21% w/w), as described by (Albaek et al. 2008). The power input at the production scale was measured directly from the electrical consumption assuming a 10% loss in the motor gearbox, bearings and seals (Hjorth et al. 2000). In the work reported in this chapter the specific power input (Power/volume) and the energy dissipation rate (Power/mass) are referred indistinctly. EDCF calculations were done as specified by (Jüsten et al. 1996) using the equations listed in Table 6.1. In the case where multiple impellers were mounted on the shaft, the EDCF was calculated separately for each of the impellers as described by (Li et al. 2000) and the highest EDCF was used for the correlations.

6.2.3 Agitation conditions

The agitation conditions for the batch phase at the pilot scale were selected to match the k_La at the production scale, as suggested by (Stocks 2013). At NT = 0.17, an agitation ramp was implemented. The agitation intensity at the end of the ramp was selected as the lowest agitation (PS4) required to prevent the dissolved oxygen to fall below the specified set-point during the process, which could otherwise have a negative impact on the morphology (Wongwicharn et al. 1999)(Fazenda et al. 2010). The highest stirrer intensity was selected as a very high agitation intensity to promote a broad range of morphological sizes (PS1). Also, the agitation conditions were chosen ensuring that the EDCF values for the pilot scale experiments were well below and above the values at the production scale, as illustrated in Table 6.2. The agitation speeds for the other two fermentations (PS2 and PS3) were selected considering $P \propto N^3$. The reported values for the energy dissipation rate and the EDCF are normalized by the values of the production batch at the end of the agitation ramp.

Table 6.2. Experimental conditions at the end of the agitation ramp (NT=0.2) for the five fed-batch fermentations at pilot and production scale.

Fermentation ID	Nominal Volume	Relative Energy Dissipation rate	Relative EDCF
PS1	≈1 m^3	3.5	9.1
PS2	≈1 m^3	2.5	5.7
PS3	≈1 m^3	1.2	2.6
PS4	≈1 m^3	0.1	0.5
FS	≈100 m^3	1	1

6.2.4 Off-line measurements

Samples were taken at different intervals and analyzed for the biomass content (cell dry weight per kg medium), particle size distribution (laser diffraction) and rheology. The biomass concentration determination was done by double centrifugation and re-suspension of the broth sample followed by drying to constant weight at 110°C. Biomass concentration results are normalized by the highest biomass concentration value observed in this chapter.

Laser diffraction was used to monitor the morphology. The Mastersizer 3000 with a Hydro SM manual small sample dispersion unit (Malvern Instruments Ltd. Worcestershire, UK) was used to measure laser diffraction. The method was similar to the one described by (Rønnest et al. 2012); however 30% laser saturation was used as maximum. Three to four successive measurements were made for each sample and the 10^{th}, 50^{th} and 90^{th} percentiles were given by the software. To calculate the mean of the PSD and the major mode, the PSD obtained from successive measurements was averaged first by the software and then exported to Matlab for manual calculations. Therefore, standard errors for these two parameters (mean and major mode) are not reported.

Rheological measurements were done in an AR-G2 rheometer (TA Instruments, New Castle, DE) in controlled shear rate mode. The vane and cup geometry was used for the measurements and a gap of 1 mm between the bigger radius of the vane and outer cylinder was used. This geometry was employed to avoid an interference of the suspended particles in the measurements. The vane and cup geometry has been previously compared to the cone and plane resulting in no differences in the rheological measurements for model non-Newtonian fluids, e.g. xanthan gum (Marten et al. 1996; Quintanilla 2013). The temperature for the rheological measurements was controlled at the operating temperature in the fermenter. A continuous shear rate ramp from 20 to 600 1/s was implemented in 6 minutes, and 16 measurements of the shear stress were taken. In all cases, a power law-type expression was fitted to the data to give a consistency index (K). The flow behavior index (n) was fixed at a value of 0.55. This parameter was fixed since it is relatively constant throughout a fermentation (Olsvik & Kristiansen 1994). A more detailed explanation for the chosen value is given in Chapter 3. The apparent viscosity in the stirred tank reactor was evaluated using two methods. The first method was the average shear rate according to the Metzner and Otto correlation (Metzner & Otto 1957):

$$\dot{\gamma} = k_s N \qquad \textbf{Equation 6-7}$$

Where k_s is the proportionality constant and has a value between 10 and 13 depending on the impeller type (Nienow 1990). In the above expression, N is the stirrer speed in s^{-1}.

The other approach was the shear rate calculation derived by (Henzler & Kauling 1985) and further developed by (Sánchez Pérez et al. 2006) to give:

$$\dot{\gamma} = \left(\frac{4P_0\,\rho D^2}{\pi 3^3 K}\right)^{1/(1+n_{PL})} N^{3/(1+n_{PL})} \qquad \textbf{Equation 6-8}$$

As in the case of the EDCF, when more than one impeller was mounted on the shaft, the shear rate was calculated separately for each impeller and the highest value was reported.

6.3 Results

6.3.1 Agitation conditions

Figure 6.1 shows the development of the energy dissipation rate and the EDCF in time. Both parameters have been normalized, each on the same basis considering the values for energy dissipation and EDCF for the production batch at the end of the agitation ramp at NT=0.2 as a reference. The energy dissipation rate is relatively low during the batch phase and then increases when the agitation ramp is implemented, Figure 6.1a. It reaches its maximum at the end of the agitation ramp followed by a slight decrease. The decrease is higher for the fermentations with the highest energy dissipation rates. The oxygen transfer increases with the agitation intensity. Hence, fermentations with higher agitation intensities will allow higher feed rates, which then will increase the volume, thereby decreasing the specific power input. The energy dissipation rate for the production scale fermentation is similar to the specific power input for PS3. The profiles of the EDCF are similar to the energy dissipation rate profiles, Figure 6.1b, but the EDCF for the production scale fermentation is not as close to PS3 as is the case for the energy dissipation rate.

6.3.2 Biomass concentration and rheology

The biomass concentration measurements and the rheological data for the five fed-batch fermentations are reported in Figure 6.2. The biomass concentration, Figure 6.2a, at NT=0 and NT=0.08 is mainly influenced by the non-soluble nitrogen source. For the production scale batch, the biomass concentration rapidly increases until NT=0.3 where it remains constant. PS1 and PS2 follow the same trend as FS. The biomass concentration values for PS1 and PS2 are very similar. For PS3 and PS4 there is a biomass concentration decrease at NT = 0.2. At NT= 0.25 the biomass concentration for PS3 increases significantly to level off at a similar level as PS1, PS2 and FS.

The values of the biomass concentration between NT=0.25 and 0.3 are similar for PS1, PS2, PS3 and FS. This is not the case for PS4. For PS4, the biomass concentration increases at t=0.3 but it is significantly lower than the other four batches; this is the batch with the lowest agitation speed, thus lowest oxygen transfer. For all five fed-batch fermentations the growth rate decreases significantly from NT=0.3 and the biomass concentration remains more or less constant. The biomass concentration values for the FS batch are right in between the biomass values of PS2 and PS3.

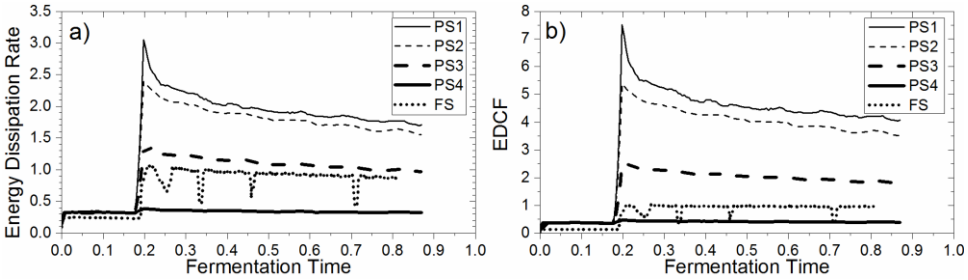

Figure 6.1. Profiles of two scale up/scale down parameters for the five fed-batch fermentations. a) Energy dissipation rate. b) EDCF. Normalization has been done on the same basis for time. The two parameters have been normalized with respect to the production scale values at NT=0.2 as a reference.

The consistency index, *K*, from the power law rheological model is plotted as indication of media viscosity before the evaluation of the shear rate in the tank, Figure 6.2b. In general, the consistency index for all fermentations increases and reaches a maximum and then decreases due to morphological changes, as described below. The maximum value of *K* for FS is achieved at NT=0.6, while the pilot scale fermentations achieve a maximum value for *K* between NT=0.35 and NT=0.45. It is observed that the consistency index for the full scale fermentation is higher than for the fermentation conducted at pilot scale.

The apparent viscosity is evaluated with two approaches to estimate the average shear rate in the tank, using the Metzner and Otto (M&O) approach, Figure 6.2c, and the Henzler and Kauling (H&K) approach, Figure 6.2d. The apparent viscosity evaluated with the M&O shear rate for the FS batch is very high in comparison to the pilot scale batches. When the H&K method is used, the apparent viscosity for FS is not very different from the pilot scale batches, but still higher. In general, the values obtained for the apparent viscosity are higher for the M&O approach compared to the H&K approach.

6.3.3 Morphology development

The morphological characterization in this work was done by determining the particle size distribution with laser diffraction. Laser diffraction has been proved as an easy and fast method to characterize other filamentous hosts, i.e. *Streptomyces coelicolor* and *Aspergillus oryzae* (Petersen et al. 2008; Rønnest et al. 2012). Chapter 5 demonstrated the applicability of laser diffraction for the characterization of *T. reesei* morphology at lab scale. Figure 6.3a shows the whole biomass particle size distribution (as volume percentage) for the five fed-batch fermentations in an early point of the fermentations, close to the end of the batch phase, NT=0.08. An important fact is the insignificant batch-to-batch variation in the morphological characterization, i.e. the processes run at pilot scale are run at the same conditions at NT=0.08 and they present very similar PSD.

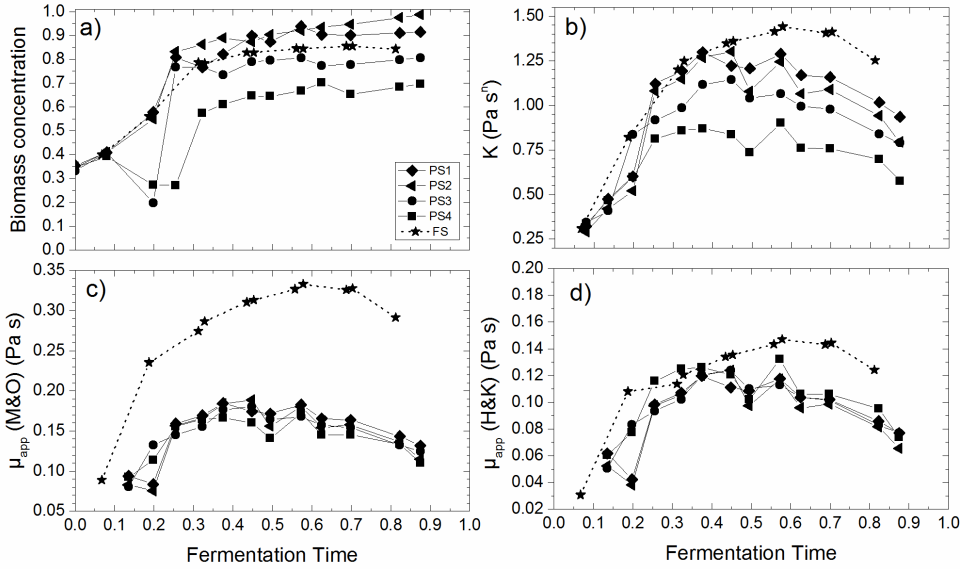

Figure 6.2. Off-line measurements for the five fed-batch fermentations. a) Biomass concentration development normalized on the same basis (highest value observed in the experiments in this chapter). b) Consistency index development. c) Viscosity evaluated with the M&O shear rate method. D) Viscosity evaluated with H&K shear rate method. Lines drawn to indicate trends.

According to a one-way ANOVA test, there is no statistical difference in the 50th percentile of the particle size distribution ($p<0.05$) for the pilot scale fed-batch fermentations at NT=0.08. This parameter has been considered for the statistical analysis at this point, because in the early stages of the fermentations, the non-soluble nitrogen source highly influences other parameters, e.g. the 90th percentile.

When the PSD for the FS batch and the pilot scale are compared, they are very similar. This is expected for two reasons: 1) because the differences in energy dissipation rate and EDCF in the batch phase are small, Figure 6.1; and 2) according to Nielsen and Krabben (1995) in the batch phase growth is larger than fragmentation, so the fungal size should be determined by the maximum growth rate. Thus, if the scale down considering the k_La was successful, no differences in particle size distribution for both scales should be observed at this time. The particle size distribution for this strain is very broad, with particles with diameters that vary between 50 µm and 400 µm. The morphological sizes reported here are smaller than the ones observed in Chapter 5. However, it is important to highlight that in the work reported here an industrial strain is used. The strain in this work has been passed through a series of strain selection stages, possibly screening for lower viscosity, which are translated in lower particle sizes.

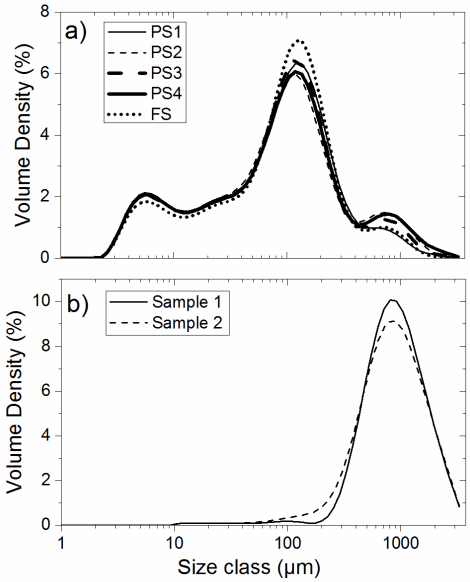

Figure 6.3. a) Particle size distribution of whole fungal biomass at the end of the batch phase for the five fed-batch fermentations. b) Particle size distribution of the non-soluble nitrogen source suspended in water.

It is possible to identify three modes in the particle size distribution: the first mode is observed at 5 µm, the second mode is around 120 µm and the last mode is at 900 µm. The last mode corresponds to the influence of the non-soluble nitrogen source. Figure 6.3b shows the PSD for two samples of the non-soluble nitrogen source suspended in water. These measurements clearly agree with the third mode in Figure 6.3a.

Figure 6.4 shows the particle size distributions at different normalized fermentation times for the five fed-batch processes. The particle sizes for the five fermentation are larger in the batch phase, i.e. NT=0.08, which is in agreement with the observations by (Amanullah et al 2002). They characterize the morphology using image analysis at different agitation rates in fed-batch fermentation with *A. oryzae* (Amanullah et al. 2002). At the end of the batch phase, the bigger clump sizes should be observed. i.e. when mycelial growth dominates over mycelial fragmentation (Amanullah et al. 2002).

The size distributions are very similar for the five fermentations at NT=0.19 (the time just before the implementation of the agitation ramp). At this point, NT=0.19, the PSD has shifted to the left, probably because of a decrease in the growth rate due to less carbon available. Thus, fragmentation starts to dominate over growth. When the agitation ramp is implemented, after NT=0.2, the distribution shifts significantly to the left (i.e. smaller size classes) as an indication of hyphal fragmentation. The shift to the left is less pronounced for the fermentation run at lower agitation intensity, as expected.

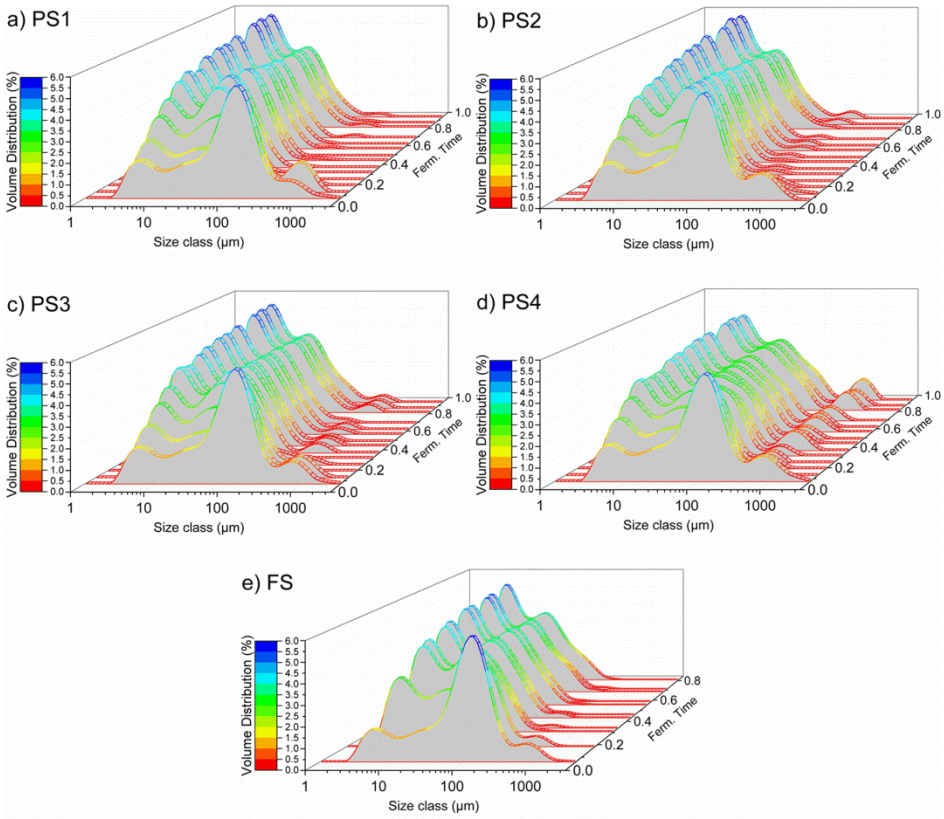

Figure 6.4. Particle size distribution of whole biomass at different normalized fermentation times for the five fed-batch fermentations

Figure 6.5 shows the profiles for different parameters estimated from the particle size distributions. By looking at a single parameter, a better understanding of the data can be achieved. Figure 6.5a shows the mean size of the volume distribution. Figure 6.5b shows the major mode of the particle size distribution. Figure 6.5c shows the profiles for the 90th percentile of the particle size distribution, s_{90}. There is a large variation in the profile of the mean size of the PSD, e.g. the mean size for PS1 never reaches a stable value. Also, for PS3 there are a lot of fluctuations in time. On the other hand, there is no variation when the major mode is employed as a morphological parameter. From the second half of the process all the major modes are around 5 µm. These factors are good reasons to choose the s_{90} as the characteristic morphological parameter, in addition to the fact that the s_{90} has already shown to give good correlation to rheological properties as seen in Chapter 5.

According to Figure 6.5c, for all the batches, s_{90} decreases in time as an indication of mycelial fragmentation over the first third of the processes. From NT=0.3 the s_{90} remains constant for each process. This behavior has been previously reported in other works

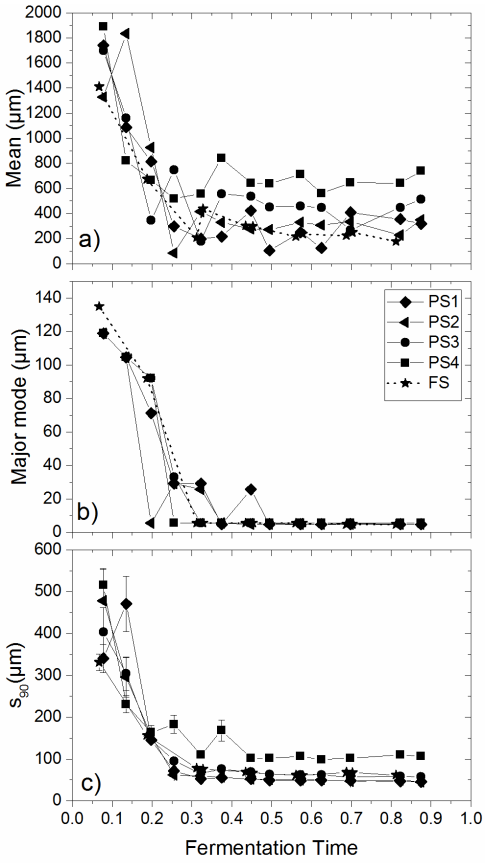

Figure 6.5. Different morphological parameters as a function of normalized time. a) Mean size, b) Major mode and c) 90th percentile of the PSD. Lines drawn to illustrate trends. Error bars represent the standard error of the successive measurements for s_{90}.

conducted in production scale fermentations. Li et al. (2000) observed that the average equivalent hyphal length decreases in time until it reaches a constant value (Li et al. 2000). According to Nielsen and Krabben, there is a point where an equilibrium between growth and fragmentation is achieved (Nielsen & Krabben 1995). For the pilot scale fermentations, the s_{90} is smaller for the batches at the highest agitation intensity as expected. The s_{90} percentile of the PSD for the FS fermentation is similar to the s_{90} for PS3.

6.3.4 Fragmentation prediction across scales

Figure 6.6 shows the 90th percentile of the particle size distribution as a function of different scale up parameters: energy dissipation rate, EDCF, tip speed and shear rate (H&K). The data presented in the graph correspond to the point when an equilibrium length is achieved, i.e. from NT=0.30 to the end of each batch.Appendix D shows a similar graph, but using the mean size of the PSD to illustrate the poor correlation for this morphological parameter.

According to Figure 6.6, there seems to be a general correlation between the energy dissipation rate, EDCF and the shear rate; the s_{90} decreases as a function of each variable, regardless the scale. The tip speed is the only parameter that does not represent a good trend, which is in accordance with (Nienow 2009). The energy dissipation rate and EDCF describe the average value of the 90th percentile rather well, while the shear rate can be used as a basis to predict the trend.

The averages for the data presented in Figure 6.6 for each batch were estimated, see Figure 6.7. A power law trend-line has been fit to the data, and the model equation and the R^2 are displayed. According to the R^2, the energy dissipation rate is the parameter which fits the data best, although the R^2 values are not very different for the other parameters.

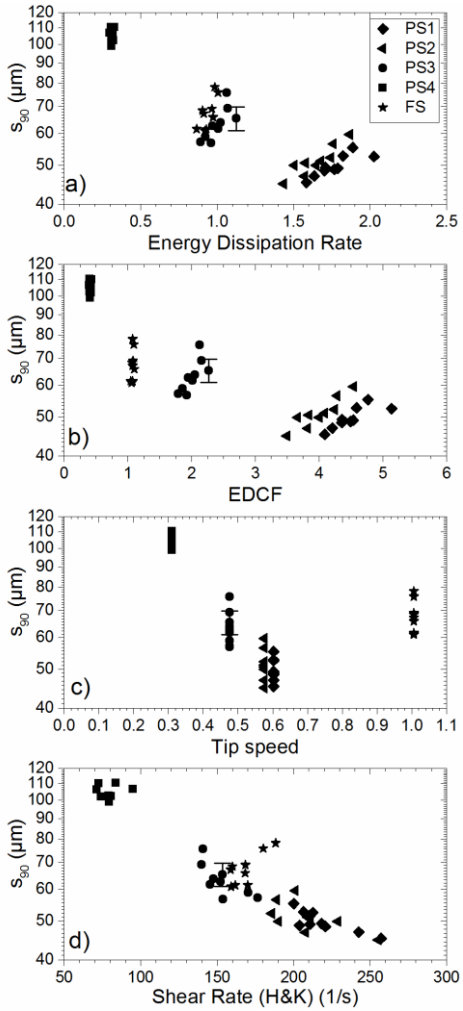

Figure 6.6. 90th percentile of the PSD as a function of different scale up models. a) Energy dissipation rate, b) EDCF, c) Tip speed and d) Shear rate (Henzler and Kauling method).

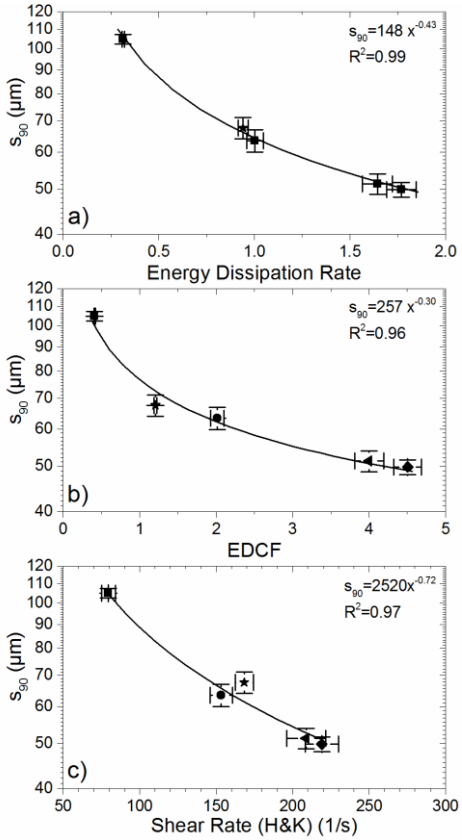

Figure 6.7. Averaged s_{90} as a function of different maximum scale-up parameters. a) Energy dissipation rate, b) EDCF and c) Shear rate. The average values of s_{90} are calculated when steady conditions over hydrodynamics and growth have been achieved (i. e. after normalized time > 0.5). The error bars represent the standard error.

6.3.5 Fermentations at bench scale

Two additional sets of three fermentations were carried out at lab scale (≈0.001 m^3). The first set was run slightly different to the fermentations at the pilot and production scale due to technical problems. The agitation ramp was implemented in an earlier stage. The fermentations for the first set are identified as SS1, SS2 and SS3. The fermentation with the higher agitation rate was SS1, followed by SS2 and then SS3. The agitation conditions were selected in the same fashion as for the pilot scale fermentations. The second set of fermentations was run as a scale-down version of the processes described at the production and the pilot scale, and they are identified as SS1-2, SS2-2 and SS3-2. Specific power input determinations at this scale were done by calorimetry as proposed by (Ding et al. 2005) and as previously described in section 5.3.5. But in this experiment the fermentation broth at the end of each process was used as model fluid. The broth was inactivated by adding 5 g/L of pure acetic acid.

The fact that the agitation ramp was implemented earlier for the first set influenced the biomass development significantly for SS1, SS2 and SS3, thus only the morphological

changes are reported. Figure 6.8 shows the s_{90} in time. As in the case of the pilot and production scale processes, the 90th percentile of the PSD decreases until it reaches equilibrium. The equilibrium is reached between NT=0.4 and NT=0.5; this is different from the time at which the pilot and production scale fermentation reach an equilibrium (NT=0.3).

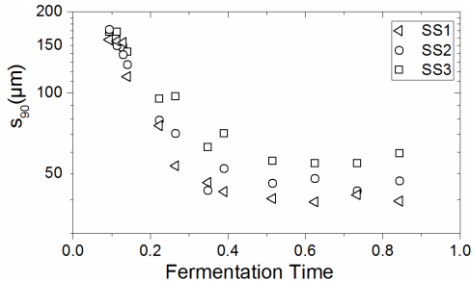

Figure 6.8. 90th percentile of the PSD as a function of normalized time for three fed-batch bench scale fermentations.

The second set of fermentations at the bench scale was run very smoothly. Figure 6.9 shows the profiles for the biomass concentration, consistency index, viscosity (M&O) and the s_{90}. The biomass concentration trend, Figure 6.9a, is similar for the batches at the pilot and production scale. The biomass concentration for the FS batch is close to the values of the SS1-2 process. See Appendix E for a direct comparison. The trend for the consistency index is different for the processes at the production and pilot scale. For the latter processes the consistency index increases and then decreases in time, while for the processes at the bench scale the consistency index keeps increasing at all times, Figure 6.9b. The viscosity for the bench scale processes was just evaluated with the M&O approach, since a lab scale fermenters with a very high viscosity – as the one typically developed by filamentous fungi – have a Reynolds number in the laminar flow (Stocks 2013). The apparent viscosity for SS1-2, SS2-2 and SS3-2 is the same, Figure 6.9c. Figure 6.9d shows the profile for the morphological parameter. According to the data, the equilibrium length is achieved between NT=0.25 and NT=0.35. This agrees with the data from the pilot and production scale batches.

6.3.6 Validation of the fragmentation prediction model

The morphological data from both bench scale fermentation sets was used as a validation for the fragmentation models presented in Figure 6.7. The s_{90} at the end of the fermentation is plotted as a function of the energy dissipation rate estimated by calorimetry, Figure 6.10a. The R^2 for the data presented in the graph is 0.75. The end data point was plotted instead of the average for the equilibrium length, since the power input was measured at the end of each process. It is expected that the power input will change with the different fillings in the bioreactor, mostly due to surface aeration but also due to the degree of filling.

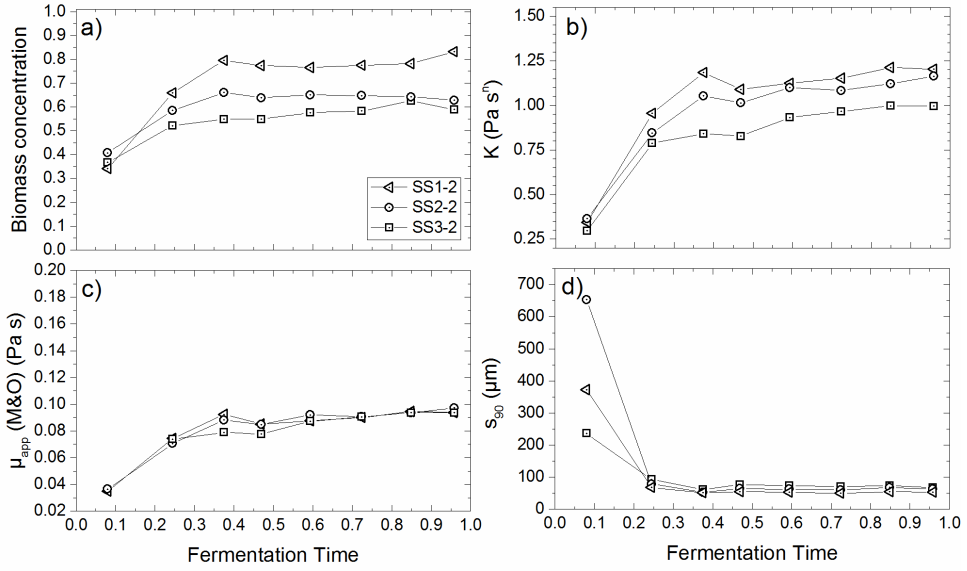

Figure 6.9. Off-line measurements for the second set of fermentations at bench scale. a) Biomass concentration development normalized on same basis (highest value of observed in the experiments in this chapter). b) Consistency index development. c) Viscosity evaluated with the Metzner and Otto shear rate method. D) Morphological parameters s_{90}. Lines drawn to indicate trends.

Figure 6.10b shows the s_{90} at the end of each process *vs* the EDCF. The EDCF at this scale was not easy to estimate. The bench scale reactors were equipped with two impellers mounted very close to each other. Therefore, it becomes very difficult to assign a corresponding volume to each impeller. In order to deal with this, the EDCF was estimated as if a single impeller was mounted on the shaft, but a factor of 2 was used when the impeller height (W) was present in the equations in Table 6.1. The EDCF correlates the s_{90} at the bench scale very poorly (R^2=-1.2).

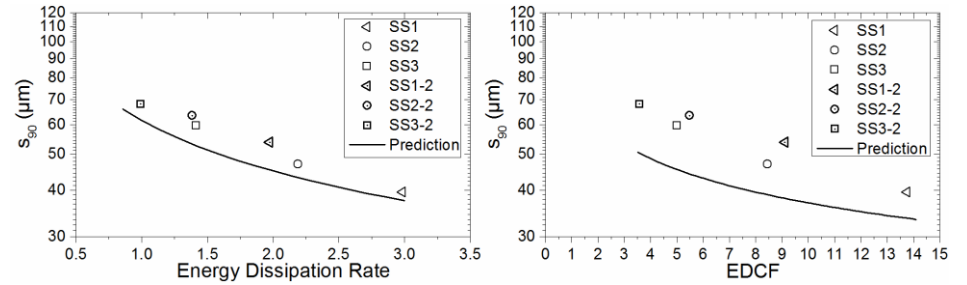

Figure 6.10. 90th percentile of the PSD as a function of the energy dissipation rate and the EDCF for the fermentations at bench scale.

6.4 Discussion

6.4.1 EDCF vs Energy Dissipation Rate

A scale-down experiment was conducted aiming to study the fragmentation behavior of *T. reesei* across scales from >100 m^3 to ≈ 0.001 m^3. The main goal was to test the applicability of the EDCF to predict on-line fragmentation in fermentations broths. The EDCF has been found to correlate better with morphological and fragmentation data than specific power input (P/V) across scales up to 180 L (Jüsten et al. 1996; Jüsten et al. 1998; Amanullah et al. 1999; Amanullah et al. 2000; Amanullah et al. 2002). Other works have used this function to report impeller power at production scales (Li et al. 2000; Li et al. 2002a; Li et al. 2002b). Thus, it is safe to say that this correlation has been accepted as a standard tool to model mycelial fragmentation. Nevertheless, in this study, the energy dissipation rate seems to correlate better across scales when actual fermentation broths are studied.

The EDCF was initially developed in highly diluted systems. Broth samples from a continuous culture were removed, diluted and then subjected to off-line fragmentation (Jüsten et al. 1996; Amanullah et al. 2000). It is hypothesized that the reason why EDCF does not correlate well for the data produced here, has to do with the high viscosities that are observed for the fermentation broths. Let us consider Kolmogorov's theory of isotropic turbulence, which represents a cascade of energy from large scales to small scales within the stirred tank reactor (Li et al. 2002). "Large eddies, generated behind the stirrer blades, are breaking up into smaller ones, thereby dissipating energy. Dissipation by viscous effect (friction losses) increases as the eddy size decreases due to breakup, until finally the small eddies are losing their energy due to viscous dissipation" (van Suijdam & Metz 1981). Kolmogorov assumed that the size of the smaller eddies is independent of external conditions and it is only determined by the amount of energy input and the viscous dissipation:

$$\eta = \left(\frac{\nu^3}{\varepsilon}\right)^{\frac{1}{4}} \qquad \textbf{Equation 6-9}$$

Where η is the so-called Kolmogorov microscale, ν is the kinematic viscosity and ε is the energy dissipation rate. Figure 6.11 shows the Kolmogorov microscale using the M&O approach and the H&K approach to evaluate the apparent viscosity. Independent of the method used for estimating the viscosity, the Kolmogorov microscale is between 200 and 1600 μm. These values are large compared to the mycelial sized observed at all fermentations (35-120 μm). This suggest that eddies in the viscous subrange are responsible for fragmentation, in agreement with (Li et al. 2002). The size of those eddies may just be a function of the energy dissipation rate, since that parameter correlated better with our morphological data in this study.

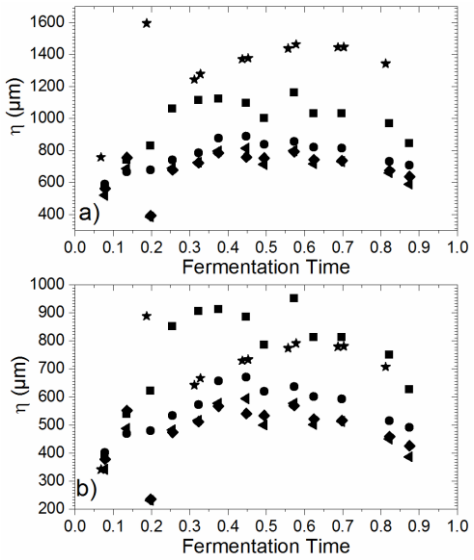

Figure 6.11. Kolmogorov microscale as a function of fermentation time. a) The viscosity is evaluated with the M&O approach b) The viscosity is evaluated with the H&K approach. Symbols as in Figure 6.6**.**

6.4.2 Shear rate in a turbulent stirred tank reactor

In this work, we used two approaches to estimate the shear rate in the tank. The M&O empirical approach and the H&K equation derived through dimensional analysis. We then used these shear rates to further evaluate an apparent viscosity in the tanks across scales. So, the question is then which shear rate should we use/ can we trust? This is a traditional problem when evaluating the apparent viscosity in fermentation tanks at large scale (Stocks 2013). It should not be forgotten that the M&O approach is an empirical correlation that was developed for Reynolds numbers in the laminar and transitional regime, i.e. lab-scale and pilot-scale fermenters (Formenti et al. 2014)(Quintanilla et al. 2015). Thus, the M&O approach is limited to these scales and should not be used in production scales where the Reynolds number calculation confirms that there are turbulent hydrodynamic conditions. In-line with this, our data shows that the viscosity estimated with the M&O approach for the production batch is very different to the viscosities developed at the pilot scale. We speculate that if this was actually the case, it would have been impossible to obtain similar productivities across scales (data not shown). Thus, our data suggest that the apparent viscosity evaluated with the shear rate from H&K is more trustworthy.

Furthermore, when the Kolmogorov microscale is determined with the apparent viscosity from M&O and H&K, Figure 6.11, the profiles for this parameter for the production batch are very different to the Kolmogorov microscale for the pilot scale processes. When the H&K equation is used, the size of the Kolmogorov microscale for the production batch lies between the batches from pilot scale, which is also in-line with the observations for s_{90}. Although, we discussed that the eddies responsible for fragmentation

are in the viscous subrange, and thus not related to the Kolmogorov microscale, it is assumed that they will be proportional to η.

Finally, we have considered the equilibrium length average for the model formulation in Figure 6.7a and Figure 6.7b, which has been validated in bench scale in Figure 6.10, Nevertheless, our data shows a very good correlation from the s_{90} to the H&K shear rate at any time from NT=0.3 onwards for the pilot and production scale batches, Figure 6.6d. This is very surprising and interesting. We suggest that the results found in this work for the shear rate for pilot and production scale could help to validate CFD models.

6.4.3 Higher viscosity at the production scale

We evaluated the apparent viscosity in the tank for the pilot and production scale batches using two approaches to estimate the shear rate. We concluded that the μ_{app} evaluated with the H&K approach seems more reliable, since the values for the apparent viscosity across scales are closer to each other when using this approach. However, it is still unclear why the values of apparent viscosity and/or consistency index for the production scale are higher than the pilot scale batches given the fact that the biomass concentration and s_{90} values for FS are in between the values for the pilot scale. I.e. it would not be possible to construct a simple rheological model, as the one described in Section 5.4.7, using only the biomass concentration and s_{90} as input. We are currently working with this data set to create a multivariate model to predict rheology across scales based on the work by (Petersen et al. 2008). It is likely that the bump between 400 and 600 µm, probably coming from the non-soluble nitrogen source only observed in the pilot scale batches in Figure 6.4, does not contribute to rheology due to the spherical shape. Preliminary work on this topic can be found in Appendix F.

6.4.4 Averages values vs maximum values

In this work, the EDCF and shear rate are reported as maximum values when multiple impellers are mounted on the shaft (i.e. the production batch). Other works have reported average values for the EDCF for multiple impellers systems, i.e. (Li et al. 2000). In our data, the maximum value correlates better than the average (see Appendix G for correlations when averages are used). A plausible explanation is the range of the growth kinetics in comparison with the circulation and mixing times. Let's consider a typical hyphal tip extension rate of 2 to 8 µm/tip/h (Nielsen & Krabben 1995); this range is very small in comparison with the mixing time for a full size reactor, which ranges from 20-25 s for a 53 m^3 bioreactor (Pollard et al. 2007) to 100-200 s for a 80 m^3 bioreactor (Li et al. 2002b). Thus, the forces that are actually dictating the size of the particles are the maximum values rather than the average values.

6.5 Conclusions

The objective of this study was to determine the applicability of the energy dissipation circulation function (EDCF) to predict hyphal fragmentation across scales in actual fermentations broths, i.e. in a situation with actively growing hyphae. In order to do this, a production batch run in a production scale bioreactor (≈ 100 m^3) was scaled down to pilot plant fermenters (≈1 m^3) and biomass concentration, rheology and particle size distribution were monitored. Furthermore, fermentations at bench scale (≈0.001 m^3) were conducted, and the morphology was analyzed. This data set functioned as a validation for demonstrating that the energy dissipation rate is better able to predict the fragmentation across scales. We suggest that this parameter is a better approach, mainly due to its simplicity.

Furthermore, this works sheds light into which is the best method to estimate the shear rate for an industrial size reactor, i.e. a reactor with turbulent conditions. The H&K equation gives better results for apparent viscosity, the Kolmogorov microscale, and the H&K equation is indeed able to correlate the s_{90} for the production and pilot scale fermentations. Also, for a multiple impeller system the maximum value for the estimated parameters gives better results than the average values.

Chapter 7. Physiological responses of filamentous fungi in submerged fermentation

7.1 Introduction

Morphology is important in industrial fermentation processes involving filamentous fungi since it affects the rheology. The deeper understanding of how fungal morphology is affected by the process conditions will allow targeted process improvements. For example, Haack et al. (2006) studied the morphology and physiology of *A. oryzae* producing lipase in submerged fermentation. They reported an increase in hyphal tip diameter, presumably connected to the increase in lipase activity; they proposed that their findings can be used to determine the fraction of producing cells in large-scale reactors as an indirect study of heterogeneities (Haack et al. 2006).

The work reported in this chapter aims to study the morphological development of *T. reesei* in pilot scale fermentations. In this study, the fungi are fed according to the estimated on-line biomass concentration and oxygen mass transfer capabilities of the system. The biomass concentration was estimated using a very sophisticated soft senor which has been reported in (Mears et al. 2017). Samples were collected at different times and the particle size distribution was measured with laser diffraction. The 90^{th} percentile was considered as the morphological parameter.

7.2 Materials and methods

7.2.1 Fermentation samples

Samples were collected from four fed-batch fermentations of a filamentous fungal strain (*Trichoderma reese*i, proprietary strain) producing an industrial enzyme. The samples were analysed for biomass concentration, viscosity and particle size distribution. This set of fermentations is part of the work reported in (Mears et al. 2017). All fermentations were conducted in bioreactors of 550 L total volume. Sixteen samples were collected from each fermentation. The time has been normalized on the same basis (NT).

A detailed description of the fermentation processes cannot be given for commercial reasons, but the processes were in general operated as follows: a stoichiometric mass balance was used along with off-gas measurements and ammonium addition to determine the current rates of product, biomass and water formation. Also, the rate of feed consumption was estimated, i.e. it was estimated how much carbon should be added to the system based on the actual amount of biomass. After these quantities were estimated, they were used as input to a mechanistic model. The model considered the mass transfer capabilities of the system and it determined whether the estimated amount of added feed would allow the dissolved oxygen tension (DOT) to follow the specified set point profile. The fermentations were conducted at the same conditions until the normalized fermentation time (NT) was equal to 0.16. From that point, ramps for changing the agitation speed, aeration and back were implemented. The new set points for those three variables were achieved at NT=0.22. The different operating conditions allowed for different levels of biomass and product concentrations due to different oxygen mass transfer capabilities. The experiment was carried as a 2^{3-1} fractional factorial design (Table 7.1). The fed addition started around NT=0.16. More details about the process and the model can be found in (Albaek et al. 2011; Albaek et al. 2012; Mears et al. 2017).

7.2.2 Sample characterization

The biomass concentration was measured in duplicates as dry cell weight by double centrifugation and re-suspension of 2-3 grams of the fermentation broth, followed by drying to constant weight at 110°C, as described by (Albaek et al. 2011). The results are reported as normalized values on the same basis. The weight from the non-soluble media components was also considered in the measurements.

Table 7.1. Experimental design of the four fermentations analysed in this study. Two levels for each factor were used, a high and a low variation, and they are indicated by the plus and minus sign, respectively. Note: the word batch is just used to label the fermentation. All experiments were carried out as fed-batch.

Fermentation ID	Agitation speed	Aeration	Back pressure
Batch 1	+	+	+
Batch 2	+	-	-
Batch 3	-	+	-
Batch 4	-	-	+

Rheological measurements were done in an AR-G2 rheometer (TA Instruments, New Castle, DE) in controlled shear rate mode. The vane and cup geometry was used for the measurements and a gap of 1 mm between the bigger radius of the vane and outer cylinder was used. Temperature was controlled at the operating temperature in the fermenter. A continuous shear rate ramp from 20 to 600 1/s was implemented in 6 minutes, and 16 measurements of shear stress were taken. In all cases a power law type fit was made to the data to find the consistency index (*K*). The flow behavior index (*n*) was fixed at a value of 0.55. This parameter was fixed since it is relatively constant throughout a fermentation (Olsvik & Kristiansen 1994). The apparent viscosity was evaluated both, with the Metzner and Otto approach using a k_s equal to 10 (Metzner & Otto 1957), and with the Henzler and Kauling equation (Henzler & Kauling 1985) derived by Sánchez Pérez et al. (2006).

$$\dot{\gamma} = \left(\frac{4P_0\,\rho D^2}{\pi 3^3 K_{PL}}\right)^{1/(1+n_{PL})} N^{3/(1+n_{PL})} \qquad \textbf{Equation 7-1}$$

The morphological characterization was done by measuring the particle size distribution with laser diffraction using the Mastersizer 3000, with a Hydro SM manual small sample dispersion unit (Malvern Instruments Ltd. Worcestershire, UK). The method was similar to the one described by Rønnest et al. (2012). Three to four successive measurements were made for each sample and the particle size distribution was reported as volume density by the Mastersizer 3000 software.

7.3 Results

7.3.1 On-line biomass estimation dynamics

Four fed-batch fermentations were conducted at pilot scale to test a soft sensor model to monitor and control the process with the filamentous fungus *T. reesei* (Mears et al. 2017). One of the core parts of the model is that it is able to estimate the biomass concentration in the bioreactor based on stoichiometric balances and off-gas measurements. Figure 7.1 presents the relative biomass concentration model estimation for the four fermentations ran at different conditions according to Table 7.1. Batch 1 is estimated to have the highest biomass concentration, followed by Batch 2. For Batch 4, and Batch 3 the model calculated lower biomass concentrations. The estimated biomass concentration profiles for Batch 1 and Batch 2 were very similar. For both fermentations the biomass concentration increased until around NT=0.6, then the rate of increase slowed down. The biomass concentration profiles given by the model for Batch 3 and Batch 4 had a comparable profile until around NT=0.7. After NT=0.7, it seemed as the biomass concentration stayed constant for Batch 3, whereas a slow increase could be seen for Batch 4.

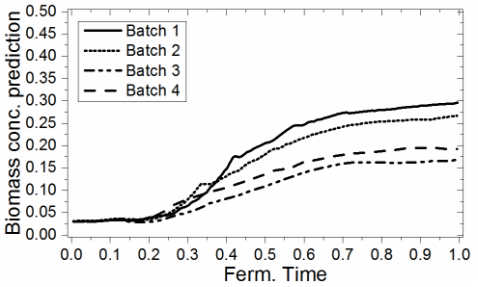

Figure 7.1. Biomass concentration model estimation for the four fed-batch fermentations run at different conditions for agitation, aeration and back pressure in pilot scale fermenters. Results are normalized on the same basis. The results are part of the work reported in (Mears et al. 2017).

7.3.2 Dry cell weight and viscosity evolution

The off-line biomass concentration measurements and the rheology data for the four fed-batch fermentations are reported in Figure 7.2. The results for the biomass concentration, Figure 7.2a, are reported as normalized values on the same basis. True results are not displayed due to confidentiality reasons, but similar values have been previously reported for other filamentous fungi processes (Booking et al. 1999; Amanullah et al. 2002; Bhargava et al. 2003b). The high values of biomass concentration at the beginning of the process observed in all fermentations were caused by the non-soluble media components. The biomass concentrations profiles for Batch 3 and Batch 4 followed each other closely throughout the fermentations although the values for Batch 4 were slightly higher than for Batch 3. This is in accordance with the estimated on-line biomass concentrations, Figure 7.1. The variation in the duplicate measurements for Batch 3 and Batch 4 was very low. The standard deviations were smaller than the symbols and thereby not visible in the figure. The similarity in the biomass concentrations for these two fermentations resulted in similar rheological development, as can be seen in Figure 7.2b, but the values determined for the consistency index, *K*, for Batch 4 were larger compared to those seen for Batch 3.

The biomass concentration measurements for Batch 1 and Batch 2 were also rather similar, although some deviations are seen and the values for Batch 1 were slightly higher, which is in agreement with the on-line biomass concentration estimation, Figure 7.1. The profiles for the consistency index for Batch 1 and Batch 2 showed the same trend, but the values for Batch 1 were higher than for Batch 2, i.e. there is a difference of 0.2 Pa s^n between Batch 1 and Batch 2 at all times from NT=0.4 onwards.

The apparent viscosity was evaluated with two approaches to estimate the average shear rate in the tank, the Metzner and Otto approach, Figure 7.2c, and the Henzler and Kauling approach, Figure 7.2d. In general, the values obtained for the apparent viscosity were higher when using the first approach. It is also important to notice that the differences are very large, i.e. more than 100%. This is a major consideration when developing correlations for viscosity prediction and oxygen transfer.

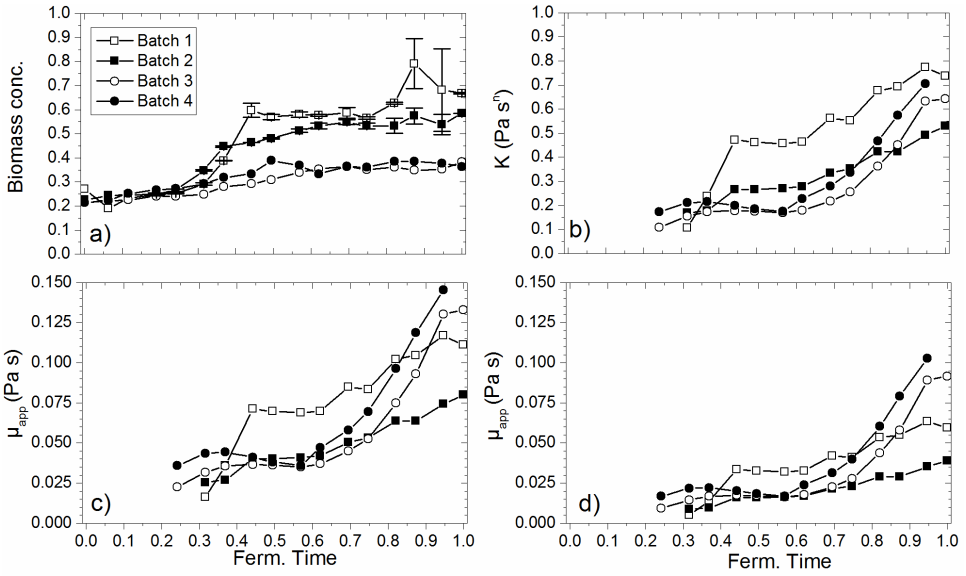

Figure 7.2. Off-line measurements for the four fed-batch fermentations. a) Biomass concentration development normalized on the same basis. Error bars represent the standard deviation. b) Consistency index development. c) Viscosity evaluated with the Metzner and Otto shear rate method. d) Viscosity evaluated with the Henzler and Kauling shear rate method. Lines were drawn to indicate trends.

7.3.3 On-line measurements

Selected on-line measurements are displayed in Figure 7.3. All axes are scaled due to confidentiality reasons. Until NT=0.75, all fermentations, except Batch 1, followed the specified DOT-set point profile, Figure 7.3a. Batch 1 was run with a higher oxygen mass transfer, Figure 7.3b. It is also the fermentation with the highest biomass concentration. Thus, it is the fermentation, which received more feed, Figure 7.3c. When the oxygen mass transfer started to decrease, at approx. NT=0.33, the feed solution addition rate slowly decreased At NT=0.4, when the DOT deviated in a negative way from the set-point, the feed was stopped for a while. After this point the DOT followed the specified DOT set point profile.

From NT=0.75, the DOT for Batch 3 and Batch 4 diverged from the specified DOT set point profile: the DOT for Batch 4 started decreasing at approx. NT=0.77 and it reached 0 at NT=0.83. The feed solution addition rate was already extremely low at NT=0.7. For Batch 3 the feed solution addition rate was dramatically reduced at NT=0.77. Batch 1 and Batch 2 stopped receiving feed from NT=0.9. These observations are important to have in mind for the later discussion of morphological development.

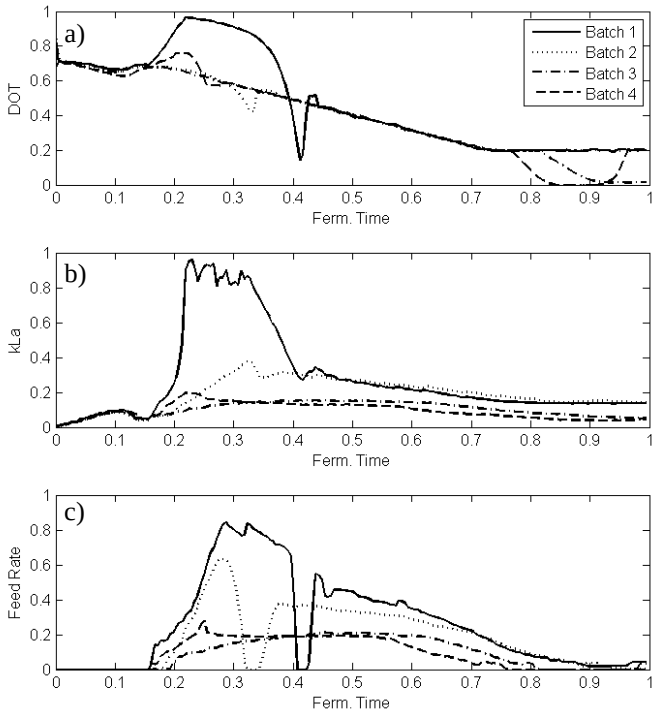

Figure 7.3. Selected **o**n-line measurements for the four fed-batch fermentations. a) Dissolved oxygen tension. b) Volumetric mass transfer coefficient (calculated with on-line data). c) Feed rate per mass of broth. Scaled axes labels for confidentiality reasons.

7.3.4 Morphology development monitored as particle size distribution with laser diffraction

Figure 7.4 displays the averaged particle size distribution (PSD) for four consecutive measurements for selected time points from the four fed-batch fermentations. The PSD for the four fermentations are very similar at a point in the batch phase, NT=0.07. Here, all the fermentations were run at the same conditions, thus the similar PSD were expected. Nevertheless, an analysis of variance (ANOVA) showed a statistical difference for the 50th percentile for Batch 1. This is not so surprising due to the biological variation. In general, the PSD for NT=0.07 was very broad and it showed a bimodal distribution, where the size of the particles ranged between 3 to 700 µm with the major mode around 180-200 µm for all fermentations. At NT=0.33, the PSD had shifted to the left, which is an indication of hyphal fragmentation. This shift was more pronounced for Batch 1 and Batch 2 as expected, since they were run at higher agitation speeds. The major mode for Batch 1 and Batch 2 at NT=0.33 lied between 50 and 60 µm; while the major mode for the other two fermentations was between 90 and 100 µm. At NT=0.50, the major mode for Batch 1 and Batch 2 had decreased by approx. 20 µm. The distribution kept shifting to the left for these two processes. At NT=0.75, a unimodal distribution with the mode at 10 µm was seen. At the end of the fermentation, the left side had shifted even more.

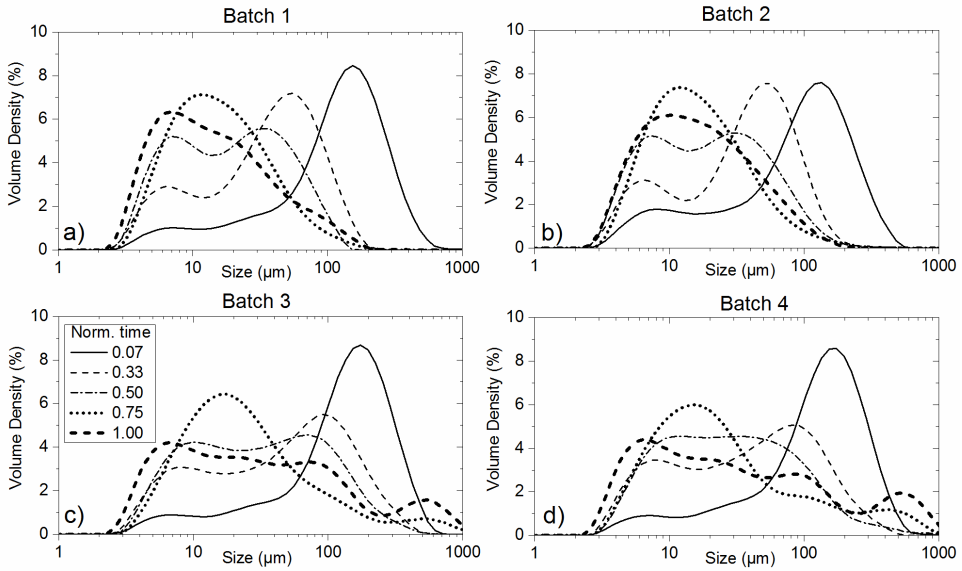

Figure 7.4. Particle size distribution estimated as volume density at different normalized times a) Batch 1, b) Batch 2, c) Batch 3 and d) Batch 4. The lines in the four graphs correspond to the legend in graph c.

For Batch 3 the PSD also showed a reduction in size from NT=0.33 to NT=0.50. The major mode reduced by approx. 20 µm. At NT=0.75 there seemed to be a unimodal distribution, with a small bump around 500 µm. The bump was very pronounced at the end of the fermentation (NT=1.0). The same trend was observed for Batch 4, but the effects were more pronounced; already at NT=0.50, the size of the particles on the right side of the distribution had overpassed the PSD for NT=0.33 at the right end. At NT=0.75, for Batch 4 the number of particles at 500 µm was larger than for Batch 3. The PSD at NT=1.0 were very similar for Batch 3 and Batch 4, with an increased number of particles at 500 µm compared to NT=0.75.

To simplify the particle size analysis for all the collected time data points, the 90th percentile of the particle size distribution, s_{90}, was considered, Figure 7.5. This parameter was used since it has shown to give a good correlation with rheological properties and fragmentation prediction across scales according to Chapter 5 and Chapter 6, respectively. Again it can be seen that the particle size distributions for Batch 1 and Batch 2 behaved very similar, as already pointed out in Figure 7.4. For Batch 1, the s_{90} decreased from 288 ± 8 µm (at NT=0.07) to 46 µm ± 0.8 µm (at NT=0.75). The numbers were very similar for Batch 2. After this point, the s_{90} slightly increased; the s_{90} increased with around 10 µm from NT=0.75 to NT=1.00.

For Batch 3 and Batch 4, the s_{90} decreased from 313 ± 15 µm (Batch 3) and 299 ± 13 µm (Batch 4) at NT=0.07, to 112 ± 2.2 µm (Batch 3) and 114 ± 14.1 µm (Batch 4) at NT=0.58. In the next data point, the s_{90} for Batch 4 started increasing, and it reached its

highest value at NT=0.83, 355 ± 120 µm. For Batch 3 the size started to significantly increase from NT=0.75 to NT=0.83, from 120 ± 11 µm to 390 ± 201.5 µm.

Figure 7.6 shows microscopic images for three time points towards the end of the fermentations for the four experiments; Batch 3 and Batch 4 present very long hyphae lacking branching.

7.4 Discussion

The morphological development for *T. reesei* was monitored in fed-batch pilot scale fermentations. The morphology was characterized by measuring the volume weighted particle size distribution with laser diffraction and the 90th percentile of the distribution was chosen as the morphological parameter.

The on-line estimated biomass concentration and the off-line analyzed dry cell weight differed due to the influence of the non-soluble media compounds considered in the off-line measurements. But, importantly, both methods presented the same trend: higher biomass concentrations were observed at the higher agitation speeds, i.e. at the higher mass transfer rates. At the same agitation speed, higher biomass concentrations were obtained when higher back pressure was applied. The aeration seemed to only play a minor effect on biomass formation. The reason for this was the higher k_La observed for Batch 1 and Batch 2, Figure 7.3b. This is contrary to the findings of Johansen et al (1998), whom observed higher biomass concentrations for *Aspergillus awamori* at the lower agitations speeds. They suggested that the maintenance requirements arising from a substantial cell damage due to the higher agitation rates resulted in less biomass concentration (Johansen et al. 1998). Our results are in accordance with the findings reported by Amanullah et al. (2002) and (Patel et al. 2009), who investigated the effect of agitation intensity on biomass formation by *Aspergillus oryzae* and *Trichoderma reesei*, respectively. Chapter 5 also reports no influence of agitation intensity on biomass development when the same amount of carbon is available.

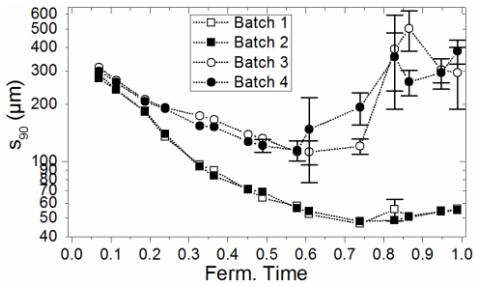

Figure 7.5. 90th percentile of the PSD for the fed-batch fermentations as a function of time. Lines drawn to indicate trends. Error bars represent standard deviation for four PSD measurements.

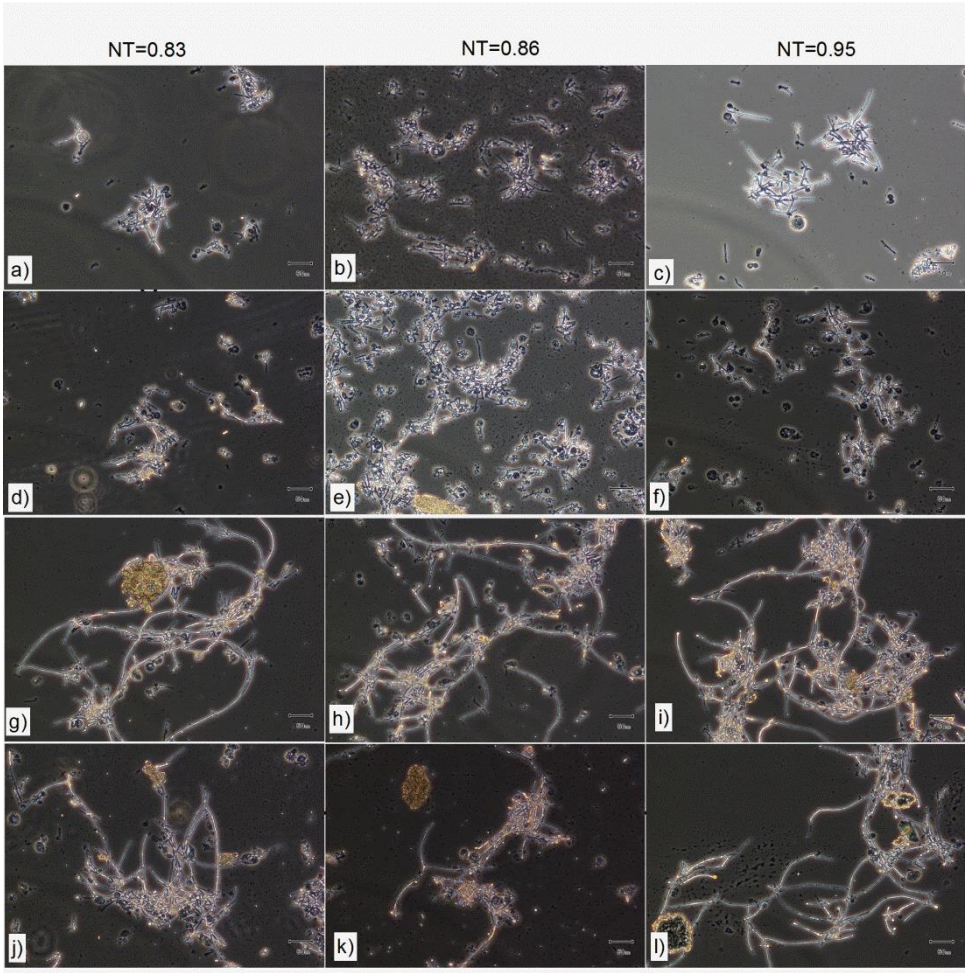

Figure 7.6 Morphological development in time for the four fed-batch fermentations. Batch 1 a) b) c). Batch 2 d) e) f). Batch 3 g) h) i). Batch 4 j) k) l). The sample time corresponding to each picture it is specified in the top of the figure.

Before discussing the morphology development, it is important to highlight the very large standard deviations in the s_{90} measurements for Batch 3 and Batch 4 for the second half of the processes, Figure 7.5. This could lead to the conclusion that the measurements are not reliable. Figure 7.7 displays the raw data for the four repetitive measurements for a specific data point with a large standard deviation: Batch 4, NT=0.83. When analysing the four repetitive measurements from the left end, the measurements seem to overlap each other, i.e. from 2 µm to 200 µm the PSDs are very similar. The measurements for the particle sizes start to differ from 200 µm onwards. In a non-homogenous sample, as fungal fermentation broths, the probability of finding large particles is lower. The measurements become very unstable because a volume weighted distribution is considered. Then, since the 90th percentile considers the right end of the distribution, a large variation is obtained when this single parameter is considered.

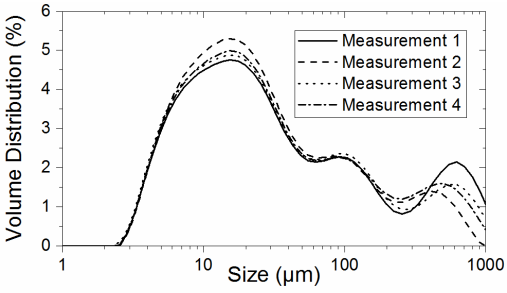

Figure 7.7. Four consecutive particle size distribution measurements for Batch 4 at NT=0.83.

For the first half of the fermentation, all the processes showed a decrease in the s_{90}. The fermentations run at the highest agitation speed had a higher degree of fragmentation, as expected. The particle size in these cultivations converts towards values representing an equilibrium between the hydrodynamic conditions and the hyphal tensile strength, as suggested by van Suijdam and Metz (1981) based on Kolmogorov's theory of isotropic turbulence. When the local shear forces are larger than the tensile hyphal strength, fragmentation occurs until equilibrium is established. The size of the hyphae at which equilibrium is achieved is called the equilibrium effective length. "Hyphae longer than this maximum value will fragment and hyphae shorter than this maximum value will not be further reduced in size" (Nielsen & Krabben 1995). Amanullah et al. (2002) observed smaller mean projected areas (measured with image analysis) for the fermentations ran at the higher agitation rates in fermentations conducted with *A. oryzae*. This is in agreement with the observations in this work.

Batch 3 and Batch 4 present a very interesting morphological phenomenon. The s_{90} for Batch 3 and Batch 4 did decrease for the first half of the processes, but then it started to increase. This is highly unexpected, given the fact that the biomass remained almost constant for the second half for these two fermentations. Another reason why this is even more interesting is the fact that the increase in size coincided with the reduction in the feed addition rate. For Batch 4, the s_{90} increased at NT=0.61, this was when the relative feed addition rate was approx. 0.1. For Batch 3, a s_{90} increase was registered between NT=0.6 and NT=0.75; at NT=0.7 the relative feed addition rate was 0.1. In Batch 1 and Batch 2, it was also possible to see a small increase in the s_{90} towards the end of the processes (after NT=0.85), and also here this increase agrees in time with the feed addition rate decreasing to 0.1 at NT=0.8. It is hypothesized that the underlying reason for the size increase is due to foraging, a physiological starvation response. *Saccharomyces cerevisiae* exhibits filamentous growth when subject to nutrient depletion (Da Silva et al. 2007; Birkaya et al. 2009). Although, foraging is a very well-known physiological response in filamentous fungi to lack of nutrients (Dowson et al. 1989; Ritz & Young 2004; Veses et al. 2008), to the best of our knowledge, it has not been reported in submerged fermentations. The increase in apical growth in these experiments was confirmed by microscopic images, Figure 7.6. As mentioned before, Batch 3 and Batch 4 present very long hyphae lacking branching.

An important point for discussion is the physiology of filamentous fungi in batch fermentation in nutrient limitation conditions. In this context, the question arises whether the same morphological phenomenon would be observed at the time of carbon depletion in a batch process. According to McIntyre et al. (2001) the mean projected area of *A. nidulans*, which is assumed to be analogue to the s_{90}, increases for the first hours and it reaches its maximum at the end of the exponential growth phase. After that, the mean projected area starts to decrease, but it never increases again (McIntyre et al. 2001). It is speculated that an increase on hyphae size is not observed in batch phase process because there is a large amount of carbon source available all the time, until the point that there is not anymore. Thus, the fungus does not have time to adapt to the environment for the point when all the carbon is exhausted. Contrary to a fed-batch process, where the carbon source is the limiting factor all the time and growth is governed by the feed rate addition. It is likely that when the feed rate is very small (maybe dictated by a relative feed addition rate = 0.1, Figure 7.3c), the fungi has time to adapt and used the available carbon source to look for nutrients.

7.5 Conclusions

In this work, while studying the morphology of filamentous fungi in fed-batch fermentation in pilot scale reactors, it was observed that the particle size distribution measured with laser diffraction cannot only give insight into the relation between morphology and rheology, as shown in Chapter 5, but it also granted the possibility to study direct physiological responses to environmental conditions in stirred bioreactors. The results obtained indicate that the nutrient depletion induced foraging due to starvation, which caused the increase in hyphal length. To our knowledge, this is the first time that this phenomenon is reported in submerged fermentations.

Foraging has been identified by image analysis in solid state fermentations (Hitchcock et al. 1996). More sophisticated fully automatic image analysis methods have suggested that foraging can be geometrically mapped on solid substrate (Barry et al. 2009). But no method has been reported in submerged fermentations. Thus, this is the first time that laser diffraction is used for that purpose. The information obtained with laser diffraction can be used as a routine measurement in fermentation processes, where it is desired to know whether the correct feeding strategy has been applied, given the fact that the measurements are very simple and fast, only requiring seconds. This method opens the door to infinite more studies. More work will require investigating whether the fungus returns to its “normal” equilibrium length when more carbon source is added.

Chapter 8. Dependence of hyphal tensile strength on environment and genetic variation

The contents of this chapter have been submitted to the Biotechnology and Bioengineering Journal "A fast and simple method to estimate relative, hyphal tensile-strength of filamentous fungi used to assess the effect of autophagy".
Quintanilla, D., Chelius, C., Gernaey, K.V., Marten, M.

8.1 Abstract

Fungal hyphal strength is an important phenotype which can have a profound impact on bioprocess behavior. Until now, there is not an efficient method which allows its characterization. Currently available methods are very time consuming; thus, compromising their applicability in strain selection and process development. To overcome this issue, a method for fast and easy, statistically-verified quantification of relative hyphal tensile strength was developed. It involves off-line fragmentation in a high shear mixer followed by quantification of fragment size using laser diffraction. Particle size distribution (PSD) is determined, with analysis time on the order of minutes. Plots of PSD 90^{th} percentile versus time allow the estimation of the specific fragmentation rate. This novel method is demonstrated by estimating relative hyphal strength during growth in control conditions and rapamycin-induced autophagy for *Aspergillus nidulans* (paternal strain) and a mutant strain (Δ*Anatg8*) lacking an essential autophagy gene. Both strains were grown in shake flasks, and relative hyphal tensile strength was compared. The mutant strain grown in control conditions appears to be

weaker than the paternal strain, suggesting that Anatg8 may play a role in other processes involving cell wall biosynthesis. Furthermore, rapamycin-induced autophagy resulted in apparently weaker cells walls even for the mutant strain. These findings confirm the utility of the developed method in strain selection and process development.

8.2 Introduction

Due to their exceptional capacity to express and secrete significant quantities of both native and recombinant protein, filamentous fungi have become indispensable for the production of industrial enzymes (Meyer 2008). Industrial enzyme production is typically carried out in large-scale aerobic fermentations. However, as fungal biomass increases, broth viscosity often increases significantly, resulting in oxygen mass-transfer limitations (Metz et al. 1979; Olsvik & Kristiansen 1994). To cope with these limitations, a simple strategy is to increase agitation intensity. Increased agitation also impacts fungal morphology, typically resulting in a reduction in the mean size of fungal elements (both freely-dispersed form and clumps; (Nienow 2009). These smaller fungal elements can have an indirect positive impact on productivity, as smaller fragments lead to reduced viscosity allowing increased oxygen mass-transfer (Johansen et al. 1998; Amanullah et al. 2002). Thus, in a DO-controlled feeding of a fungal fermentation, productivity will be enhanced with smaller fragments (Bhargava et al. 2003b).

During a submerged fermentation, the average size of fungal elements is the result of two opposing phenomena. Fragmentation occurs due to shear forces, imposed by hydrodynamic conditions in the tank, while resistance to fragmentation is dependent on hyphal tensile strength. van Suijdam and Metz (1981) suggested, based on Kolmogorov's theory of isotropic turbulence, that when the local shearing forces are larger than hyphal tensile strength, fragmentation occurs. The size of the hyphae at which equilibrium is achieved is called the equilibrium effective length (van Suijdam & Metz 1981). "Hyphae longer than this maximum value will fragment and hyphae shorter than this maximum value will not be further reduced in size" (Nielsen & Krabben 1995). This implies there is a limit on how agitation can be manipulated to control broth rheology. Another significant limitation in using increased agitation to control broth rheology is the significant capital investment required to purchase larger motors and the increased power requirements required to operate them. These ideas suggest that when attempting to control fungal broth rheology, an alternative to increased agitation is manipulation of hyphal tensile strength. While a number of authors have assumed fungal tensile strength to be constant (van Suijdam & Metz 1981; Nielsen & Krabben 1995; Johansen et al. 1998), more recent studies show this is not the case, and that tensile strength of fungal hyphae changes during growth (Li et al. 2002b; Li et al. 2002c). This raises clear questions regarding the dependence of hyphal strength on culture conditions and/or genetic variables. And, even more importantly, the question should be raised also whether we can actively manipulate these in order to favor fragmentation and thus positively impact fermentation productivity.

These ideas imply hyphal strength is a particularly important phenotype in fungal bioprocesses, and thus it would be ideal to have an easy, fast and reproducible method that allows its characterization. Different approaches have been developed to measure hyphal strength based on pressure or mechanical forces (Money & Hill 1997; Stocks & Thomas 2001). However, these methods rely on sophisticated equipment or measuring techniques, and generally measure the strength of a single cell, not the population. A population-based method has been developed (Li et al. 2002c), which is based on off-line fragmentation to quantify the relative hyphal tensile strength. Fungal broth is removed from a growing culture, and subjected to high shear in a mixer over a very short period of time; samples are removed every few seconds and the change of average size for the fungal elements is quantified by image analysis (Li et al. 2002c). While off-line fragmentation in a high shear mixer is fast and relatively simple, the image analysis required is extremely time consuming, and requires several days to be performed. Therefore, there is need for a method which allows rapid characterization of hyphal strength phenotype to be used in strain selection and process development.

In this work, the technique originally reported by Li et al (2002c) was further developed to create an easy and rapid method that allows reproducible quantification of relative hyphal strength. The first part of the assay, i.e., off-line fragmentation, remains unchanged. Here though, instead of using image analysis, average size of fragmented samples is analyzed using laser diffraction. Changes in hyphal morphology (i.e., fungal element size) are quantified by measuring particle size distribution (PSD). Plots of the 90^{th} percentile of the PSD versus time in the high shear mixer allow estimation of the instantaneous specific fragmentation rate, k_{frag}, which is inversely proportional to hyphal tensile strength.

To test reproducibility and applicability of the new method, we used shake flask cultures, grown under autophagy induced conditions (i.e., added rapamycin), to determine the impact on specific fragmentation rate. It was previously suggested that one of the effects of rapamycin-induced autophagy is the degradation of cell wall components, even in the presence of available exogenous carbon (Kim et al. 2011). Thus, we hypothesized a weaker hyphal cell wall should be observed during induced autophagy in comparison to control conditions. Additionally, the role of *A. nidulans* Anatg8 was examined using an *Anatg8* gene deletion mutant. Anatg8 plays a key role in the autophagy pathway, and *Anatg8* deletion mutants are autophagy deficient (Pollack et al. 2009; Zustiak et al. 2008). The hyphal cell wall strength was tested both under control and rapamycin-induced autophagy conditions and compared to the isogenic parental strain (ie., *Anatg8*+). This further allowed testing the applicability of the method for strain selection by measuring the hyphal strength phenotype-response on genetic variations. Furthermore, since we are aware that fragmentation rate measured in the fashion reported in this paper is a function of mixer geometry and speed, we propose a strategy to enable inter-laboratory comparisons.

8.3 Materials and Methods

8.3.1 Strains and growth conditions

Wild type *A. nidulans* (FGSC A4) was used for the method development experiments. Spores were propagated from freeze-dried ampoules onto MAG plates, following incubation for 3 days at 28°C. The MAG plates were made with 10 g/L glucose, 20 g/L malt extract, 15 g/L agar, 2 g/L peptone, 1 ml/L vitamin mix solution and 1 ml/L trace elements solution. The trace element solution was made of: 22 g/L $ZnSO_4 \cdot 7H_2O$, 11 g/L H_3BO_3, 5 g/L $MnCl_2 \cdot 4H_2O$, 5 g/L $FeSO_4 \cdot 7H_2O$, 1.7 g/L $CoCl_2 \cdot 6H_2O$, 1.6 g/L $CuSO_4 \cdot 5H_2O$, 1.5 g/L $Na_2MoO_4.2H_2O$ and 50 g/L EDTA (Na_4). The vitamin solution contained: 100 mg/L biotin, 100 mg/L pyridoxine, 100 mg/L thiamine, 100 mg/L riboflavin, 100 mg/L p-aminobenzoic acid, and 100 mg/L nicotinic acid. The spores were harvested with deionized water. Approximately 10^7 spores were used to inoculate a 250 mL shake flask containing 50 ml media. The shake flask media consisted of: 10 g/L glucose, 20 g/L malt extract, 2 g/L peptone, 1 ml/L trace metal solution and 1 ml/L vitamin mix solution. The pH of the media was adjusted to 3.3 ± 0.2 with the addition of 1M HCl to ensure dispersed growth (Carlsen et al. 1996). After inoculation, the shake flasks were placed in an orbital shaker at 250 rpm and 28°C. The 12 h vegetative growth from this shake flask was used to inoculate a 2.8 L baffled Fernbach flask containing 1.2 L of the same media. The initial pH of the media in this shake flask was not adjusted, but did not vary significantly (pH 6 ± 0.2). All flasks were incubated at 28 °C on an oscillating shaker at 250 rpm.

The applicability of the method was tested by measuring the specific fragmentation rate on a strain lacking a particular autophagy gene (Δatg8) and its paternal strain (TNO2A3) obtained from Dr. Steven D. Harris (Department of Plant Pathology and Center for Plant Science Innovation, University of Nebraska, NE, USA). For the control conditions (no autophagy), the strains were grown in the same media as for *A. nidulans* A4 but the media was enriched with uracil (1.2 g/L) and uridine (1.3 g/L), in addition to the MAG plates. Autophagy was induced in the exponential phase by adding 20 mg/L of a rapamycin solution (20 g/L). Rapamycin addition occurred at 10 h for the TNO2A3 strain and at 13 h for the Δatg8 strain. Samples were taken at different time intervals and dry cell weight measurements were performed along with k_{frag} measurements. The amount of withdrawn sample depended on the expected biomass concentration, since it is required to have a minimal biomass concentration in order to achieve a stable reading in the particle size determination, as further described.

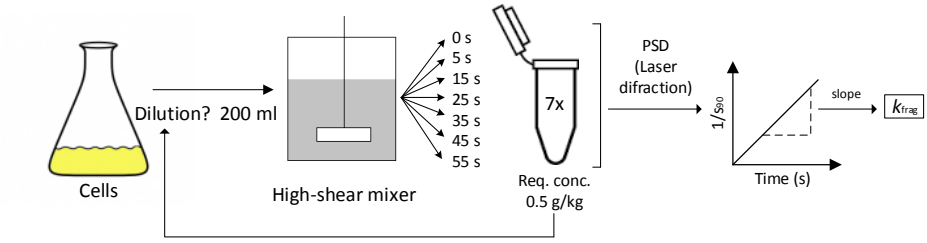

Figure 8.1. Schematic representation of the protocol to determine the relative hyphal tensile strength.

8.3.2 Modifications to the fragmentation test of fungal hyphae

In this work, the relative hyphal tensile strength was also estimated by measuring the relative fragmentation rate using a high-shear mixer (Black+Decker, BL2010BPA). The procedure was very similar as the one described by Li et al. (2002c) and it is illustrated in Figure 8.1. When the biomass concentration in the shake flasks was above 2 g/L, the samples were diluted 2x. 200 ml of properly diluted sample was placed in the high-shear mixer and the slowest speed was chosen. After short time intervals, approx. 1 ml samples were taken from the mixer with a cut pipette tip (to prevent size exclusion) and placed in Eppendorf tubes. The times for sample removal from the high shear mixer were: 0s, 5s, 15s, 25s, 35s, 45 s and 55 s. The particle size distribution of these samples was measured using laser diffraction. The Mastersizer 3000 with a Hydro SM manual small sample dispersion unit (Malvern Instruments Ltd. Worcestershire, UK) was used. The 1 ml sample from the high shear mixer was dispersed in tap water with a refractive index of 1.33. Using tap water ensured that no bubbles seated on the measurement area of the optical bench. The stirring was set to 1,800 rpm. A laser saturation of at least 1% was required in order to have a stable reading. Two or three successive measurements were performed for each sample, and a volume-weighted particle size distribution was calculated automatically in the Mastersizer 3000 software. The 90th percentile of the particle size distribution, s_{90}, was used as the parameter to characterize the morphological changes. Samples with biomass concentration less than 1 g/kg were analyzed right away, while samples with a higher biomass concentration were fixed with 1 ml fixative solution.

8.4 Results and Discussion

8.4.1 Method Development

Relative hyphal tensile strength was determined with an approach similar to a method developed by Li et al. (2002c). The difference in the method proposed here is in how average particle size is characterized after samples have been fragmented in a high shear mixer. In the original method of Li et al., (2002c) image analysis was used. Here, we use laser diffraction to characterize morphological changes. Using laser diffraction for these type of measurements has been shown to be an easy and fast method to characterize fungal morphology (Petersen et al. 2008; Rønnest et al. 2012). Experience has shown that

the relative fragmentation rate determination for one sample using image analysis for morphology characterization typically takes on the order of 20 hours. Thus a faster, more efficient, method would facilitate using this approach to evaluate phenotype for strain selection and process development procedures.

Figure 8.2 shows the particle size distribution (PSD) of *A. nidulans* A4 samples taken from the high shear mixer. Broth samples were taken from a shake flask at 15 h (Figure 8.2a) and 52 h (Figure 8.2b). The PSD represents the average of three successive measurements. It can be seen clearly that the laser diffraction method accounts for the changes in size due to the high shear forces in the mixer. The particle size distribution shifts to the left during high shear mixer operation, as an indication of particle size reduction in both figures. The time required to measure each broth sample is approximately 15 minutes, which is a dramatic (approximately 50x) reduction in processing time compared to the previous image analysis method (Li et al. 2002c).

The 90th percentile of the particle size distribution, s_{90}, was chosen as the morphological parameter to account for the changes in size in the high shear mixer. The s_{90} has been shown to correlate well with rheological properties of fermentation broths (unpublished data), in a manner similar as other morphological parameters (e.g., maximum projected area and the mean maximum dimension) (Riley et al. 2000). Figure 8.3a shows s_{90} for the PSD illustrated in Figure 8.2 as a function of time exposed to the high shear mixer. For the sample removed at 15 h, the s_{90} is at 1350 µm before being exposed to the high shear mixer, then decreases in size over time until it reaches approximately 300 µm. The sample removed at 52 h has a different fragmentation pattern; at 0 s the s_{90} is 1230 µm, and decreases in size until it reaches 380 µm at 55 s.

We used the same kinetic model applied in previous work (Li et al. 2002c) to determine the relative fragmentation rate:

$$\left(\frac{1}{s_{90}} - \frac{1}{s_{90,0}}\right) = k_{frag}t \qquad \textbf{Equation 8-1}$$

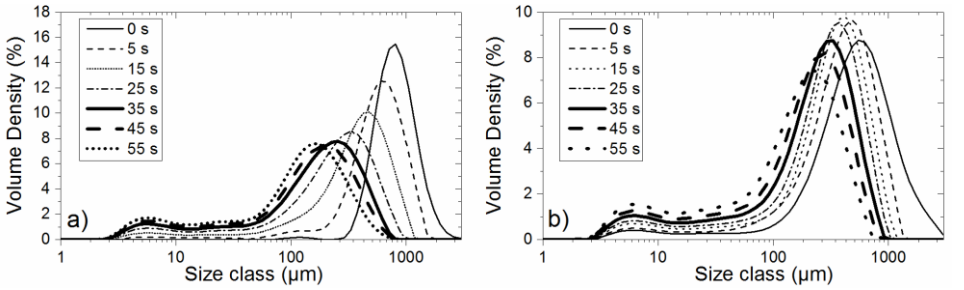

Figure 8.2. Particle size distributions of *A. nidulans* A4 samples taken from the high shear mixer at short time intervals, i.e. 0 s, 5 s, 15 s, 25 s, 35 s, 45 s and 55 s. a) PSD from a broth sample removed from the shake flasks at 15 h growth. b) PSD from a broth sample removed from the shake flask at 52 h growth.

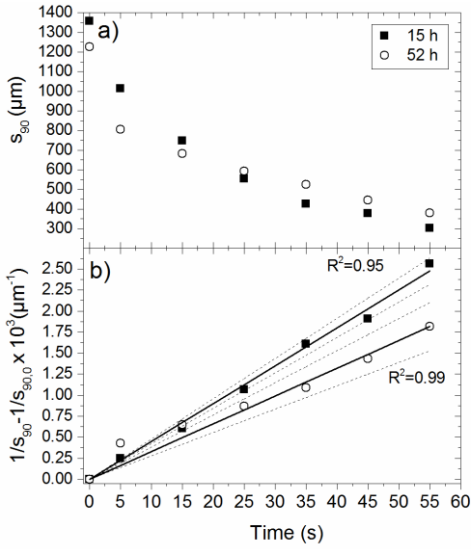

Figure 8.3. Preliminary results from the fragmentations test performed in *A. nidulans* A4 grown in complex media, samples taken at different fermentations times: 15 h (■) and 52 h (○). a) Evolution of the 90th percentile of the PSD in the high shear mixer. b) Results after the normalization with Equation. (1). the slope of the curves corresponds to the relative fragmentation rate, k_{frag}. The dotted lines represent the 95% confidence intervals of the slope.

where $s_{90,0}$ is the 90th percentile of the PSD at the beginning of a fragmentation test, i.e. the size of the particles in the shake flasks at the time the sample was removed and t is the time the particles have been exposed to the high shear mixer. Thus the relative fragmentation rate, k_{frag}, is the slope of plotting the left hand side of Eq. (1) versus the time the sample has been blended in the high shear mixer, Figure 8.3b. The values for each slope, 95% confidence intervals and regression coefficients can be found in Table 8.1. Assuming k_{frag} to be inversely proportional to the tensile strength, in this study it was found that the hyphae become stronger in the shake flask in time. This result contradicts the findings of Li et al (2002c). However, it should be emphasized that the experiments performed previously used a different species, *A. oryzae*, which might explain the differences in observed trends.

8.4.2 Finding a measuring window to estimate a constant specific fragmentation rate

Shake flask cultivations were performed to monitor the development of hyphal tensile strength of *A. nidulans* A4 during exponential growth in complex media. Results are shown in Figure 8.4. This allowed us to establish a time window where the k_{frag} measurements should be performed. Thus, a valid comparison can be conducted when evaluating hyphal strength of different strains which may have different growth curves. Since broth volume is the limiting factor in fragmentation experiments, dry cell weight samples were taken in the early growth phase for some flasks and late growth phase for the others. This ensured having enough broth to fragment mycelia and estimate k_{frag} values at several time points.

Table 8.1. Fragmentation rate (k_{frag}), confidence intervals (CI) and regression coefficient (R^2) for the slopes shown in Figure 8.3b. Samples were taken from a shake flask with *A. nidulans* A4 with complex media at two different time points (15 and 52 h).

Ferm. Time (h)	k_{frag} ($\mu m^{-1} s^{-1}$)	95% CI	R^2
15	4.5 E-05	[4.21E-05, 4-78E-05]	0.99
52	3.3 E-05	[2.77E-05, 3-82E-05]	0.95

Figure 8.4a the biomass concentration as a function of time for three shake flask cultivations run as biological replicates. The exponential phase is from 5 to 11 h, and ceases when biomass concentration reaches approximately 2 g/L due to oxygen transfer limitations. Similar growth curves are observed in (Zaho et al. 2005). Figure 8.4b displays the 90th percentile of the particle size distribution, s_{90}, as a function of time for five different shake flask fermentations. The morphology parameter s_{90} aligns well for the 5 biological replicates. According to the s_{90} profiles, the size of the cells increases linearly, i.e. there is no exponential increase in size, which indicates that further increase in biomass in the exponential phase is due to branching. This is indeed the mechanism that allows exponential growth of filamentous microorganisms (Spohr et al. 1998).

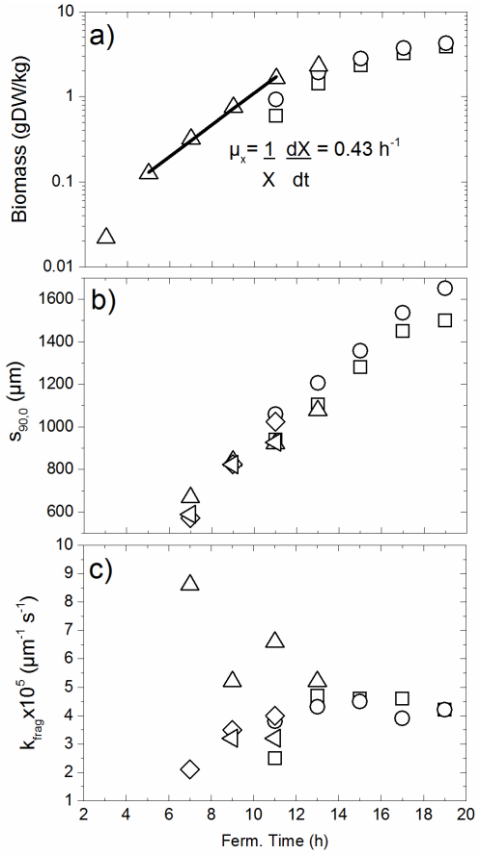

Figure 8.4. Profiles for *A. nidulans* A4 shake-flask fermentation with complex medium. a) biomass concentration (dry cell weight), b) 90th percentile of the particle size distribution as indication of morphology and c) fragmentation rate k_{frag}. The different symbols represent a biological replicate.

The relative fragmentation rate is illustrated in Figure 8.4c; there is significant variation in the k_{frag} measurements at the early stages of the cultivation. The variation however decreases in the latter portion of the flask culture i.e. 13 h. Early variation is due to unstable laser diffraction measurements due to low biomass concentrations. Thus we recommend performing the k_{frag} measurements when a biomass concentration of at least 1 g/L is achieved. Analysis of variance of k_{frag} from 13 h to 19 h shows no significant difference ($p>0.05$), with a mean value of 4.51E-05 ± 3.01 E-06 $\mu m^{-1}s^{-1}$ (95% CI).

8.4.3 Hyphal tensile strength in autophagy conditions

It has been suggested that rapamycin-induced autophagy boosts the expression levels of a-glucosidase B (AgdB) to increase glucose monomers from the α–glucan fraction of the cell wall, even in the presence of excess external carbon (David et al. 2006). Furthermore, rapamycin-induced autophagy leads to a reduction in the UDP-*N*-acetylglucosamine pyrophosphorylase (UngA), which is an important enzyme in cell-wall biosynthesis in yeasts (Milewski et al. 2006). Thus the effects of rapamycin-induced autophagy are likely to be the degradation of cell wall components, making the cell wall weaker as a result (Kim et al. 2011). To test this hypothesis, we measured the fragmentation rate constant, k_{frag}, for a strain of *A. nidulans* (TNO2A3) under rapamycin-induced autophagy with the method described above.

TNO2A3 was grown in complex media (control conditions) and k_{frag} was measured at different times between 12 and 25 h after the start of the cultivation. For the rapamycin-induced fermentations, 20 mg/L of rapamycin was added at 10 h, and k_{frag} was measured between 14 and 24 h after the start of the cultivation. Figure 8.5 shows biomass, s_{90} and k_{frag} profiles for control and rapamycin-induced autophagy conditions for four biological replicates. In control conditions, cells grow in exponential phase from 3 to 12 h. A biomass concentration of 1 g/L is observed approximately at the end of the exponential growth phase. For rapamycin treated cells, the growth rate is reduced from the point the rapamycin was added (10 h), and the biomass concentration is lower in comparison to control conditions from this point onwards. The s_{90} (Figure 8.5b) increases linearly from 6 to 16 h, and then remains constant with an average size of 706 ± 32 µm (95% CI) (control conditions). In the autophagy induced experiment, the rapamycin was added at 10 h and the s_{90} suddenly decreased and then eventually increased until achieving a size similar to untreated cells, 736 µm. The k_{frag} for the control conditions is 3.6E-05 ± 2.8 E-06 $\mu m^{-1}s^{-1}$ (95% CI), while the k_{frag} for the rapamycin treated cells is 6.6E-05 ± 5.4 E-06 $\mu m^{-1}s^{-1}$ (95% CI). There is a statistically significant difference ($p=1.4E-10$). The data suggest rapamycin addition resulted in weaker cell walls, observable as a reduction in size, s_{90}, coinciding with rapamycin addition.

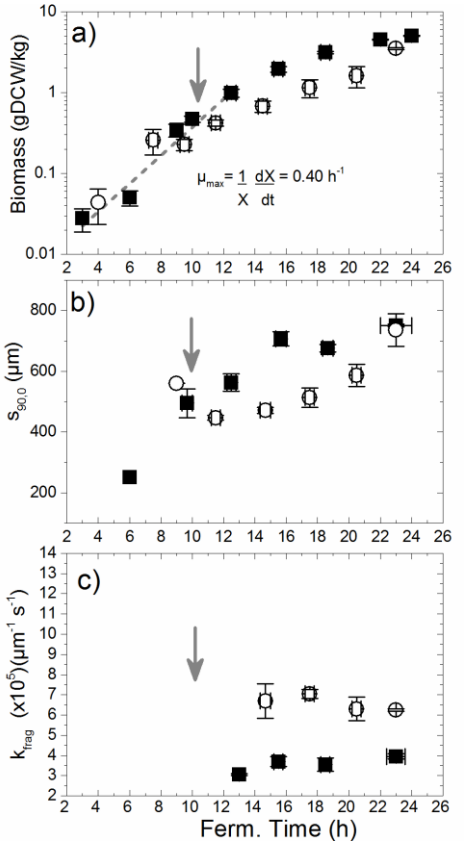

Figure 8.5. Results from *A. nidulans* TNO2A3 shake flasks cultivations with complex media at control conditions (■) and with autophagy induction by rapamycin addition (○). a) Biomass concentration (dry cell weight), b) 90th percentile of the PSD (morphological parameter) c) specific fragmentation rate k_{frag}. Error bars represent standard error for four biological replicates. The gray arrow indicates the rapamycin addition.

8.4.4 Studying the role of Anatg8 in hyphal strength

To test the ability of the developed method for assessing the hyphal strength phenotype in response to genetic variations, we measured k_{frag} for a mutant strain (Δ*Anatg8*) lacking a key gene in the autophagy pathway. Cultures of Δ*Anatg8* and its isogenic parent (ie., control strain) were grown in complex media (control) and complex media + rapamycin (autophagy).

Under control conditions, the autophagy deficient mutant strain, Δ*Anatg8*, has a very similar growth profile, to the autophagy capable strain (Figure 8.6a), with maximum growth rates of 0.40 and 0.37 h^{-1}, respectively, i.e. no significant difference between both strains. However, the lag phase for Δatg8 is longer, thus the rapamycin addition was at 13h for this strain. It is expected that both strains will have similar growth profiles when grown in complex media since autophagy is largely inactive when adequate nutrients are available (Moss 2013). For the rapamycin treated cells, the growth rate is reduced after 13 h, Figure 8.6a.

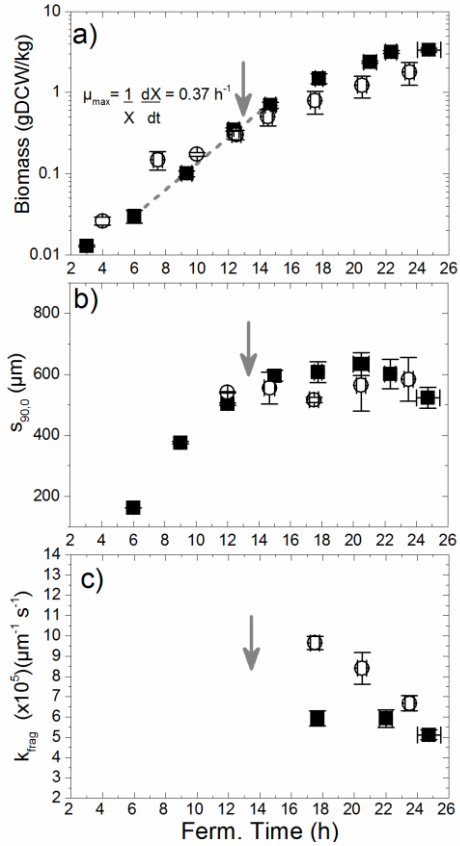

Figure 8.6. Results from *A. nidulans* Δatg8 shake flasks cultivations with complex media at control conditions (■) and with autophagy induction by rapamycin addition (○). a) Biomass concentration (dry cell weight); b) 90th percentile of the PSD (morphological parameter); c) specific fragmentation rate k_{frag}. Error bars represent standard error for four biological replicates. The gray arrow indicates the rapamycin addition.

Figure 8.6b shows the profile for the 90th percentile of the PSD. In general, the s_{90} increases linearly up to 600 µm at 14 h. Then s_{90} increases very slowly up to 20 h at which point it then begins a slight decrease. The s_{90} for the rapamycin treated cells is similar. The fragmentation rate for the control conditions for Δ*Anatg8* is 5.8E-05 ± 5.8 E-06 µm^{-1}s^{-1}. This implies the hyphal tensile strength for the mutant is lower than the paternal strain (TNO2A3), even when autophagy is inactive. There is a statistically significant difference between the k_{frag} for TNO2A3 under control conditions and the values for Δ*Anatg8* (p=7.66 E-08). These data suggest the Anatg8 protein may play a role outside the autophagy pathway or that the autophagy pathway is required for cell wall strength, even during growth on abundant nutrients. The k_{frag} value for Δ*Anatg8* at 18 h (after rapamycin addition) is significantly higher than the control conditions. However, the effect of rapamycin seems to be transient, as the k_{frag} values steadily decrease until they align with the control conditions. Although short-lived, the influence of rapamycin causes the autophagy deficient strain to become weaker.

Table 8.2. Summary of hyphal fragmentation results for two strains of *A. nidulans* (TNO2A3 and Δatg8) under control conditions and rapamycin-induced autophagy.

Strain	Rap (mg/L)	k_{frag} x 10^-5 (μm^{-1} s^{-1})	CI (95% confidence)	n
TNO2A3	0	3.64	± 0.28	14
Δatg8	0	5.81	± 0.58	12
TNO2A3	20	6.62	± 0.56	13
Δatg8	20	8.12	± 0.79	15

8.4.5 Normalization of the relative fragmentation rate for inter-laboratory comparison

Here, we propose a method to estimate the relative tensile strength of fungal hyphae by measuring the specific rate of fragmentation. We are aware that the rate of fragmentation evaluated in this fashion will depend on the geometry of the high shear mixer, the motor power of that mixer, and potentially other external factors related to the mixer-induced fragmentation. Thus, we propose results be reported as the ratio of fragmentation rate for the strain being tested and that for wild type *Aspergillus nidulans* A4. I.e. the values of k_{frag} reported in Table 8.2 are divided by the k_{frag} determined for A4, 4.51E-05 μm^{-1} s^{-1}, resulting in the normalized k_{frag} values shown in Figure 8.7.

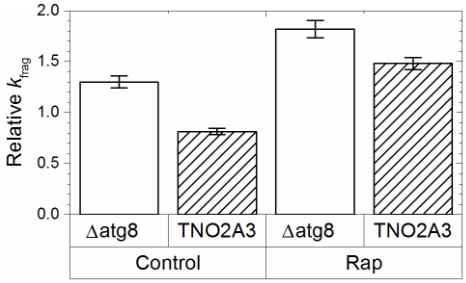

Figure 8.7. Normalized hyphal fragmentation rate for two strains of *A. nidulans* (Δatg8 and TNO2A3) at control and rapamycin induced conditions. Error bars represent the standard error divided by the average k_{frag} for A4.

8.5 Conclusions

In this work, we developed a rapid method to assess a bioprocess-relevant phenotype – the hyphal strength. The developed method allowed us to estimate the fragmentation rate which was assumed to be inversely proportional to the tensile strength. This new tool is inexpensive, fast and simple. This opens the door for future studies where the impact and changes of genetic manipulations on hyphal strength can be assessed in a quantitative way. This will provide the ability to make rational genetic or environmental changes that will likely impact bioprocess performance.

Chapter 9. General conclusion and future perspectives

Filamentous fungi are widely used as host for the production of industrial enzymes due to a number of advantages. However, the main disadvantage of working with filamentous fungi is the risk for oxygen transfer limitation that is encountered due to the high viscosity of the broth this type of host develops. Thus, this PhD thesis aimed to study and connect the viscosity to the morphology of filamentous fungi.

The literature review highlighted one of the biggest challenges with respect to the study of filamentous fungi in the production of enzymes: i.e. the lack of relevant industrial data. The difference between data generated by academia and the industry is enormous. E.g. processes studied in Chapter 2 are typically reported as a result of a study that has taken place at a university department, dealing with titers of barely a couple of grams per liter of extracellular protein. In industry there are reports of titers up to hundreds of grams per liter (Cherry & Fidantsef 2003). It is expected that the behavior of the industrial microorganisms would be completely different compared to lab-scale conditions due to the stress on the host organism that is caused by such high expression levels. Therefore, the work developed in this project deals with this issue. At the beginning of this project, a considerable amount of work was done to establish a platform which allowed high enzymes titers. The platform developed in Chapter 4 produced very high specific protein titers (amount of protein produced per amount of biomass). Thus, it can be used as reference process for a highly productive system for further studies.

The platform developed in Chapter 4 was further used to study the effect of agitation (a very important process variable) on enzyme production, rheology and morphology. This is an important issue, since according to Chapter 2, the different investigations reported

in the literature have not been able to manipulate one variable while keeping the rest of the parameters constant. In Chapter 5, we ran a set of 8 fermentations at different conditions; the agitation speed and the media concentration were varied. The fermentations were fed at very slow feed rates, thus ensuring that no oxygen limiting conditions were encountered. No difference in biomass, product formation and carbon dioxide production per unit of carbon feed were observed in our experiments, even at very high power inputs. This is great news for scientists and engineers, since it means that process scale up/scale down can be performed without further considerations to potential physiological damage caused by the energy dissipation rate. Chapter 5 also showed that the morphology, characterized as the 90^{th} percentile of the particle size distribution, was significantly affected by the stirrer speed. This study has therefore allowed us to conclude that agitation intensity can be manipulated in order to reduce oxygen transfer limitations and improve bulk mixing. But it can also be used to reduce viscosity by affecting the morphology without affecting productivity and it is in agreement with Johansen et al. (1998) and Amanullah et al.(2002).

This PhD thesis introduced the laser diffraction as an easy method to characterize dispersed fungal morphology by measuring the particle size distribution (PSD). This very simple/straightforward method is a very interesting new possibility to be used as a routine measurement in strain selection stages to get quantitative descriptions of strain morphology, since the time required to obtain the required information is very short. The data produced in Chapter 5 was used to construct a simple model to predict rheology based on knowledge of the 90^{th} percentile of the PSD and biomass concentration. This method and model could be used in strain selection stages for the production of industrial enzymes when an oxygen transfer limitation is an issue due to the high viscosities developed by the strain.

The knowledge described above was put in context in Chapter 6 by scaling down a production batch run at Novozymes A/S. This was done in order to evaluate the applicability of different literature models to predict hyphal fragmentation across scales in actual fermentations broths, i.e. in a situation with actively growing hyphae. Thus a production scale batch (≈ 100 m^3) was scaled down to pilot plant fermenters (≈ 1 m^3) and biomass concentration, rheology and particle size distribution were monitored. Furthermore, three more fermentations at bench scale (≈ 0.001 m^3) were conducted, and the morphology was analyzed. This data set functioned as a validation for demonstrating that the energy dissipation rate is better able to predict the fragmentation across scales. We suggested that P/V is a better approach, mainly due to its simplicity. Furthermore, this work also sheds light into which is the best method to estimate the shear rate for an industrial size reactor, i.e. a reactor with turbulent conditions. On our data, the H&K shear rate approach gives better results for the apparent viscosity, the Kolmogorov microscale, and the H&K equation is indeed able to correlate the s_{90} for the production and pilot scale fermentations. It was furthermore suggested that the results obtained in

this work for the shear rate for pilot and production scale could help to validate CFD models.

The last section of the thesis deals with the study of philological responses to environment conditions and to genetic variation. In Chapter 7 it was observed that the particle size distribution measured with laser diffraction cannot only give insight into the relation between morphology and rheology, as shown in Chapter 5, but it also granted the possibility to study direct physiological responses to environmental conditions in stirred bioreactors. The results obtained indicate that the nutrient depletion induced foraging due to starvation, which caused the increase in hyphal length. To our knowledge, this is the first time that this phenomenon is reported in submerged fermentations. This method therefore opens the door to a considerable number of additional studies.

Finally, Chapter 8 described a method which can be used to assess a bioprocess-relevant phenotype – the hyphal strength. The developed method allowed estimating the fragmentation rate which was assumed to be inversely proportional to the tensile strength. This new tool is inexpensive, fast and simple. This opens the door for future studies where the impact and changes of genetic manipulations on hyphal strength can be assessed in a very quantitative way. This will further allow making rational changes that will likely impact bioprocess performance.

In general, this PhD thesis brings more knowledge to the understanding of the relationship between growth kinetics, environmental conditions and the morphological structure of the filamentous fungi, which can help to tailor the morphology for a given industrial strain.

Appendix A

FBRM Further background

Since a couple of years, FBRM is widely considered as a useful technique for particle size analysis. FBRM can give in-line particle growth measurements even in a wide range of solid concentrations (Alshihabi et al. 2013). This is highly desirable when dealing with filamentous fungi, due to the high biomass concentration values that are achieved.

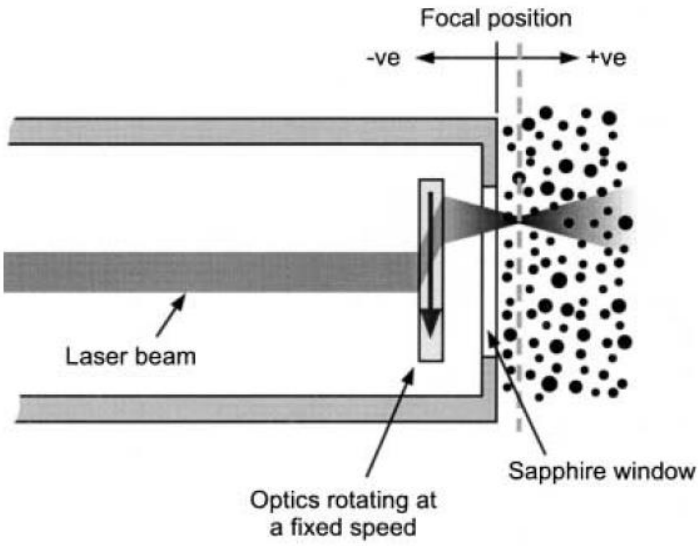

Fig. I Schematic of the FBRM probe (not to scale). Retrieved from (Heath et al. 2002)

The FBRM instrument directs a laser with a wavelength near the infrared region through the fiber-optics to the probe tip. A rotating optical lens located at the probe tip deflects the laser beam, as shown in Fig. I. When the probe is inserted into a particulate system, the emitted laser light is reflected if it scans across the surface of a particle, as indicated inFig. II. The probe measures the reflectance time, i.e. the time that passes between emitting the laser beam and capturing the reflected light, and estimates the chord length by making the product of the reflectance time and the laser scan speed (which can vary from 2 to 16 m/s). The results are given as number of counts of chord length of a specific size per second. . The size domain used in this work is 1 – 1000 μm. The size discretization is done automatically by the iCare Software based on a geometric progression. The domain is subdivided in 100 intervals which are referred as channels.

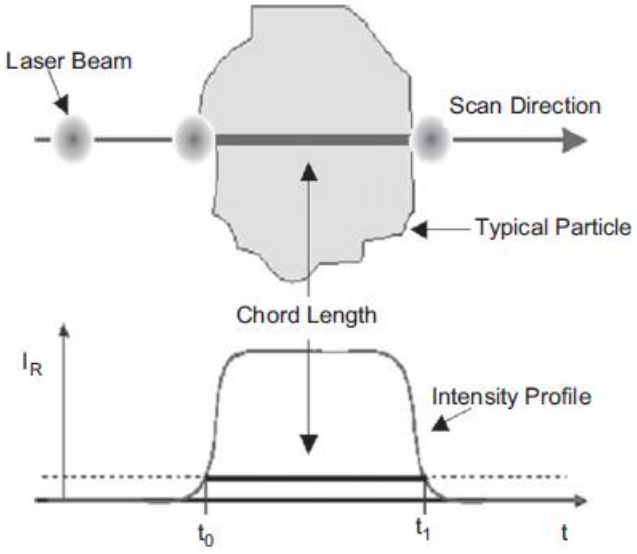

Fig. II Measurement of a particle chord length using the FBRM technology. Retrieved from (Greaves et al. 2008)**.**

The analysis of the data for chord length estimation can be done in two different ways: the Fine and the Coarse electronics processing regime. The main differences between these two electronics modules relies in the faster preamplification and greater edge definition with the Fine electronics setting; this is the most widely used electronics module in particle studies due to sharper resolution and higher sensitivity to fine chords that is achieved (Heath et al. 2002). The used of the coarse electronics is recommended in the study of aggregated particles, e.g. in flocculation applications. Turner (2005) suggested that agglomerates should be studied using the coarse setting of the instrument since the less detectable edges would be bypassed (Turner 2005). Also, Greaves et al. (2008) stated: "It is believed that by using the coarse setting, smaller portions of the agglomerates (like bumps and crevices) would be ignored and the whole agglomerate would be measured." Thus, this suggests that the study of filamentous morphology, including hyphal aggregation and clump formation, should be performed with the coarse electronics setting.

Appendix B

Estimation of maximum growth rates

The Carbon Dioxide Production Rate (CPR) was used to estimate the maximum specific growth rate for RedTr. The CPR evolution for the first hours is plotted below to determine the time where the cells were in exponential growth phase. For Soy fermentation, the exponential growth phase is from 5 to 14 h. For PP it is from 5 to 15 hours and for Inorg-N it is from 5 to 23 hours.

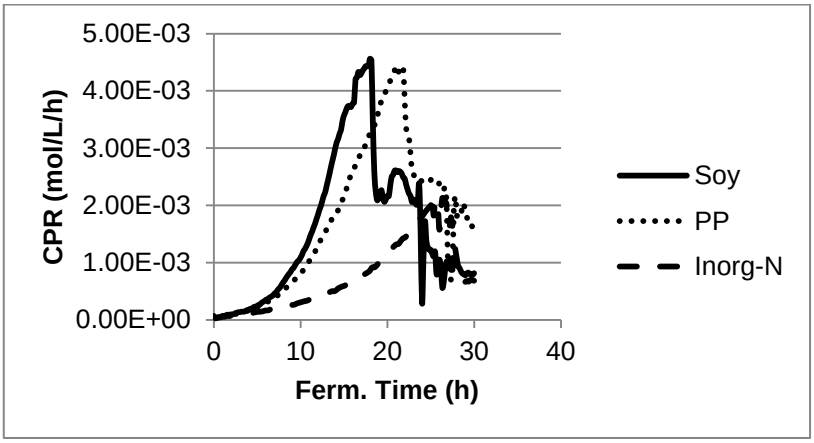

An exponential trend line is fit to the selected data and the maximum growth rate corresponds to μ:

$$CPR = CPR_0 e^{\mu t}$$

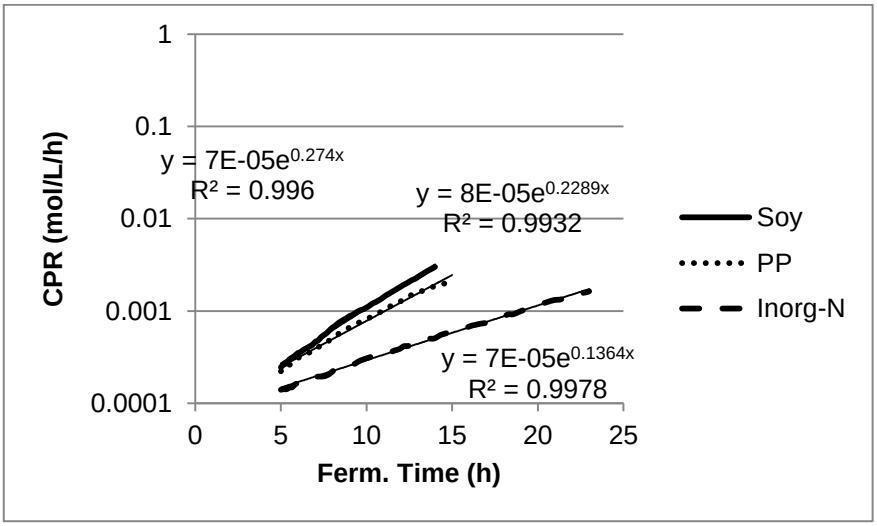

Appendix C

Mass Balances Calculations

Detailed calculations for the mass balances are illustrated here. This example corresponds to the fermentation named as PP

General Carbon Balance (C-mol) in time:

Ferm. Time (h)	**In Carbon (C-mol)**				**Out Carbon (C-mol)**				**Carbon error**
	Glc	N-source	Feed	Total	X	CO_2	P	Total	%
0	0.26	1.16	0.00	1.42	0.00	0.00	0.21	0.21	-85%
17	0.26	1.16	0.01	1.43	0.29	0.08	0.17	0.55	-62%
25	0.26	1.16	0.07	1.49	0.78	0.25	0.18	1.21	-19%
40	0.26	1.16	0.30	1.72	0.76	0.41	0.29	1.46	-15%
69	0.26	1.16	1.01	2.43	1.02	0.77	0.51	2.30	-5%
96	0.26	1.16	1.66	3.08	1.16	1.12	0.65	2.93	-5%

The **In Carbon** from the different sources is estimated as:

Glc corresponds to the added glucose in the batch phase:

$$Glc = \frac{conc \cdot Initial\ vol}{MW_{Glc}\ (C-mol)} = \frac{6\frac{g}{L} \cdot 1.3L}{30\frac{g}{C-mol}} = 0.26\ C-mol$$

The N-source corresponds to the added peptone in the batch phase:

$$N-source = \frac{conc \cdot Initial\ vol}{MW_{Pep}\ (C-mol)} = \frac{20\frac{g}{L} \cdot 1.3L}{22.5\frac{g}{C-mol}} = 1.16\ C-mol$$

The molecular weight in C-mol base for the peptone was taken from Nielsen et al (2003)

The Feed carbon source corresponds to the added Lactose solution:

$$Feed_{96h} = \frac{\frac{\Delta Weight_{LacSol}}{\rho_{LacSol}} Conc_{LacSol}}{MW_{Lac}\ (C-mol)} = \frac{\frac{0.34\ kg}{1.075\frac{kg}{L}} 150\frac{g}{L}}{28\ \frac{g}{C-mol}} = 3.08\ C-mol$$

The **Out Carbon** for the different sources is estimated as:

X corresponds to the carbon going to the biomass.

$$X_{96h} = X_{tank} + X_{loss} = \frac{W_{tank_{96h}} X_{Conc_{96h}}}{MW_X\ (C-mol)} + \frac{\sum_0^{96} X_{Conc_{t-1}} W_{loss_{\Delta t}}}{MW_X\ (C-mol)} =$$

$$= \frac{1.22kg \cdot 19.14 \frac{g}{kg}}{24.9 \frac{g}{C-mol}} + \frac{5.48\ g}{24.9 \frac{g}{C-mol}} = 1.16\ C-mol$$

The molecular weight in C-mol base for the biomass was assumed to be the same as for *A. niger* and it was taken from Villadsen et al. (2011) .

P corresponds to the carbon that is directed to the product.

$$P_{96h} = P_{tank} + P_{loss} = \frac{W_{tank_{96h}} P_{Conc_{96h}}}{MW_P\ (C-mol)} + \frac{\sum_0^{96} P_{Conc_{t-1}} W_{loss_{\Delta t}}}{MW_X\ (C-mol)} =$$

$$= \frac{\frac{1.22kg}{1.08 \frac{kg}{L}} \cdot 10.9 \frac{g}{kg}}{22.4 \frac{g}{C-mol}} + \frac{2.35\ g}{22.4 \frac{g}{C-mol}} = 0.65\ C-mol$$

The molecular weight in C-mol base for the product was assumed to be the same as for the peptone and it was taken from Nielsen et al (2003).

CO_2 corresponds to the carbon converted to Carbon dioxide, and it was measured continuously by the gas analyzer.

Appendix D

Mean of the PSD as a function of different scale up models.

a) Energy dissipation rate, b) EDCF, c) Tip speed and d) Shear rate (Henzler and Kauling method).

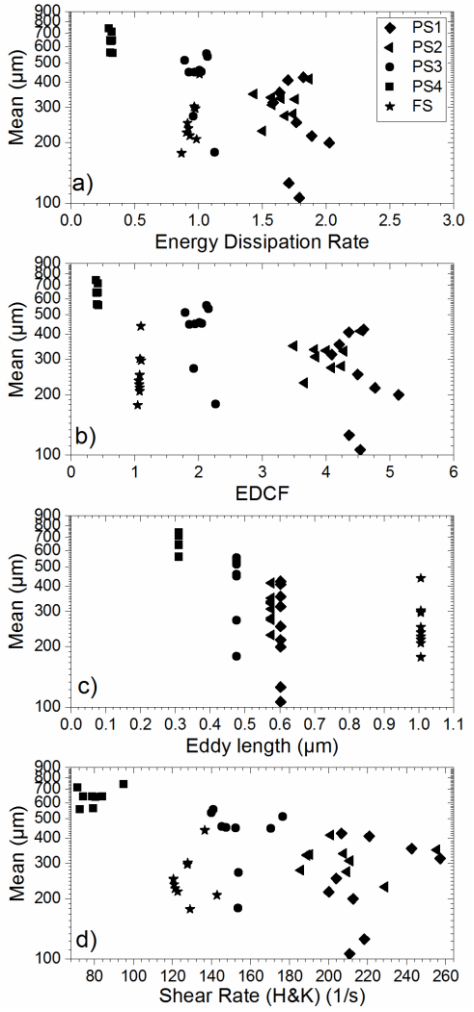

Appendix E

Direct comparison for off-line measurements for production, pilot and bench scale.
a) Biomass concentration development. b) Consistency index. c) 90th percentile of the PSD. d) Apparent viscosity. The apparent viscosity for the pilot and production scale is evaluated with H&K while the apparent viscosity for the bench scale fermentations is evaluated with the M&O approach. Lines drawn to indicate trends.

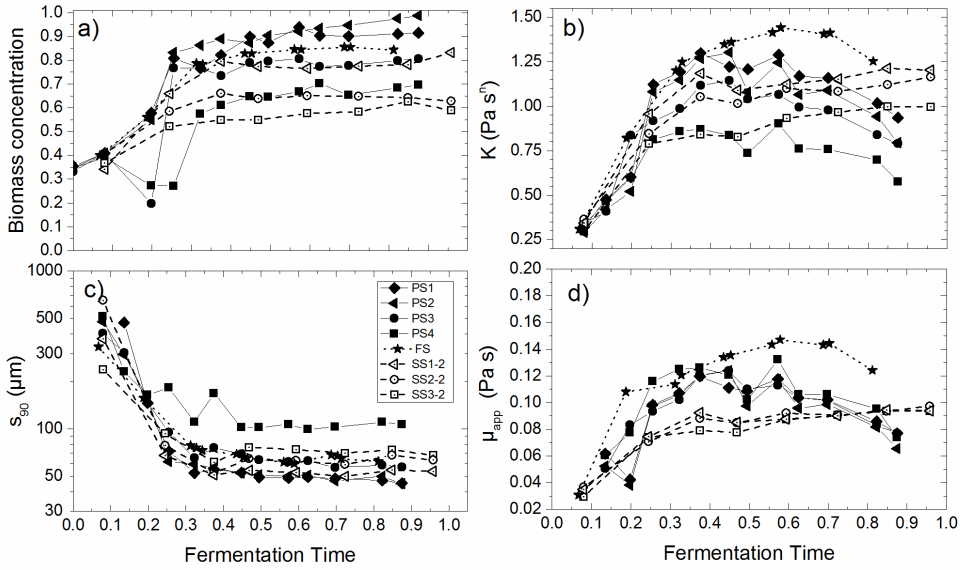

Appendix F

Preliminary work for comparison of rheological models

This appendix presents exploratory work that compares simple models, as the one described in section 5.4.7, *vs* multivariate models, as the ones described by (Petersen et al. 2008) with respect to their ability to predict rheological properties.

SIMPLE MODEL

The data set consist of:

-5 batches (4 pilot scale, 1 production scale)

-16 time points for each batch (all data points)

The data set contains:

- Consistency index, *K*
- 90th percentile of the particle size distribution, s_{90}
- Biomass concentration, X
- .

Half of the data have been chosen for the calibration of the next simple model

$$K = 9.57(X)^{-0.04}(s_{90})^{-0.49}$$

The graph below shows the validation of the model

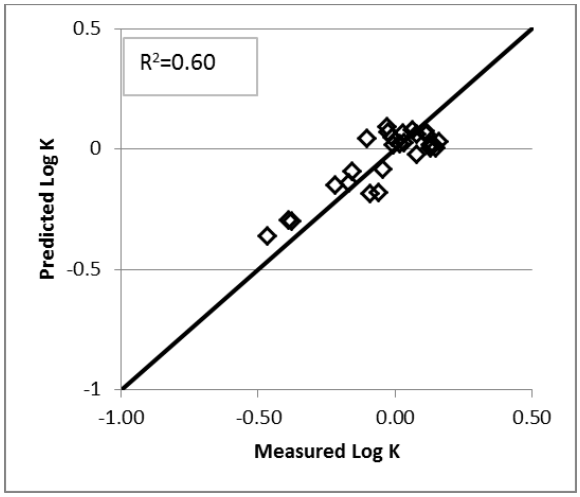

The R^2 is acceptable, but contrary to the model presented in section 5.4.7, the parameters for this model do not mean anything. I.e. the parameters presented in the model in section 5.4.7 tell us that the consistency index/viscosity increases with increase in biomass concentration and particle size; while the parameters in this appendix indicate the contrary.

MULTIVARIATE MODELS

We used the data set described above to create a multivariate model.

a) presents the scores for the PC1 and PC2. b) presents the loadings, c) is the biplot of the loading and scores, while d) presents the scree plot. According to this last plot, 90% of the variance is described with 4 components.

a)

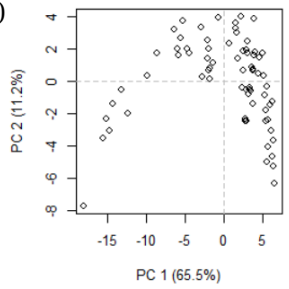

b)

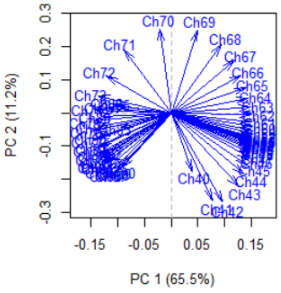

c)

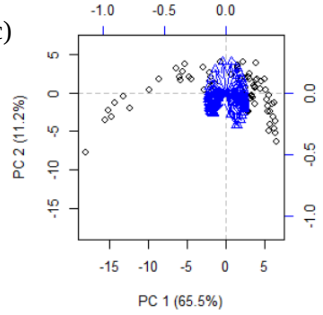

c)

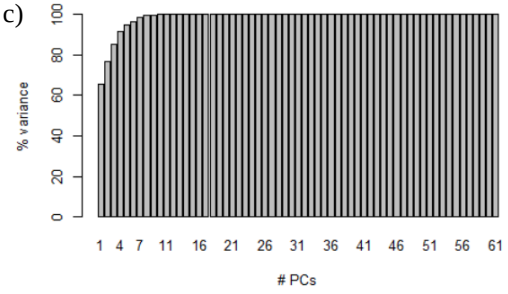

According to the graph before, 4 components are enough to describe 90% of the variation for the consistency index *K*. Thus, a PCR (principal component regression) model is constructed with 4 components. The model is shown in the figure below. The R^2 is around 0.80. This is an improvement with respect to the simple rheological model.

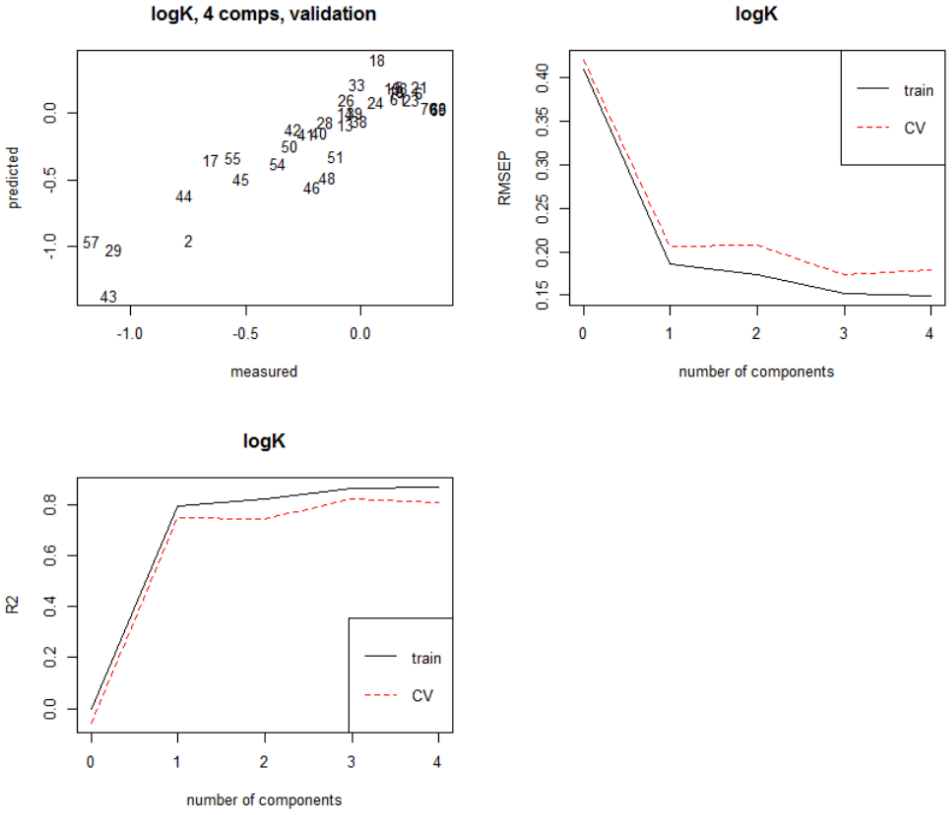

Appendix G

Averaged s_{90} as a function of different averaged scale-up parameters.

a) Energy dissipation rate, b) EDCF and c) Shear rate. The average values of s_{90} are calculated when steady conditions over hydrodynamics and growth have been achieved (i. e. after normalized time > 0.5). The error bars represent the standard error.

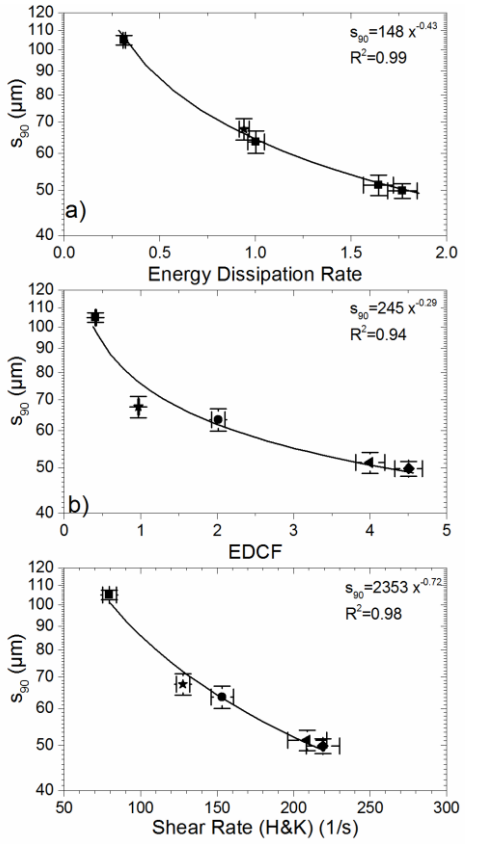

Bibliography

Agger, T. et al., 1998. Growth and product formation of Aspergillus oryzae during submerged cultivations: Verification of a morphologically structured model using fluorescent probes. Biotechnology and Bioengineering, 57(3), pp.321–329.

Ahamed, A. & Vermette, P., 2008. Culture-based strategies to enhance cellulase enzyme production from Trichoderma reesei RUT-C30 in bioreactor culture conditions. Biochemical Engineering Journal, 40(3), pp.399–407.

Ahamed, A. & Vermette, P., 2009. Effect of culture medium composition on Trichoderma reesei's morphology and cellulase production. Bioresource Technology, 100(23), pp.5979–5987.

Albaek, M.O. et al., 2012. Evaluation of the energy efficiency of enzyme fermentation by mechanistic modeling. Biotechnology and Bioengineering, 109(4), pp.950–961.

Albaek, M.O. et al., 2011. Modeling enzyme production with Aspergillus oryzae in pilot scale vessels with different agitation, aeration, and agitator types. Biotechnology and Bioengineering, 108(8), pp.1828–1840.

Albaek, M.O., Gernaey, K. V. & Stocks, S.M., 2008. Gassed and ungassed power draw in a pilot scale 550 litre fermentor retrofitted with up-pumping hydrofoil B2 impellers in media of different viscosity and with very high power draw. Chemical Engineering Science, 63(24), pp.5813–5820.

Allen, D.G. & Robinson, C.W., 1990. Measurements of rheological properties of filamentous fermentation broths. Chemical Engineering Science, 45(1), pp.37–48.

Alshihabi, F., Vandamme, T. & Betz, G., 2013. Focused beam reflectance method as an innovative (PAT) tool to monitor in-line granulation process in fluidized bed. Pharmaceutical development and technology, 18(1), pp.73–84

Amanullah, A. et al., 2000. Agitation induced mycelial fragmentation of Aspergillus oryzae and Penicillium chrysogenum. Biochemical Engineering Journal, 5(2), pp.109–114.

Amanullah, A. et al., 2002. Dependence of morphology on agitation intensity in fed-batch cultures of Aspergillus oryzae and its implications for recombinant protein production. Biotechnology and Bioengineering, 77(7), pp.815–826.

Amanullah, A. et al., 1999. Effects of agitation intensity on mycelial morphology and protein production in chemostat cultures of recombinant aspergillus oryzae. Biotechnology and Bioengineering, 62(4), pp.434–446.

Barry, D.J., Chan, C. & Williams, G. a., 2009. Morphological quantification of filamentous fungal development using membrane immobilization and automatic image analysis. Journal of Industrial Microbiology and Biotechnology, 36(6), pp.787–800.

Barry, D.J. & Williams, G. a., 2011. Microscopic characterisation of filamentous microbes: Towards fully automated morphological quantification through image analysis. Journal of Microscopy, 244(1), pp.1–20.

Bartnicki-García, S., 1999. Glucans, walls, and morphogenesis: On the contributions of J. G. H. Wessels to the golden decades of fungal physiology and beyond. Fungal genetics and biology : FG & B, 27(2–3), pp.119–127.

de Bekker, C. et al., 2011. Heterogeneity of Aspergillus niger microcolonies in liquid shaken cultures. Applied and environmental microbiology, 77(4), pp.1263–1267.

Berry, D.R., 1988. Physiology of Industrial Fungi, Oxford: Blackwell Scientific Publications.

Bhargava, S. et al., 2003a. Pulsed feeding during fed-batch fungal fermentation leads to

reduced viscosity without detrimentally affecting protein expression. Biotechnology and bioengineering, 81(3), pp.341–347.
Bhargava, S., Wenger, K.S. & Marten, M.R., 2003b. Pulsed addition of limiting-carbon during Aspergillus oryzae fermentation leads to improved productivity of a recombinant enzyme. Biotechnology and bioengineering, 82(1), pp.112–117.
Bhargava, S. et al., 2005. Effect of cycle time on fungal morphology, broth rheology, and recombinant enzyme productivity during pulsed addition of limiting carbon source. Biotechnology and bioengineering, 89(5), pp.525–529.
Birkaya, B. et al., 2009. Role of the cell wall integrity and filamentous growth mitogen-activated protein kinase pathways in cell wall remodeling during filamentous growth. Eukaryotic Cell, 8(8), pp.1118–1133.
Blainey, P., Krzywinski, M. & Altman, N., 2014. Points of Significance: Replication. Nature Methods, 11(9), pp.879–880.
Booking, S.P. et al., 1999. Effect of branch frequency in Aspergillus oryzae on protein secretion and culture viscosity. Biotechnology and Bioengineering, 65(6), pp.638–648.
Carlsen, M. et al., 1996. Morphology and physiology of an alpha-amylase producing strain of Aspergillus oryzae during batch cultivations. Biotechnology and Bioengineering, 49(3), pp.266–276.
Cascaval, D., Oniscu, C. & Galaction, A., 2003. Rheology of Fermentation Broths II. Influence of the rheological behavior on biotechnological processes. Revue Roumaine de Chimie, 48, pp.339–356.
Cherry, B., Bashkirova, E. V & Leon, A.L. De, 2009. Analysis of an Aspergillus niger glucoamylase strain pedigree using comparative genome hybridization & real-time quantitative polymerase chain reaction. Industrial Biotechnology, 5(4), pp.237–244.
Cherry, J.R. & Fidantsef, A.L., 2003. Directed evolution of industrial enzymes: an update. Current Opinion in Biotechnology, 14(4), pp.438–443.
Cooke, M., Middleton, J.C. & Bush, J.R., 1988. Mixing and mass transfer in filamentous fermentations. In 2nd International Conference on Bioreactor Fluid Dynamics. pp. 37–64.
Cox, P.W., Paul, G.C. & Thomas, C.R., 1998. Image analysis of the morphology of filamentous micro-organisms. Microbiology, 144(1 998), pp.817–827.
Davey, H.M. et al., 1999. Variable selection and multivariate methods for the identification of microorganisms by flow cytometry. Cytometry, 35(2), pp.162–168.
David, H. et al., 2006. Metabolic network driven analysis of genome-wide transcription data from Aspergillus nidulans. Genome biology, 7(11), p.R108.
Deindoerfer, F.H. & Gaden, E.L.J., 1955. Oxygen Transfer in Penicillin Fermentation Effects of Liquid Physical Properties on Oxygen Transfer in Penicillin Fermentation. Applied Microbiology, 3(5), pp.253–257.
Demain, A.L. & Vaishnav, P., 2009. Production of recombinant proteins by microbes and higher organisms. Biotechnology Advances, 27(3), pp.297–306.
Ding, P. et al., 2005. A process for the manufacture of chemically produced toner (CPT). II. Effect of operating conditions. Industrial and Engineering Chemistry Research, 44, pp.6012–6021.
Dowson, A.C.G. et al., 1989. Resource systems of relationships fascicu are in of foraging soil and Phanerochaete velutina Hypholoma. New Phytologist, 111(3), pp.501–509.
El-Deen, A.M.N., Shata, H.M.A.H. & Farid, M.A.F., 2014. Improvement of β-glucosidase production by co-culture of Aspergillus niger and A. oryzae under solid state fermentation through feeding process. Annals of Microbiology, 64(2),

pp.627–637.
Fazenda, M.L., Harvey, L.M. & McNeil, B., 2010. Effects of dissolved oxygen on fungal morphology and process rheology during fed-batch processing of Ganoderma lucidum. Journal of Microbiology and Biotechnology, 20(4), pp.844–851.
Fleissner, A. & Dersch, P., 2010. Expression and export: recombinant protein production systems for Aspergillus. Applied microbiology and biotechnology, 87(4), pp.1255–1270.
Formenti, L.R. et al., 2014. Challenges in industrial fermentation technology research. Biotechnology journal, 9(6), pp.727–738.
Ge, X.M., Zhao, X.Q. & Bai, F.W., 2005. Online monitoring and characterization of flocculating yeast cell flocs during continuous ethanol fermentation. Biotechnology and Bioengineering, 90, pp.523–531.
Ghose, T.K., 1987. Measurements of cellullase activities. Pure and Applied Chemistry, 59(2), pp.257–268.
Gibbs, P.A., Seviour, R.J. & Schmid, F., 2000. Growth of Filamentous Fungi in Submerged Culture : Problems and Possible Solutions. Critical Reviews in Biotechnology, 20(1), pp.17–48.
Greaves, D. et al., 2008. Measuring the particle size of a known distribution using the focused beam reflectance measurement technique. Chemical Engineering Science, 63, pp.5410–5419.
Gupta, K., Mishra, P.K. & Srivastava, P., 2007. A correlative evaluation of morphology and rheology of Aspergillus terreus during lovastatin fermentation. Biotechnology and Bioprocess Engineering, 12, pp.140–146.
Haack, M.B. et al., 2006. Change in hyphal morphology of Aspergillus oryzae during fed-batch cultivation. Applied microbiology and biotechnology, 70(4), pp.482–487.
Harold, F.M., 1997. New Ideas in Cell Biology. Protoplasma, 197, pp.137–147.
Heath, A.R. et al., 2002. Estimating average particle size by focused beam reflectance measurement (FBRM). Particle and Particle Systems Characterization, 19, pp.84–95.
Henzler, H.J. & Kauling, J., 1985. Scale-up of mass transfer in highly viscous liquids. In Fifth European Conference on Mixing. Wurzburg, Germany, pp. 303–312.
Hille, A. et al., 2005. Oxygen profiles and biomass distribution in biopellets of Aspergillus niger. Biotechnology and Bioengineering, 92(5), pp.614–623.
Hitchcock, D., Glasbey, C.A. & Ritz, K., 1996. Image analysis of space-filling by networks: Application to a fungal mycelium. Biotechnology Techniques, 10(3), pp.205–210.
Hjorth, S. et al., 2000. An Analysis of the Use of Electrical Power Measurements for Process Control in Large-Scale Stirred Vessels. The Canadian Journal of Chemical Engineering, 78, pp.1127–1132.
Horn, S.J. et al., 2012. Novel enzymes for the degradation of cellulose. Biotechnology for biofuels, 5(1), p.45.
Irfan, M., Nadeem, M. & Syed, Q., 2012. Influence of Nutritional Conditions for Endoglucanase Production by Trichoderma viride in SSF. Global Journal of Biotechnology and Biochemistry, 7(1), pp.7–12.
Johansen, C., Coolen, L. & Hunik, J., 1998. Influence of morphology on product formation in Aspergillus awamori during submerged fermentations. Biotechnology progress, 14(98), pp.233–240.
Juhász, T. et al., 2005. Characterization of cellulases and hemicellulases produced by Trichoderma reesei on various carbon sources. Process Biochemistry, 40(11), pp.3519–3525.

Jüsten, P. et al., 1996. Dependence of mycelial morphology on impeller type and agitation intensity. Biotechnology and Bioengineering, 52(6), pp.672–684.
Jüsten, P. et al., 1998. Dependence of Penicillium chrysogenum growth, morphology, vacuolation, and productivity in fed-batch fermentations on impeller type and agitation intensity. Biotechnology and Bioengineering, 59, pp.762–775.
Kamrani, A.K. & Salhieh, S.M., 2002. Product Design for Modularity 2nd ed., New York: Springer Science + Business Media.
Kim, Y. et al., 2011. Autophagy induced by rapamycin and carbon-starvation have distinct proteome profiles in Aspergillus nidulans. Biotechnology and Bioengineering, 108(11), pp.2705–2715.
Kold, D., 2010. Study of Mass Transfer in Viscous Fermentations - using a Rotating Jet Head Mixing System. PhD thesis. Technical University of Denmark.
Kossen, N.W.F., 2000. The Morphology of Filamentous Fungi. Advances in Biochemical Engineering/Biotetchnology, 70, pp.1–33.
Krull, R. et al., 2013. Characterization and control of fungal morphology for improved production performance in biotechnology. Journal of Biotechnology, 163(2), pp.112–123.
Lee, S.-M. & Koo, Y.-M., 2001. Pilot Scale Production of cellulase using Trichoderma reesei Rut-c30 in fedbatch mode. J. Microbiol. Biotechnol., 11(2), pp.229–233.
Lehmann, L., 2011. Physiological characterization of enzyme production in Trichoderma reesei, Kgs. Lyngby. PhD thesis. Technical University of Denmark
Li, Z.J. et al., 2000. Fungal morphology and fragmentation behavior in a fed-batch Aspergillus oryzae fermentation at the production scale. Biotechnology and Bioengineering, 70(3), pp.300–312.
Li, Z.J. et al., 2002a. Effects of increased impeller power in a production-scale Aspergillus oryzae fermentation. Biotechnology Progress, 18(3), pp.437–444.
Li, Z.J. et al., 2002b. Estimation of hyphal tensile strength in production-scale Aspergillus oryzae fungal fermentations. Biotechnology and Bioengineering, 77(6), pp.601–613.
Li, Z.J., Bhargava, S. & Marten, M.R., 2002c. Measurements of the fragmentation rate constant imply that the tensile strength of fungal hyphae can change significantly during growth. Biotechnology Letters, 24(1), pp.1–7.
Lin, P.J., Scholz, A. & Krull, R., 2010. Effect of volumetric power input by aeration and agitation on pellet morphology and product formation of Aspergillus niger. Biochemical Engineering Journal, 49(2), pp.213–220.
Lubertozzi, D. & Keasling, J.D., 2009. Developing Aspergillus as a host for heterologous expression. Biotechnology advances, 27(1), pp.53–75.
Lynd, L.R. et al., 2005. Consolidated bioprocessing of cellulosic biomass: an update. Current opinion in biotechnology, 16(5), pp.577–83.
Ma, L. et al., 2013. Kinetic studies on batch cultivation of Trichoderma reesei and application to enhance cellulase production by fed-batch fermentation. Journal of Biotechnology, 166(4), pp.192–197.
Machado, J.J.B., Coutinho, J.A. & Macedo, E.A., 2000. Solid – liquid equilibrium of lactose in ethanol / water. , 173, pp.121–134.
Makagiansar, H.Y. et al., 1993. The influence of mechanical forces on the morphology and penicillin production of Penicillium chrysogenum. Bioprocess Engineering, 9, pp.83–90.
Malouf, P., 2008. Study of the Relationship of Rheology , Morphology and Biomass Concentration of Trichoderma reesei Fermentation. MSc thesis. University of Ottawa.

Marten, M.R. et al., 1996b. Rheological , Mass Transfer , and Mixing Characterization of Cellulase-Producing Trichoderma reesei Suspensions. Biotechnol. Prog., 7938(95), pp.602–611.

Martinez, D. et al., 2008. Genome sequencing and analysis of the biomass-degrading fungus Trichoderma reesei (syn. Hypocrea jecorina). Nature biotechnology, 26(5), pp.553–560.

McDonald, K.A., Jackman, A.P. & Hurst, S., 2001. Characterization of plant suspension cultures using the focused beam reflectance technique. Biotechnology Letters, 23, pp.317–324.

McIntyre, M., Dynesen, J. & Nielsen, J., 2001. Morphological characterization of Aspergillus nidulans: growth, septation and fragmentation. Microbiology, 147(Pt 1), pp.239–246.

McNeil, B. et al., 1998. Measurement of autolysis in submerged batch cultures of Penicillium chrysogenum. Biotechnology and Bioengineering, 57(3), pp.297–305.

Mears, L. et al., 2017. Application of a mechanistic model as a tool for on-line monitoring of pilot scale filamentous fungal fermentation processes-The importance of evaporation effects. Biotechnology and Bioengineering, 114(3), pp.589–599.

Metz, B., Kossen, N.W.F. & van Suijdam, J.C., 1979. The rheology of mould suspensions. Advances in Biochemical Engineering, 11, pp.103–156.

Metzner, A. & Otto, R.E., 1957. Agitation of Non-Newtonian Fluids. AIChe Journal, 3(1), pp.3–10.

Meyer, V., 2008. Genetic engineering of filamentous fungi--progress, obstacles and future trends. Biotechnology advances, 26(2), pp.177–85.

Milewski, S., Gabriel, I. & Olchowy, J., 2006. Enzymes of UDP-GlcNAc biosynthesis in yeast. Yeast, 23(1), pp.1–14.

Money, N.P. & Hill, T.W., 1997. Correlation between endoglucanase secretion and cell wall strength in oomycete hyphae : implications for growth and morphogenesis. Micologya, 89(5), pp.777–785.

Moore, D., 1998. Fungal Morphogenesis, Cambridge.

Moss, B.J., 2013. Proteomic analysis of Aspergillus nidulans during autophagy and the role of autophagy genes Anatg13 and Anatg8. PhD thesis. University of Maryland Baltimore County.

Mukataka, S. et al., 1987. Variation in Cellulase-Constituting Components from Trichoderma reesei with Agitation Intensity. Biotechnology and Bioengineering, 32, pp.760–763.

Nakari-Setälä, T. et al., 2009. Genetic modification of carbon catabolite repression in Trichoderma reesei for improved protein production. Applied and Environmental Microbiology, 75(14), pp.4853–4860.

Nevalainen, K.M.H., Te'o, V.S.J. & Bergquist, P.L., 2005. Heterologous protein expression in filamentous fungi. Trends in biotechnology, 23(9), pp.468–74.

Nielsen, A., 2015. Promoting Pelleted and Mycelial Morphology In Filamentous Fermentation Broth. MSc thesis. Technical University of Denmark.

Nielsen, J. & Krabben, P., 1995. Hyphal Growth and Fragmentation of Penicillium chrysogenum in Submerged Cultures. Biotechnology and Bioengineering, 46, pp.588–598.

Nienow, A.W., 1990. Agitators for mycelial fermentations. Trends in Biotechnology, 8(1990), pp.224–233.

Nienow, A.W., 1998. Gas-liquid mixing studies: a comparison of Rushton turbines with some modern impellers. Trans IChemE, 74(Part A), pp.417–423.

Nienow, A.W., 2009. Scale-Up Considerations Based on Studies at the Bench Scale in Stirred Bioreactors. Journal of Chemical Engineering of Japan, 42(11), pp.789–796.
Olsson, L. et al., 2003. Influence of the carbon source on production of cellulases, hemicellulases and pectinases by Trichoderma reesei Rut C-30. Enzyme and Microbial Technology, 33(5), pp.612–619.
Olsvik, E. et al., 1993. Correlation of Aspergillus niger broth rheological properties with biomass concentration and the shape of mycelial aggregates. Biotechnology and Bioengineering, 42(9), pp.1046–1052.
Olsvik, E. & Kristiansen, B., 1994. Rheology of filamentous fermentations. Biotechnology Advances, 12(1), pp.1–39.
Oniscu, C., I., G.A. & Cascaval, D., 2003. Rheology of Fermentation Broths I. Rheological behaviors and influencing factors. Revue Roumaine de Chimie, 48(2), p.2003.
Osborn, T.W., 1977. Elemental Composition of Soybean Meal and Interlaboratory Performance. J. Agric. Food. Chem., 25(2), pp.229–232.
Papagianni, M., 2014. Characterization of Fungal Morphology using Digital Image Analysis Techniques. Journal of Microbial & Biochemical Technology, 6(4), pp.189–194.
Papagianni, M., 2004. Fungal morphology and metabolite production in submerged mycelial processes. Biotechnology Advances, 22(3), pp.189–259.
Patel, N. et al., 2009. Growth of Trichoderma reesei RUT C-30 in stirred tank and reciprocating plate bioreactors. Process Biochemistry, 44(10), pp.1164–1171.
Peberdy, J.F., 1994. Protein secretion in filamentous fungi--trying to understand a highly productive black box. Trends in biotechnology, 12(2), pp.50–57.
Persson, I., Tjerneld, F. & Hahn-Hägerdal, B., 1991. Fungal cellulolytic enzyme production: A review. Process Biochemistry, 26(2), pp.65–74.
Peter, C.P. et al., 2004. Impact of out-of-phase conditions on screening results in shaking flask experiments. Biochemical Engineering Journal, 17(3), pp.205–215.
Petersen, N., Stocks, S. & Gernaey, K. V., 2008. Multivariate models for prediction of rheological characteristics of filamentous fermentation broth from the size distribution. Biotechnology and Bioengineering, 100(1), pp.61–71.
Peterson, R. & Nevalainen, H., 2012. Trichoderma reesei RUT-C30--thirty years of strain improvement. Microbiology (Reading, England), 158(Pt 1), pp.58–68.
Pollack, J.K., Harris, S.D. & Marten, M.R., 2009. Autophagy in filamentous fungi. Fungal genetics and biology : FG & B, 46(1), pp.1–8.
Pollard, D.J. et al., 2007. Scale Up of a Viscous Fungal Fermentation: Application of Scale-Up Criteria With Regime Analysis and Operating Boundary Conditions. Biotechnol. Bioeng., 96(2), pp.307–317.
Punt, P.J. et al., 2002. Filamentous fungi as cell factories for heterologous protein production. Trends in biotechnology, 20(5), pp.200–206.
Quintanilla, D. et al., 2015. Fungal Morphology in Industrial Enzyme Production-Modelling and Monitoring. Advances in biochemical engineering/biotechnology, 149, pp.29–54.
Quintanilla, D., 2013. Oxygen Transfer in Aerated Stirred Tanks of Different Sizes. MSc thesis. Technical University of Denmark.
Ratkovich, N. et al., 2013. Activated sludge rheology: a critical review on data collection and modelling. Water research, 47(2), pp.463–482.
Reinhardt, M.O., 1892. Das Wachstum der Pilzhyphen. Jahrbücher für wissenschafftliche Botanik, 23, pp.479–565.
Rieseberg, M. et al., 2001. Flow cytometry in biotechnology. Applied Microbiology and

Biotechnology, 56(3–4), pp.350–360.
Riley, G.L. et al., 2000. Effect of biomass concentration and mycelial morphology on fermentation broth rheology. Biotechnology and Bioengineering, 68(2), pp.160–172.
Riley, G.L. & Thomas, C.R., 2010. Applicability of Penicillium chrysogenum rheological correlations to broths of other fungal strains. Biotechnology letters, 32(11), pp.1623–1629.
Ritz, K. & Young, I.M., 2004. Interactions between soil structure and fungi. Mycologist, 18(2), pp.52–59.
Rodriguez-Gomez, D. et al., 2012. Examining the potential of plasma-assisted pretreated wheat straw for enzyme production by Trichoderma reesei. Applied Biochemistry and Biotechnology, 166(8), pp.2051–2063.
Rodriguez-Gomez, D. & Hobley, T.J., 2013. Is an organic nitrogen source needed for cellulase production by Trichoderma reesei Rut-C30? World Journal of Microbiology and Biotechnology, 29(11), pp.2157–2165.
Rønnest, N.P. et al., 2012. Comparison of laser diffraction and image analysis for measurement of Streptomyces coelicolor cell clumps and pellets. Biotechnology Letters, 34(8), pp.1465–1473.
Sánchez Pérez, J. a. et al., 2006. Shear rate in stirred tank and bubble column bioreactors. Chemical Engineering Journal, 124(1–3), pp.1–5.
Schafner, D.W. & Toledo, R.T., 1992. Cellulase production in continuous culture by Trichoderma reesei on xylose-based media. Biotechnology and bioengineering, 39, pp.865–869.
Schöll, J., Kempkes, M. & Mazzotti, M., 2012. Focused Beam Reflectance Measurement Jochen Schöll, Michael Kempkes, Marco Mazzotti Pages 21-28. , p.2012.
Da Silva, P.C. et al., 2007. Characterization of industrial strains of Saccharomyces cerevisiae exhibiting filamentous growth induced by alcohols and nutrient deprivation. World Journal of Microbiology and Biotechnology, 23(5), pp.697–704.
Sin, G., Gernaey, K. V & Lantz, A.E., 2009. Good modelling practice (GMoP) for PAT applications: Propagation of input uncertainty and sensitivity analysis. Biotechnology Progress, 25, pp.1043–1053.
Sivaramakrishnan, S. et al., 2006. a -Amylases from Microbial Sources – An Overview on Recent Developments. , 44(2), pp.173–184.
Smith, J.J., Lilly, M.D. & Fox, R.I., 1990. The effect of agitation on the morphology and penicillin production of penicillium chrysogenum. Biotechnology and Bioengineering, 35(10), pp.1011–1023.
Spohr, A. et al., 1997. Morphological characterization of recombinant strains of Aspergillus oryzae producing alpha-amylase during batch cultivations. Biotechnology Letters, 19(3), pp.257–261.
Spohr, A. et al., 1998. Quantitative Morphology of Filamentous Micro-organisms. In M. H. F. Wilkinson & F. Schut, eds. Digital Image Analysis of Microbes. pp. 373–410.
Stocks, S.M., 2013. Industrial enzyme production: Process scale up/scale down. In B. McNeil et al., eds. Microbial Production of Food Ingredients, Enzymes and Nutraceuticals. Woodhead Publishing, pp. 144–172.
Stocks, S.M. & Thomas, C.R., 2001. Strength of mid-logarithmic and stationary phase Saccharopolyspora erythraea hyphae during a batch fermentation in defined nitrate-limited medium. Biotechnology and Bioengineering, 73, pp.370–378.
van Suijdam, J.C. & Metz, B., 1981. Influence of engineering variables upon the morphology of filamentous molds. Biotechnology and Bioengineering, 23, pp.111–

148.
Thomas, C.R., 1992. Image analysis : putting filamentous microorganism in the picture. Trends in biotechnology, 10(10), pp.343–348.
Turner, D., 2005. Clathrate hydrate formation in water-in-oil dispersions. Colorado School of Mines.
Velkovska, S., Marten, M.R. & Ollis, D.F., 1997. Kinetic model for batch cellulase production by Trichoderma reesei Rut C30. Journal of Biotechnology, 54, pp.83–94.
Veses, V., Richards, A. & Gow, N.A., 2008. Vacuoles and fungal biology. Current Opinion in Microbiology, 11(6), pp.503–510.
Villadsen, J., Nielsen, J. & Lidén, G., 2011. Bioreaction Engineering Principles, Boston, MA: Springer US.
Ward, O.P., 2012. Production of recombinant proteins by filamentous fungi. Biotechnology advances, 30(5), pp.1119–39.
Weber, J. & Agblevor, F.A., 2005. Microbubble fermentation of Trichoderma reesei for cellulase production. Process Biochemistry, 40(2), pp.669–676.
Wessels, J.G.H., 1990. Role of Cell Wall Architecture in Fungal Tip Growth Generation. In I. B. Heath, ed. Tip Growth in Plant and Fungal Cells. Academic Press, Inc., pp. 1–29.
Wessels, J.G.H., 1993. Wall growth, protein excretion and morphogenesis in fungi. New Phytol., 123(45), pp.397–413.
White, S. et al., 2002. The Autolysis of Industrial Filamentous Fungi. , 22(1), pp.1–14.
Wongwicharn, A., McNeil, B. & Harvey, L.M., 1999. Effect of oxygen enrichment on morphology, growth, and heterologous protein production in chemostat cultures of Aspergillus niger B1-D. Biotechnology and Bioengineering, 65(4), pp.416–424.
Wösten, H. a et al., 1991. Localization of growth and secretion of proteins in Aspergillus niger. Journal of general microbiology, 137(8), pp.2017–2023.
Wucherpfennig, T. et al., 2010. Morphology and rheology in filamentous cultivations 1st ed., Elsevier Inc.
Wucherpfennig, T., Hestler, T. & Krull, R., 2011. Morphology engineering - Osmolality and its effect on Aspergillus niger morphology and productivity. Microbial Cell Factories, 10(1), p.58.
Wucherpfennig, T., Lakowitz, A. & Krull, R., 2013. Comprehension of viscous morphology-Evaluation of fractal and conventional parameters for rheological characterization of Aspergillus niger culture broth. Journal of Biotechnology, 163(2), pp.124–132.
Xiao, Z., Storms, R. & Tsang, A., 2004. Microplate-based filter paper assay to measure total cellulase activity. Biotechnology and Bioengineering, 88(7), pp.832–837.
Xu, J. et al., 2014. Intracellular beta-glucosidases CEL1a and CEL1b are essential for cellulase induction on lactose in Trichoderma reesei. Eukaryotic Cell, 13(8), pp.1001–1013.
Yu, L. et al., 2012. Hydrodynamic and kinetic study of cellulase production by Trichoderma reesei with pellet morphology. Biotechnology and Bioengineering, 109(7), pp.1755–1768.
Zaho, L. et al., 2005. Elastic Properties of the Cell Wall of Aspergillus nidulans Studied with Atomic Force Microscopy. Biotechnology Progress, 21, pp.292–299.
Zustiak, M.P. et al., 2008. Feast or famine: autophagy control and engineering in eukaryotic cell culture. Current Opinion in Biotechnology, 19(5), pp.518–526.

Process and Systems Engineering Centre (PROSYS)
Department of Chemical and Biochemical Engineering
Technical University of Denmark
Søltofts Plads, Building 229
DK - 2800 Kgs. Lyngby
Denmark

Phone: +45 45 25 28 00
Web: www.kt.dtu.dk/forskning/prosys